

MaCKiE–2015

Mathematics in (bio)Chemical
Kinetics and Engineering

Book of Abstracts

Ghent, July 2–3, 2015.

On the detailed modelling of high temperature nanoparticles synthesis

*M. Kraft*¹

New findings and models of high temperature nanoparticle synthesis and, in particular, particle formation and growth from gas phase precursors are presented. The model construction starts by identifying possible chemical species relevant to the synthesis and growth of nanoparticles. Subsequently, a detailed chemical mechanism is proposed. The chemical mechanism is then reduced and coupled to a stochastic particle system which describes the evolution of nanoparticles from clusters of molecules to aggregates of nano-size. In order to do this we use automated modelling techniques, advanced stochastic algorithms and statistical methods. The following systems will be discussed: silicon nanoparticle synthesis from silane, titania nanoparticles from titanium tetra-isopropoxide (TTIP) and titanium tetrachloride (TiCl_4) and silica nanoparticles from tetraethoxysilane (TEOS).

¹University of Cambridge, U.K.

On reactive settling of activated sludge*

Raimund Bürger¹, Stefan Diehl², and Ingmar Nopens³

¹CI²MA and Departamento de Ingeniería Matemática, Facultad de Ciencias Físicas y Matemáticas, Universidad de Concepción, Casilla 160-C, Concepción, Chile. E-Mail: rburger@ing-mat.udec.cl
(corresponding author)

²Centre for Mathematical Sciences, Lund University, P.O. Box 118, S-221 00 Lund, Sweden. E-Mail: diehl@maths.lth.se

³BIOMATH, Department of Mathematical Modelling, Statistics and Bioinformatics, Ghent University, Coupure links 653, B-9000 Ghent, Belgium. E-Mail: ingmar.nopens@ugent.be

April 1, 2015

Keywords: batch sedimentation; numerical scheme; degenerate parabolic PDE; sequencing batch reactor

Introduction

The authors have previously launched a model for the sedimentation process of the secondary clarifier in wastewater treatment plants (Bürger et al., 2011). The model originates from the conservation of mass and can be stated as a scalar, nonlinear partial differential equation (PDE) for the sludge concentration as function of depth and time. A special feature of this PDE is that it is parabolic wherever the solution exceeds a certain critical concentration of sludge and hyperbolic for lower concentration values. Thus, this equation is called strongly degenerate parabolic or parabolic-hyperbolic. Note that the location of the type-change interface is not known beforehand. Moreover, due to the nonlinear and degenerate nature discontinuities appear and special techniques for the numerical solution have to be used. The mathematical foundation of the model by Bürger et al. (2011) is provided by Bürger et al. (2005).

Sedimentation is often modeled under the assumption that no reaction takes place. However, there is an interest to model and simulate reactive settling, for example, in sequencing batch reactors (SBRs) (Alex et al., 2011; Kazmi and Furumai, 2000a,b; Keller and Yuan, 2002; Maruejouis et al., 2012). It is the purpose of this contribution to make a first step towards extending the advances made by Bürger et al. (2011) for the numerical treatment of non-reactive settling to the reactive case. To this end, we focus on a heavily reduced-order problem as a first approach to reactive settling partly in SBRs, and partly in the secondary clarifier. Despite the simplicity of the model, it accounts for three constitutive assumptions that determine its mathematical nature: i) the hindered settling of the flocculated particles; ii) compression of the flocculated particles at high concentrations when a network is formed; iii) a growth rate kinetic function.

Governing model

We study one-dimensional batch sedimentation of suspended particles in a closed vessel of height L with a constant cross-sectional area. The depth z is measured from the suspension surface downwards. The particulate microorganisms (biomass) may be active or inert with the concentrations X_a and X_i , respectively. The biomass is assumed to be flocculated into large particles, having the concentration $X = X_a + X_i$. Each particle is assumed to settle with a velocity $v = v(X, X_z)$ given by a constitutive assumption involving the

*Extended abstract submitted to *Mathematics in (bio)Chemical Kinetics and Engineering. An International Conference (MACKIE-2015)*, to be held at Ghent University, Belgium, July 2 and 3, 2015.

local concentration X and its gradient $X_z := \partial X / \partial z$. The active biomass consumes the substrate, which is soluble in the water and has the concentration S . For simplicity, the spatial movement of the substrate is assumed to be caused by diffusion and some dispersion due to the movement of the particles, both captured by a single diffusion coefficient ε .

A batch settling experiment starts naturally with a homogeneous suspension of particles at the concentration X_0 and substrate at the concentration S_0 . Each particle consists of a certain percentage p_0 of active biomass and the remaining is inert. The conservation of mass yields the following initial-value and zero boundary-flux problem for $0 < z < L$ and $t > 0$:

$$\frac{\partial X_a}{\partial t} = -\frac{\partial}{\partial z}(v(X, X_z)X_a) + (\mu(S, X) - b)X_a, \quad (1)$$

$$\frac{\partial X_i}{\partial t} = -\frac{\partial}{\partial z}(v(X, X_z)X_i) + bX_a, \quad (2)$$

$$\frac{\partial S}{\partial t} = \varepsilon \frac{\partial^2 S}{\partial z^2} - \frac{\mu(S, X)}{Y}X_a, \quad (3)$$

$$X_a(z, 0) = p_0X_0, \quad X_i(z, 0) = (1 - p_0)X_0, \quad S(z, 0) = S_0, \quad (4)$$

$$v(X, X_z)X|_{z=0} = v(X, X_z)X|_{z=L} = 0 = S_z(0, t) = S_z(L, t). \quad (5)$$

where Y is a dimensionless yield factor and b [s^{-1}] is a constant decay rate. The growth rate function is the following:

$$\mu(S, X) := \mu_{\max} \frac{S}{K_s + K_C X + S}, \quad (6)$$

where μ_{\max} is the maximum specific growth rate and $K_s, K_C \geq 0$ are constants. The common special case of Monod kinetics is obtained for $K_C = 0$, whereas $K_s = 0$ gives the one by Contois. The constitutive function for the particle velocity is assumed to take into account both hindered settling and compression and is of the following form (Bürger et al., 2011):

$$v(X, X_z) = \begin{cases} v_{\text{hs}}(X) & \text{for } X < X_c, \\ v_{\text{hs}}(X) \left(1 - \frac{\rho_s \sigma'_e(X)}{Xg\Delta\rho} \frac{\partial X}{\partial z}\right) & \text{for } X > X_c. \end{cases}$$

Here, $v_{\text{hs}}(X)$ is the hindered settling velocity function, σ_e the effective solids stress, ρ_s the density of the solids, $\Delta\rho$ the density difference between solids and liquid, and X_c is a critical concentration above which the particles touch each other and form a network which can bear a certain stress.

Numerical example

For the numerical simulation, we note that the sum of (1) and (2) gives an equation, which apart from the reaction term $\mu(S, X)X_a$, only contains derivatives of the total concentration X . This means that we can utilize the numerical method presented by Bürger et al. (2012a, 2013). Hence, in each discrete time step in the numerical method, this equation is updated first. This means, in particular, that the total numerical flux is known between the computational cells during the discrete time step. With this, the (numerical approximate) velocity $v(X, X_z)$ is known and it is straightforward to update Eqs (1)–(3). In the figure, we show a simulation where the Monod growth kinetics have been used with the initial data $X_0 = 4 \text{ kg/m}^3$, $X_a(z, 0) = 0.9X_0$ and $S_0 = 1 \text{ kg/m}^3$.

References

- J. Alex, S. G. E. Rönner-Holm, M. Hunze, and N. C. Holm. A combined hydraulic and biological SBR model. *Wat. Sci. Tech.*, 64(5):1025–1031, 2011. ISSN 0273-1223. doi: 10.2166/wst.2011.472.
- R. Bürger, S. Diehl, S. Farås, and I. Nopens. On reliable and unreliable numerical methods for the simulation of secondary settling tanks in wastewater treatment. *Computers & Chemical Eng.*, 41:93–105, 2012.

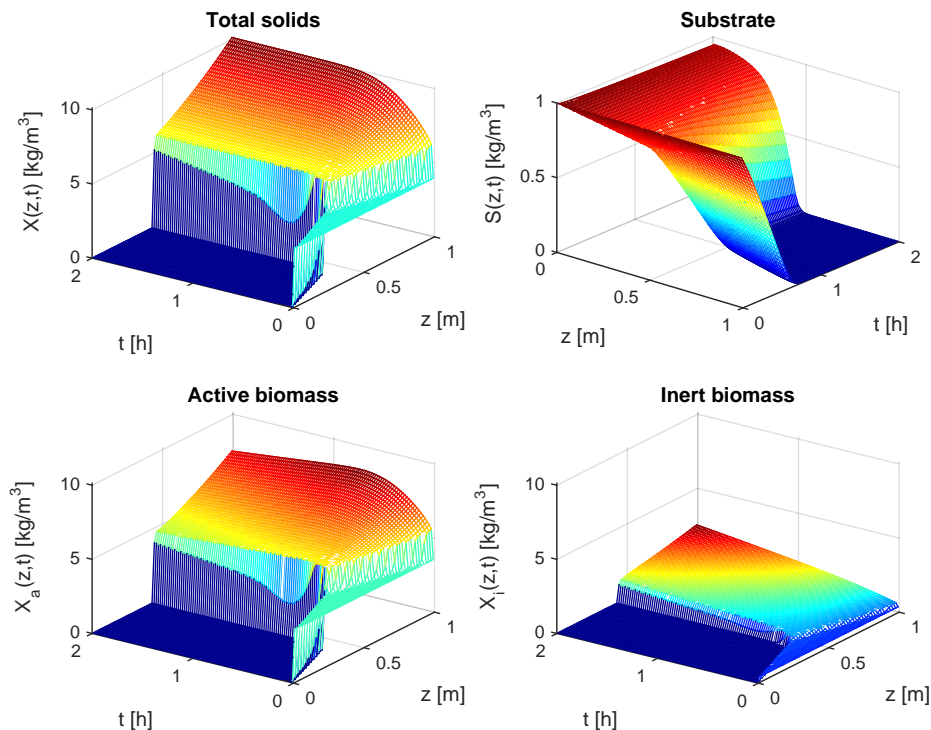


Figure 1: Simulation of reactive settling of an initially homogeneous suspension: (top left) total biomass (solids) concentration X , showing formation of a sediment with downwards-increasing concentration and slowly increasing sludge blanket, (top right) corresponding substrate concentration S , showing the consumption of substrate within the sediment, (bottom left) concentration X_a of active biomass, whose total amount slowly decreases in time, and (bottom right) concentration X_i of inert biomass, whose total amount increases in time.

- R. Bürger, S. Diehl, S. Farås, I. Nopens, and E. Torfs. A consistent modelling methodology for secondary settling tanks: a reliable numerical method. *Water Sci. Tech.*, 68:192–208, 2013.
- R. Bürger, S. Diehl, and I. Nopens. A consistent modelling methodology for secondary settling tanks in wastewater treatment. *Water Res.*, 45(6):2247–2260, 2011.
- R. Bürger, K.H. Karlsen, and J.D. Towers. A model of continuous sedimentation of flocculated suspensions in clarifier-thickener units. *SIAM J. Appl. Math.*, 65:882–940, 2005.
- A. A. Kazmi and H. Furumai. Field investigations on reactive settling in an intermittent aeration sequencing batch reactor activated sludge process. *Water Sci. Tech.*, 41(1):127–135, 2000a.
- A. A. Kazmi and N. Furumai. A simple settling model for batch activated sludge process. *Water Sci. Tech.*, 42(3-4):9–16, 2000b.
- J. Keller and Z. Yuan. Combined hydraulic and biological modelling and full-scale validation of SBR process. *Water Sci. Tech.*, 45(6):219–228, 2002.
- T. Maruejols, P. A. Vanrolleghem, G. Pelletier, and P. Lessard. A phenomenological retention tank model using settling velocity distributions. *Water Res.*, 46(20):6857–6867, 2012.

PARAMETER FITTING: WHICH ALGORITHM TO CHOOSE ?

Benoit Celse*, J. Becker, D. Sinoquet and V. Costa
 IFPEN, Lyon Establishment – Rond Point de l’Echangeur de Solaize
 BP 3 – 69360 Solaize - France

Optimization algorithms, Derivative Free Optimization fit, nonlinear model, Hydrocracking, kinetic model

Mackie 2015, Paper format, Style template files, Word, .pdf files.

Introduction

Hydrocracking (HCK) is one of the most versatile petroleum refining processes. It usually converts a heavy, low quality feedstock (VGO: Vacuum Gas Oil) into lighter, valuable transportation fuels, contributing significantly to the overall profitability of the refinery [1]. A robust kinetic model allows the optimal process design and operating conditions to be chosen to maximize the desired cuts and product characteristics. Hydrocracking of VGO residue performed in a two-step process: 1) a hydrotreatment step in the first reactor, which serves mainly to remove nitrogen and sulfur from the feed; 2) a hydrocracking step in the second reactor, which performs the main hydrocracking reactions on a zeolite-type catalyst. A kinetic model is defined by its structure and its parameters, which are estimated from collected data. The main difficulty is the parameter fit on real data. The aim of this paper is to compare several optimization algorithms on a continuous lumping model of the hydrocracking step. It is structured as follows:

- Case study description,
- Description of the chosen optimization algorithms,
- Results.

Case study: hydrocracking

The experimental runs presented in this study were performed in a pilot plant at IFP Energies Nouvelles, Solaize, France. The hydrocracking step was performed on a commercial zeolite cracking catalyst. The plant consists of a number of fixed beds, up-flow reactors, designed to mirror the operating conditions in industrial hydrocracking units. A series of mass balances with different operating conditions is thus taken from each experimental run. Each mass balance corresponds to a single experimental point.

Analyses were performed on the feedstocks, the liquid and gaseous effluents. The most relevant measurements in this study were the feed sulfur and nitrogen contents, the partial pressures of NH_3 , H_2S , and H_2 gasses, as well as the simulated distillation (SIMDIS).

A calibration database, consisting of 29 mass balances, was compiled. This database was used for the identification of the empirical parameters in a continuous lumping model originally developed for the first reactor but extended to the second one [2]. The range of the main operating conditions, temperature and liquid hourly space velocity (LHSV) is classical: $T \in [370; 400^\circ\text{C}]$, $\text{LHSV} \in [0.5; 3 \text{ h}^{-1}]$. The conversion of the 370°C fraction (X370+) is between 50 to 90%w/w.

Optimization method tested

The parameter fit problem is formulated as the following least-square minimization problem

$$\min_{l \leq x \leq u} \sum_{i=1}^{N_d} \left(\frac{m_i(x) - d_i}{\sigma_i} \right)^2 \quad (1)$$

with

- x , vector of model parameters to be tuned,
- l, u , lower and upper bounds of x ,
- N_d , size of experimental data,
- $m_i(x) \in \mathbb{R}^{N_d}$, vector of simulated data to be compared with experimental data,
- $d_i \in \mathbb{R}^{N_d}$, vector of experimental data to be fit,
- σ_i , weights modeling the measure uncertainties.

This optimization problem belongs to the class of derivative free or black-box optimization problems. Indeed, the simulator associated with the kinetic model computes the simulated data to be compared with experimental ones but does not provide the associated derivatives with respect to the parameters. Classical optimization methods, namely gradient based methods, require those derivatives: therefore, when they are not available as simulator outputs, they are usually estimated by finite difference scheme, which requires NP simulations for each gradient computation (NP being the number of parameters). The associated computational cost may thus become too high when the number of parameters increases. Moreover, the tuning of the perturbation step may be cumbersome in practice when numerical noise is present in the simulation.

An alternative is derivative free optimization methods which have become very popular with the emergence of adapted trust region methods [3,4]. SQA, developed by [5] at IFPEN, is a trust region method coupled with interpolating quadratic models. It has been applied successfully on several industrial applications [6,7] and has shown better performances than gradient based methods with finite difference estimate of derivatives. This method is an extension of the method proposed by Powell in [3] to nonlinear constrained problems. The main principle of the method is the following: in order to save simulations, quadratic interpolating models are used as surrogate of the simulator responses. These quadratic models are minimized and updated thanks to additional simulations performed along the optimization process iterations. For least-square formulations, the quadratic models approximate the residuals (differences between experimental and simulated data) instead of the single objective function, in order to improve the accuracy of the approximation.

In the following section, SQA method is compared to the Gauss-Newton method implemented in Port library (DN2FB method) [8]. For this latter method, the Jacobian matrix (derivatives of simulated data with respect to parameters) is estimated by finite differences.

Results

The performances of the SQA and Port algorithms for the Hydrocracking model parameter identification have been compared. The continuous lumping model requires a total of NP=28 experimental parameters to be identified. A target function, based on the yield structure (standard cuts: <150°C, 150-250°C, 250-370°C, >370°C and C1-C4 gas) is defined. The same target function and initial parameters were used for both algorithms.

The SSQ is decreased by an order of magnitude, from 1.7×10^9 to 4.1×10^8 by the Port algorithm and to 4.2×10^8 by the SQA algorithm. The evolution of the sum of square residuals with the number of function evaluations for the SQA and Port (DN2FB) algorithms are shown in figure 2. Both methods attain a minimum. The gradient base method (DN2FB) reached a minimum after around 240 function calls. The response-surface based method (SQA) reached a minimum after 190 function calls. The decrease of the SSQ is very gradual for the DN2FB algorithm. The SQA algorithm first constructs the interpolation of the response surface for a total of $2 \times NP + 1 = 57$ function calls. This is characterized by an exploration phase around the initial value of the SSQ. Once the response surface has been constructed, the algorithm rapidly descends towards the minimum (about 60 function calls). The baseline of the SSQ does not decrease significantly after this step. A number of oscillations can be observed, as the algorithm refines the search for the local minimum.

Both of the local optimization algorithms, DN2FB and SQA are found to converge to a local minimum with the same square residual. The trust-region method (SQA) shows better performance on the test case than the gradient based-method with finite difference approximation (DN2FB). Once the response surface has been constructed (i.e. exploration around initial point in Figure 1), the SQA algorithm rapidly attains the local minimum. The DN2FB algorithm decreases the residuals much more gradually. Furthermore, the parameter space is explored much more thoroughly by the SQA algorithm, which is illustrated by the large spikes in Figure 1. The finite difference algorithm perturbs only slightly the parameters around each iterate for gradient estimation. This feature makes SQA less likely to be caught in a local minimum.

Conclusion

This paper compares two optimization methods for fitting kinetic model parameters. In this example, the SQA method proves to be more efficient than classical gradient method.

The fact that two different sets of parameters yield to the same sum of square residuals suggests the presence of local minima. Adding chemical/physical *a-priori* information can help to constrain the system and to remove this under-determination.

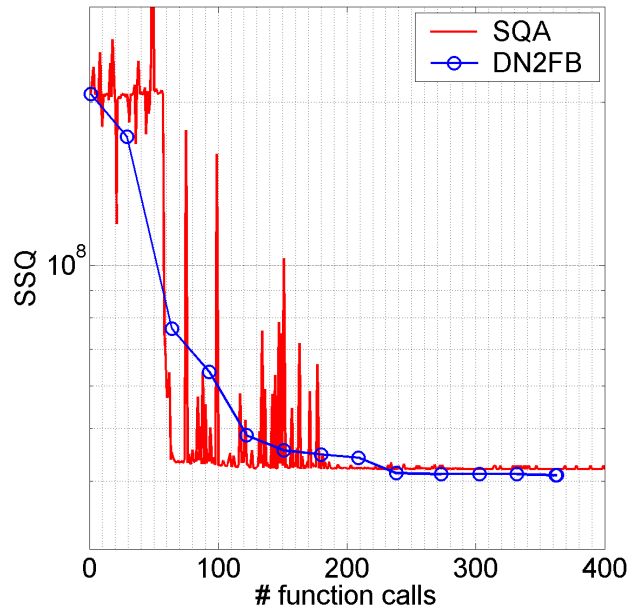


Figure 1 : Sum of Square Residuals (SSQ) with function evaluations for SQA and Port (DN₂FB) algorithms

Bibliography

- [1] N. Charon-Revellin, H. Dulot, C. López-García, and J. Jose, "Kinetic Modeling of Vacuum Gas Oil Hydrotreatment using a Molecular Reconstruction Approach," *Oil Gas Sci. Technol. – Rev. d'IFP Energies Nouv.*, vol. 66, no. 3, pp. 479–490, Oct. 2010.
- [2] P. J. Becker, B. Celse, D. Guillaume, H. Dulot, and V. Costa, "Hydrotreatment modeling for a variety of VGO feedstocks: A continuous lumping approach," *Fuel*, vol. 139, pp. 133–143, Jan. 2015.
- [3] M.J.D. Powell, "The NEWUOA software for unconstrained optimization", Centre for Mathematical Sciences, Cambridge: Department of Applied Mathematics and Theoretical Physics, 2006.
- [4] A. R. Conn, K. Scheinberg, and L. N. Vicente, "Introduction to Derivative-Free Optimization" , MPS-SIAM Series on Optimization, SIAM, Philadelphia, 2009.
- [5] H. Langouët, "Optimisation sans dérivées sous contraintes. Deux applications industrielles en ingénierie de réservoir et en calibration des moteurs", PhD thesis, Université de Nice-Sophia Antipolis, 2011.
- [6] G. Font, D. Sinoquet, H. Langouët, M. Castagné and S. Magand, "Derivative free optimization method and physical simulations coupled with statistical models for transient engine calibration", In 6th Conference "Design of Experiments (DoE) in Engine Development - Innovative Development Methods for Vehicle Engines" Berlin, Germany, May 23-24, 2011.
- [7] H. Langouët, F. Delbos, D. Sinoquet, and S. Da Veiga, "A derivative free optimization method for reservoir characterization inverse problem". In ECMOR European Conference on the Mathematics of Oil Recovery, 12th, Oxford, UK, 6-9 september 2010.
- [8] J.E. Dennis, D.M. Gay and , R.E. Welsch, "An Adaptive Nonlinear Least-Squares Algorithm", *Acm Trans. Math. Software*, Vol. 7, No. 3, 1981.

PROBING PORE BLOCKING EFFECTS ON MULTIPHASE REACTIONS AT THE PARTICLE LEVEL USING A DISCRETE MODEL

Guanghua Ye ^{a,b}, Xinggui Zhou ^{a,*}, Marc-Olivier Coppens ^b, Weikang Yuan ^a

^a State Key Laboratory of Chemical Engineering, East China University of Science and Technology, Shanghai 200237, China

^b Department of Chemical Engineering, University College London, London WC1E 7JE, UK
Email: G. Ye (gh_ye@mail.ecust.edu.cn); X. Zhou (xgzhou@ecust.edu.cn); M.-O. Coppens (m.coppens@ucl.ac.uk); W. Yuan (wkyuan@ecust.edu.cn)

1. Introduction

Multiphase catalytic reactions, including hydrocracking and hydrodesulphurization, are of great importance in the chemical industry. Despite their significance, modeling remains a very complicated process. The overall process consists of diffusion, viscous flow, reaction, multilayer adsorption, capillary condensation, and pore blocking; besides, it involves vapour, liquid, and solid phases. Hence, simulating the whole process is still challenging, in particular how pore blocking affects multiphase reactions.

Pore blocking phenomenon is well studied in adsorption/desorption processes at the particle level. How pore blocking affects the sorption hysteresis has been investigated in numerous works; however, how pore blocking affects multiphase reactions has not been reported up to now, although a similar reaction hysteresis phenomenon has been observed in numerous experiments. In multiphase reaction catalysts, some liquid-filled pores, which are supposed to empty at low pressure or high temperature, can be blocked by the adjacent liquid-filled pores during the evaporation. This is the pore blocking phenomenon. Pore blocking can change the wetting level of catalysts, and subsequently influence the apparent reaction rate, because the reaction rate in vapor phase can be different from the one in liquid phase. To study the pore blocking effects, a proper model should be established.

We build a discrete model to probe pore blocking effects on reaction hysteresis, because only the discrete models can include pore blocking. The proposed model can describe coupled mass transfer, reaction, phase transition, and pore blocking in internally and partially wetted catalysts. Benzene hydrogenation into cyclohexane is taken as the reaction system because of its industrial and academic significance.

2. Discrete Model

2.1 Pore Network

The pore network is generated by occupying an area with uniformly distributed nodes, and then inscribing cylindrical pores between two adjacent nodes according to the connectivity. The amount of nodes increases until obtaining consistent simulation results [1, 2]. The radius of the pores is randomly assigned, following a Gaussian distribution.

2.2 Phase Transition and Pore Blocking

Capillary condensation occurs in narrow pores during the multiphase reaction, resulting in the internally and partially wetted catalysts. The phase state in each pore can be predicted by using the critical pore radius of capillary condensation (r_c), which is calculated by Eq. (1).

$$r_c = t + r_k \quad (1)$$

* Corresponding author. Tel.: +86-21-64253509. Fax.: +86-21-64253528. Email address: xgzhou@ecust.edu.cn

where t is layer thickness obtained from Halsey equation and r_k is Kelvin radius. The pores are vapor-filled when their radius is larger than r_c during the condensation, but not all the pores with $r > r_c$ are vapor-filled because of the pore blocking effects during the evaporation. These blocked pores are identified by using the extended Hoshen-Kopelman algorithm [3].

2.3 Mass Transfer and Reaction

In individual pores, the continuity equation involving diffusion and reaction is given by

$$D_{i,eff} \frac{d^2 C_i}{dl_n^2} - R_i = 0 \quad (2)$$

In the inner nodes, there is no adsorption and chemical reaction because the node volume is assumed to be zero. Therefore, Kirchhoff's law is satisfied, i.e.,

$$\sum_{n=1}^{n=Z} \pi r_n^2 J_n = - \sum_{n=1}^{n=Z} \pi r_n^2 D_{i,eff} \frac{dC_i}{dl_n} = 0 \quad (3)$$

As to the boundary nodes, the boundary condition is given as follows

$$C_i = C_0 \quad (4)$$

2.4 Monte Carlo Simulation

The simulations are carried out by using a Monte Carlo method, details of which can be found elsewhere [1, 2].

3. Results and Discussion

3.1 Validation with Experiment

The proposed discrete model is validated by comparing with the continuum model [4] and experiments in the literature [4], as shown in Fig.1. The effectiveness factors calculated by the discrete model are much closer to experimental ones, and therefore better than the ones predicted by the continuum model. The continuum model cannot include pore blocking, which could be the reason why the discrete model is better.

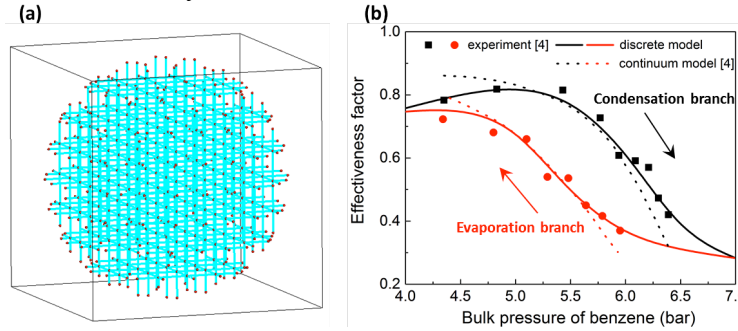


Figure 1. (a): An illustration of constructed spherical pore network, (b): comparison of the experimental effectiveness factors [4] with the predicted ones by the continuum model [4] and the proposed discrete model. (The arrows indicate the direction of bulk pressure change of benzene.)

3.2 Pore Blocking Effects on Reaction Hysteresis

The proportion of reaction hysteresis loop area caused by pore blocking (f_{PB}) is proposed as the evaluation criterion to quantify the effects of pore blocking on reaction hysteresis, as illustrated in Fig. 2. Pore blocking affects reaction hysteresis largely, indicating that pore blocking must be included in the models when simulating multiphase reactions in porous catalysts.

The relationships between pore blocking effects and pore network parameters are also investigated, as shown in Fig. 3. The f_{PB} increases significantly with the decrease of

connectivity and the increase of standard deviation, indicating that pore blocking effects are strengthened with poorly-connected pore network or wide distribution of pore size; the f_{PB} is not sensitive to the volume-averaged pore size.

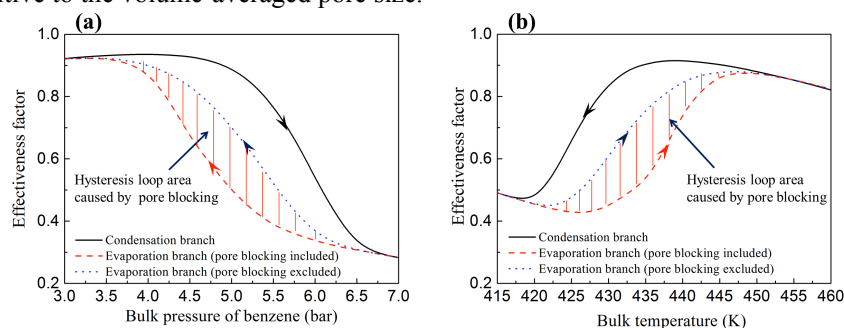


Figure 2. The illustrations of the hysteresis loop area caused by the pore blocking effects (f_{PB}). (a): the effectiveness factor as a function of the bulk pressure of benzene, (b): the effectiveness factor as a function of the bulk temperature. (The arrows indicate the direction of bulk pressure change of benzene or bulk temperature change.)

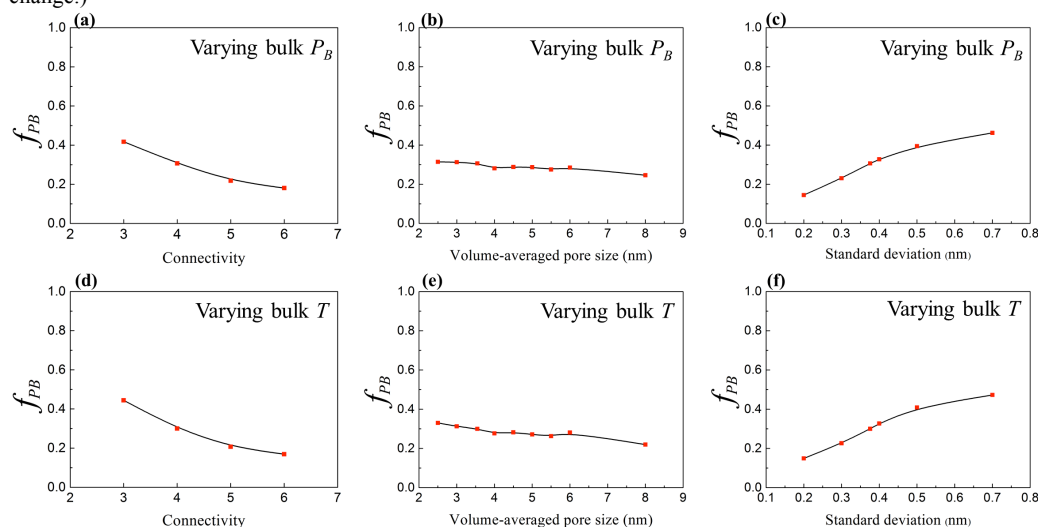


Figure 3. The relationships between f_{PB} and pore network parameters. (a)-(c): based on the reaction hysteresis caused by varying bulk pressure of benzene; (d)-(f): based on the reaction hysteresis caused by varying bulk temperature.

4. Conclusion

A discrete model, which combines mass transfer, reaction, capillary condensation, and pore blocking, is proposed to probe the pore blocking effects on multiphase reaction hysteresis. The model is solved by using the Monte Carlo method, and validated by comparing with the experiment. The simulation results show that pore blocking affects reaction hysteresis significantly, and these effects can even be strengthened when the pore network connection is poor or the distribution of pore size is wide.

References

1. J. Wood, L. F. Gladden. *Chem. Eng. Sci.*, 2002, **57**, 3033-3045.
2. J. Wood, L. F. Gladden, F. J. Keil. *Chem. Eng. Sci.*, 2002, **57**, 3047-3059.
3. A. Al-Futaisi, T. W. Patzek. *Physica A.*, 2003, **321**, 665-678.
4. Z. Zhou, Z. Cheng, Z. Li, W. Yuan. *Chem. Eng. Sci.*, 2004, **59**, 4305-4311.

A comparative study of Optimization Algorithms for a Cellular Automata model

Saurajyoti Kar^a, Saibal Majumder^b, Denis Constaes^c, Tandra Pal^{b*}, Abhishek Dutta^d

^a Department of Water Technology & Environmental Engineering, University of Chemistry and Technology, 166 28 Prague 6, Czech Republic

^b Department of Computer Science & Engineering, National Institute of Technology, Durgapur 713209, West Bengal, India

^c Department of Mathematical Analysis, Ghent University, Galglaan 2, B-9000 Ghent, Belgium

^d Departement Materiaalkunde, KU Leuven, Kasteelpark Arenberg 44 bus 2450, B-3001 Heverlee-Leuven, Belgium

Simulation of (bio)-chemical processes have always been an active field of interest and innovation, inspiring researchers from various specializations to use different approaches for optimal design and control. Increased availability of computational resources have facilitated such research and opened new dimensions for process optimization. Representation of (bio)-chemical systems at various levels of details give different insights. Although an equation-based system provides an overall characteristic of the system, it usually overlooks the effect of the intrinsic parameters that influence the behaviour of the system. On the other hand, a rule-based system such as Cellular automata (CA) is often considered as an alternative approach and complements the existing mathematical basis. The state variables are always discrete but the numbers of degrees of freedom are large (Wolfram, 1984). Since CA consists of space and time, it is essentially equivalent to a dynamical system that is discrete in both space and time. The evolution of such a discrete system is governed by certain updating rules rather than differential equations.

Previous study on a generalized CA model (Dutta et al., 2015) possessed the flexibility to model reaction interactions of all possible two-agent combinations on both reactant and product side. In Kar et al. (2014) the authors have optimized the probability parameters using a widely used multi-objective genetic algorithm (MOGA) called NSGA-II. However, due to high sensitivity of these parameters, the authors have concluded that further studies need to be carried out in order to find a suitable algorithm regarding the optimality of the solution (set of the probability parameter values) as well as the time of computation. For this purpose, along with NSGA-II, three more recently developed and popular optimization algorithms based on Genetic Algorithm (GA) called AbYSS (Nebro et al., 2008), and MOEA/D (Zhang et al., 2007) have been considered for investigation in this study using various performance measuring parameters. Ideally, an optimal solution that is insensitive to these parameter variations is desirable. The goal of a robust optimization is to optimize the performance and at the same time minimize its sensitivity to parameter variations (Deb et al., 2006). If variation in the parameter or variable space is unavoidable, search for robust solutions (Bui et al., 2012) is required. Again, this perturbation affects the degree of optimality of the solutions. In this work, similar to the previous work, the same CA model representing a (bio)-chemical kinetic reaction system is used as the basis to find a robust optimization algorithm based on GA.

References

- A. Dutta, S. Kar, A. Apte, I. Nopens and D. Constaes, "A generalized Cellular Automata approach to modelling first order enzyme kinetic", *Sadhana*, vol. 40, no. 2, 2015.
- A. J. Nebro, F. Luna, E. Alba, B. Dorronsoro, J. J. Durillo, and A. Beham, "AbYSS: Adapting scatter search to multiobjective optimization", *IEEE Tans. Evol. Comput.*, vol. 12, no. 4, pp. 439-453, 2008.
- K. Deb and H. Gupta, "Introducing robustness in multi-objective optimization," *Evolutionary Computation*, vol. 14, no. 4, pp. 463 – 494, 2006.
- L. T. Bui, H. A. Abbass, M. Barlow, and A. Bender, "Robustness against the decision-maker's attitude to risk in problems with conflicting objectives," *Evolutionary Computation*, *IEEE Transactions on*, vol. 16, no. 1, pp. 1 – 19, 2012.
- Q. Zhang, H. Li, "MOEA/D: A multiobjective Evolutionary algorithm based on decomposition", vol. 11, no. 6, pp. 712 – 731, 2007.
- S. Kar, K. Nag, A. Dutta, D. Constaes and T. Pal, "An improved cellular automata model of enzyme kinetics based on genetic algorithm", *Chemical Engineering Science*, vol. 110, pp. 105 – 118, 2014.
- S. Wolfram, "Cellular Automata as models of complexity", *Nature*, vol. 311, pp. 419 – 424, 1984.

The Sectional Quadrature Method of Moments (SQMOM): An Application to Liquid-liquid Extraction Columns

Samer Alzyod^b, Menwer Attarakih^{a,b}, Abhishek Dutta^{c,d}, Hans-Jörg Bart^b

^aFaculty of Engineering & Technology, Chem. Eng. Dept., The University of Jordan, 11942-Amman, Jordan

^bChair of Separation Sciences, The University of Kaiserslautern, 67637- Kaiserslautern, Germany

^cDepartement Materiaalkunde, KU Leuven, Kasteelpark Arenberg 44 bus 2450, B-3001 Heverlee-Leuven, Belgium

^dFaculteit Industriële Ingenieurswetenschappen, KU Leuven, Campus Groep T Leuven, Andreas Vesaliusstraat 13, Leuven, Belgium

Abstract

During the last few decades, the Droplet Population Balance Model (DPBM) development constituted a comprehensive mathematical framework for modeling and simulation of the discrete and multiphase flow problems. The DPBM takes into account different physical and chemical phenomena that lead to the evolution of the discrete particulate phase. These phenomena include droplet growth, breakage and coalescence, which results in a coupled hydrodynamics and inter-phase mass transfer. This allows the prediction of droplet size distribution (DSD), holdup and mass transfer along the column height and provides more realistic information about flooding conditions. The DPBM is a geometrical dependent transport equation with highly nonlinear source terms and hence it has no general analytical solution. As a result of this, accurate and robust numerical algorithms with low computational cost are needed. In this contribution, the Sectional Quadrature Method of Moments (SQMOM) [1] is implemented and extended in the physical space with a 1D finite volume scheme for grid refinement with flux vector splitting technique. The resulting discrete Ordinary Differential Equation (ODE) system is solved using the standard MATLAB ODE solvers. The required quadrature nodes and weights are calculated based on the analytical solution (for two unequal quadrature points) derived by Attarakih et al. [1]. The SQMOM performance has been tested at two different levels namely: Numerical and experimental levels. At the numerical level, the SQMOM results are compared with the PPBLAB detailed population balance solver, which is based on the extended fixed pivot technique [2]. At the experimental level, the SQMOM is validated using the available steady state experimental data for two different EFCE chemical test systems: Toluene-acetone-water and butyl acetate-acetone-water. The only adjusted model parameter is the pre-exponential parameter in the droplet coalescence model. Figure (1) shows a comparison between the simulated and experimental [3] mass transfer profiles in a Kühni extraction column at two different rotational speeds: 150 and 200 rpm respectively.

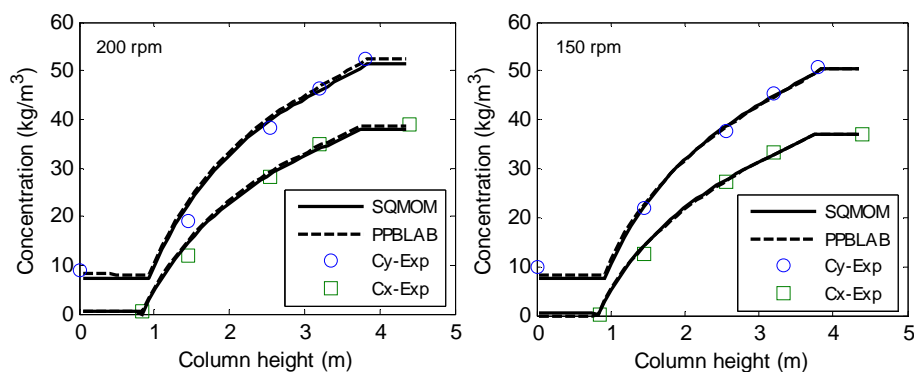


Figure (1): Comparison between simulated and experimental [3] steady state mass transfer profiles responses in a Kühni extraction column at two different rotational speeds: 150 and 200 rpm.

References:

- [1] Menwer M. Attarakih, Christian Drumm, Hans-Jörg Bart . Solution of the population balance equation using the sectional Quadrature Method of Moments (SQMOM). *Chem. Eng. Sci.*, 64, 742--752.
- [2] M. Attarakih, M. Hlawitschka, M. Abu-Khader, S. Al-Zyod, H-J. Bart, CFD-PopulationBalance Modelling and Simulation of Coupled Hydrodynamics and Mass Transfer in Liquid Extraction Columns, *Appl. Math. Modelling* (2015), doi: [dx.doi.org/10.1016/j.apm.2015.04.006](https://doi.org/10.1016/j.apm.2015.04.006)
- [2] Garthe, D., (2006), Fluidynamics and mass transfer of single particles and swarms of particles in extraction columns, Published Ph-D thesis, TechnischeUniversitstMünchen, Germany.

Slow Manifolds identification for dimensionality reduction of chemical kinetics: a computational route

Alessandro Ceccato^{*}, Paolo Nicolini^{**}, Diego Frezzato^{*}

^{*} Department of Chemical Sciences, University of Padova,
Via Marzolo 1, I-35131, Padova, Italy. E-mail: diego.frezzato@unipd.it

^{**} Department of Control Engineering – K335, Faculty of Electrical Engineering, Czech Technical University in Prague, Karlovo náměstí 13, 121 35, Prague 2, Czech Republic. E-mail: nicolpao@fel.cvut.cz

It is known that trajectories of a reacting system, when represented in the concentrations space, may rapidly approach hypersurfaces, named Slow Manifolds (SMs), and remain in their neighbourhood up to equilibrium. By considering that the dimensionality of the SMs may be much smaller than that of the whole space, such mutual correlation between species concentrations on the “slow tail” of the system evolution can be exploited to achieve a simplification (in the sense of reduction of dynamical variables) in the description of the kinetics.

In recent communications [1, 2] we have proposed a definition of SM which spontaneously “emerges” from the intrinsic properties of a universal quadratic format into which the system of Ordinary Differential Equations (ODEs) of any mass-action-based kinetic scheme (with N species and M elementary steps/reactions) can be transformed, regardless of the degree of non-linearity.

The global transformation consists in turning from the set of volumetric concentrations of the species, x_j for $j=1, \dots, N$, to the following $N \times M$ rate-variables which are mutually correlated by non-linear constraints (such that only N of them are independent),

$$V_{jm, j'm'}(\mathbf{x}) = \left[v_{P_j}^{(m')} - v_{R_j}^{(m')} \right] \left[\delta_{j, j'} - v_{R_j}^{(m)} \right] k_m \prod_i x_i^{v_{R_i}^{(m)} - \delta_{i, j'}} \quad (1)$$

where $v_{R_j}^{(m)}$ and $v_{P_j}^{(m)}$ are the stoichiometric coefficients of species j as reactant and product, respectively, in the m -th elementary step/reaction, and k_m is the kinetic constant. By introducing the cumulative index $Q = (j, m)$ for the pair species-step, the evolution of these rates is specified by the quadratic ODEs system

$$\dot{V}_{QQ'} = -V_{QQ'} \sum_{Q''} V_{Q''Q'} \quad (2)$$

A backward transformation $\mathbf{V}(\mathbf{x}) \rightarrow \mathbf{x}$ then allows one to retrieve the actual state of the system in the concentrations space.

In ref. [2] we have shown that the following rates

$$z_Q(\mathbf{x}) := \sum_Q V_{QQ}(\mathbf{x}) \quad (3)$$

and their time-derivatives $z_Q^{(n)}(\mathbf{x}(t)) = d^n z_Q(\mathbf{x}(t)) / dt^n$ are strictly related to the SM feature. Namely, by means of phenomenological inspections we formulated the conjecture that a “typical” trajectory for a “typical” kinetic scheme enters an “Attractiveness Region” (AR) which includes the SM. We then defined the SM as that hypersurface where $z_Q^{(n)}(\mathbf{x}) = 0$, for all Q , as $n \rightarrow \infty$ (while the stronger and exact condition $z_Q^{(n \geq 1)}(\mathbf{x}) = 0$ holds on the equilibrium manifold). In practice, it would suffice to search for local minima of the Euclidean norm $\|\mathbf{z}^{(n)}(\mathbf{x})\|$ along relevant directions (to be defined), or to find points where the values of such norm fall below a given threshold (to be fixed). Apart from ambiguities to be removed, the crucial problem lies in the fact that “spurious solutions” (possibly very many) must be excluded *a posteriori* by checking if the candidate points belong or not the AR. Unfortunately, a simple and direct way to guess the dimensionality, the location and the boundaries of the AR in the whole concentrations space is still missing. Also considering that the computation of the derivatives $z_Q^{(n)}(\mathbf{x})$ becomes cumbersome (although a recursive scheme can be employed [1]) and possibly inaccurate as the order n increases, some low-computational-cost route is required. The idea is to devise a strategy which yields only an acceptable approximation of the SM but with a lower computational effort.

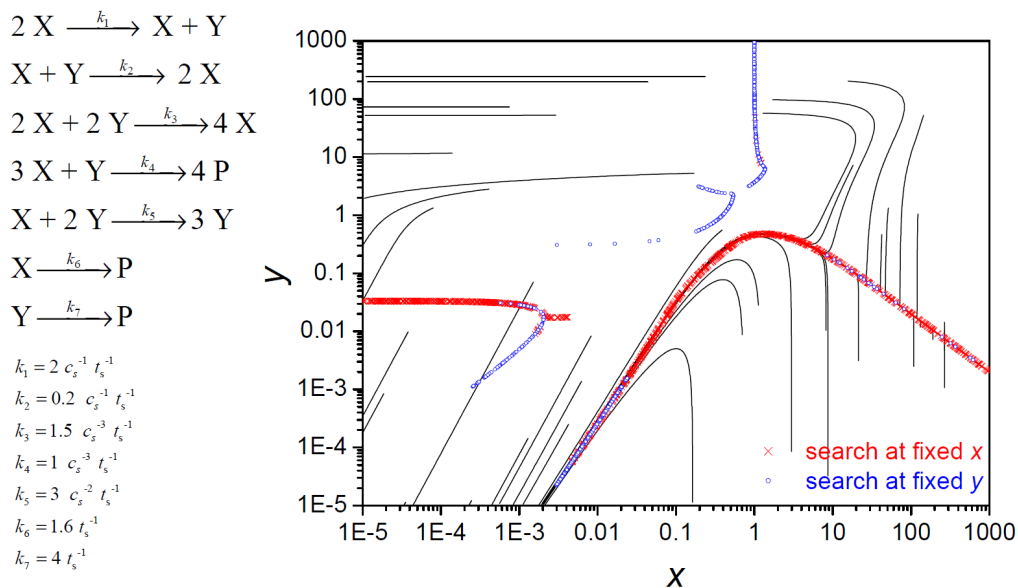
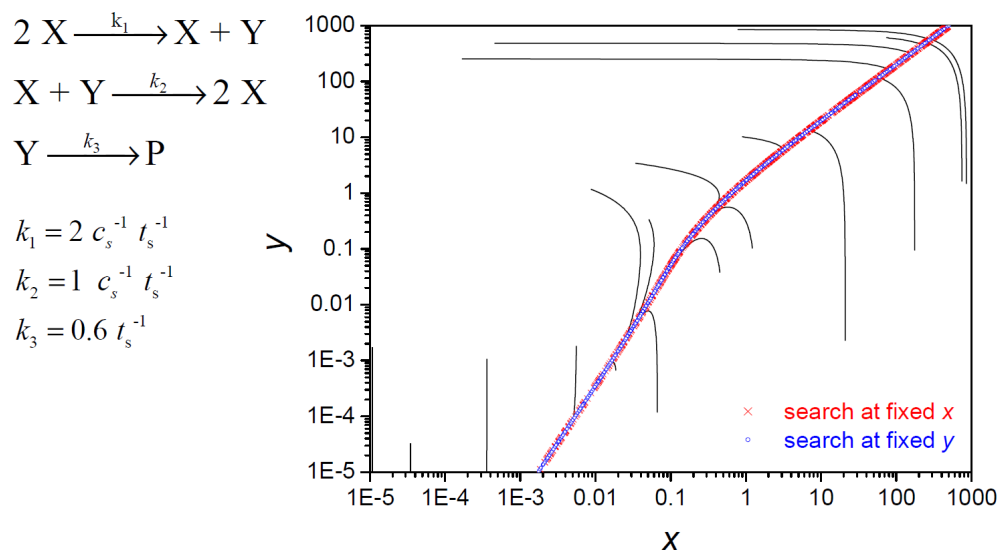
Our work in such a direction is still in progress. Here we only sketch out the essential traits to give the qualitative picture behind the formal treatment. The starting point is to note that Eqs (2) and (3) yield directly the following system of ODEs

$$\dot{\mathbf{z}} = -\mathbf{V} \mathbf{z} \quad (4)$$

which appears in a pseudo-linear format, where the term “pseudo” recalls that the matrix \mathbf{V} is point-dependent. Suppose that the dynamics in the concentrations space, $\mathbf{x}(t)$, are such that the vector $\mathbf{z}(t) \equiv \mathbf{z}(\mathbf{x}(t))$, in the extended space, is brought to be confined into a subspace of eigenvectors of \mathbf{V} . Then Eq. (4) states that $\dot{\mathbf{z}}$, and hence \mathbf{z} at the next step of the trajectory, is still confined into such a subspace. Now consider that the components of \mathbf{z} are nothing but the rates of evolution of the matrix \mathbf{V} through Eq. (2), and hence, ultimately, they control the evolution of its eigenvalues/eigenvectors. Thus, the condition of small Euclidean norm $\|\mathbf{z}\|$ enforces the confinement of \mathbf{z} itself on the subspace of the “slow” eigenvectors of \mathbf{V} . These two facts, taken together, lead to invoke the smallness of the norm $\|\dot{\mathbf{z}}\|$. By considering the mapping between matrix \mathbf{V} and state-point \mathbf{x} via backward transformation [1], the guess is that points \mathbf{x} which fall in the neighbourhood of the SM could be found by operating with these two norms. As a whole, a tentative recipe is to find points where $\|\mathbf{z}\|$ takes small values and then, starting *from* each of these points, find the closest one where $\|\dot{\mathbf{z}}\|$ has a minimum. As side-note, consider that condition of smallness of $\|\dot{\mathbf{z}}\|$ resembles a quasi-stationary-state approximation applied to the evolution of the z_Q functions in the ODEs of Eq. (4).

We have tested this idea on some simple kinetic schemes, namely the benchmark case studied by Fraser in ref. [3] (Lindemann-Hinshelwood mechanism) and a fictitious scheme where elementary

steps up to the fourth order are added. The two-step minimization of norms $\|\mathbf{z}(\mathbf{x})\|$ and $\|\dot{\mathbf{z}}(\mathbf{x})\|$ has been made by selecting initial points $\mathbf{x}=(x, y)$ at random within a box spanning 8 orders of magnitude in both directions, and then moving either at fixed x or at fixed y . Powell's method has been employed for the minimization. The results are displayed in the figure. Solid lines are trajectories of the reacting system, while the coloured marks are the outcomes of the algorithm.



Kinetic schemes for model calculations: the Lindemann-Hinshelwood mechanism with Fraser's parameterization (top) and a fictitious fourth-order mechanism (bottom). The panels show two-dimensional projections on the reactants concentrations subspace. Solid lines are trajectories from points generated at random; coloured marks are candidate points (expected to fall close to the perceived SM, but to be "screened") which are produced by the route here proposed. Volumetric concentrations and time are expressed in arbitrary units c_s and t_s .

We see that for the Lindemann-Hinshelwood scheme, the produced points fall on the *perceived* SM. For the second scheme, the majority of the produced points are very close to the perceived SM, but some spurious solutions also appear. These spurious solutions should be automatically recognized (with acceptable likelihood) and filtered-out *a posteriori* in a proper way to be conceived. Both panels display 1000 produced points. Generation of the whole set of points for the second scheme took about 5 seconds on a PC.

These illustrative tests encourage us to pursue such a route, and check if the same idea works well even with kinetic schemes of higher complexity. The work on the theoretical foundation of such a kind of low-order strategy is currently underway.

References

- [1] P. Nicolini and D. Frezzato *J. Chem. Phys.* **138**, 204101 (2013)
- [2] P. Nicolini and D. Frezzato *J. Chem. Phys.* **138**, 204102 (2013)
- [3] S. J. Fraser, *J. Chem. Phys.* **88**, 4732 (1988)

Acknowledgements: This work is funded by the University of Padova – Progetti di Ricerca di Ateneo 2013 (PRAT2013).

Traits of regularity in stochastic chemical kinetics: analogy with the “Slow Manifolds” feature in deterministic kinetics

Sara Dal Cengio^{*,§}, Alessandro Ceccato^{*}, Paolo Nicolini^{**}, Diego Frezzato^{*}

^{*} *Department of Chemical Sciences, University of Padova,
Via Marzolo 1, I-35131, Padova, Italy. E-mail: diego.frezzato@unipd.it*

[§] *Presently a scholar at “Corso di Laurea Magistrale in Fisica dei Sistemi Complessi”,
Department of Physics, University of Torino, Italy*

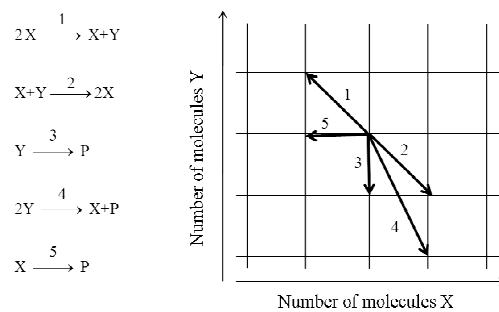
^{**} *Department of Control Engineering – K335, Faculty of Electrical Engineering, Czech Technical
University in Prague, Karlovo náměstí 13, 121 35, Prague 2, Czech Republic. E-mail:
nicolpao@fel.cvut.cz*

For reactions involving a low number of particles (like processes occurring in micro-reactors or in the cellular membranes and interior), the deterministic mass-action law which is suited for macroscopic size systems has to be abandoned in favour of a stochastic description of the kinetics [1-3]. In such a context, each elementary reaction, or elementary step of a mechanism, is associated to the so-called “propensity function” which quantifies, once multiplied by a time-step δt , the probability that the given reaction occurs. Under the assumption that the propensity functions can be indeed specified for any of the elementary processes, the progression of the system towards equilibrium, at fixed temperature and volume, is expressed by the evolution of the conditioned probability $P(\mathbf{x}, t | \mathbf{x}_0, 0)$ of finding the system in the state \mathbf{x} at time t (\mathbf{x} is an array which collects the actual number of particles of each species) if it was initially observed in the state \mathbf{x}_0 . The evolution of such probability is governed by the partial-derivatives equation termed as Chemical Master Equation (CME), whose solution is known to be a quite hard task [1-3]. Considering such a technical difficulty, together with the need to handle kinetic schemes with very many species involved (e.g., in biochemical networks), one aims to devise likely routes to reduce the complexity of the mathematical modelling of stochastic reactions. This means to work out some reduced but accurate description (i.e., with few relevant dynamic variables) able to catch the essential traits of the whole system with lower computational cost and a more transparent level of representation. Several efforts are currently devoted to this aim, especially from the scientific community working in the context of complex biochemical networks. Just to mention one recent communication on methodological issues, in ref. [4] the authors propose a route to simplify the CME by applying concepts borrowed from the Information Theory.

In this communication we illustrate that the reduction of stochastic chemical kinetics could be faced by considering that a feature known at the deterministic level, namely the presence of the so-called Slow Manifolds (SMs), is somehow found even for the stochastic counterpart. In deterministic kinetics, where volumetric concentrations are the dynamic variables, a SM is a subspace (of the whole concentrations space) in whose neighbourhood the slow tail of the evolution towards

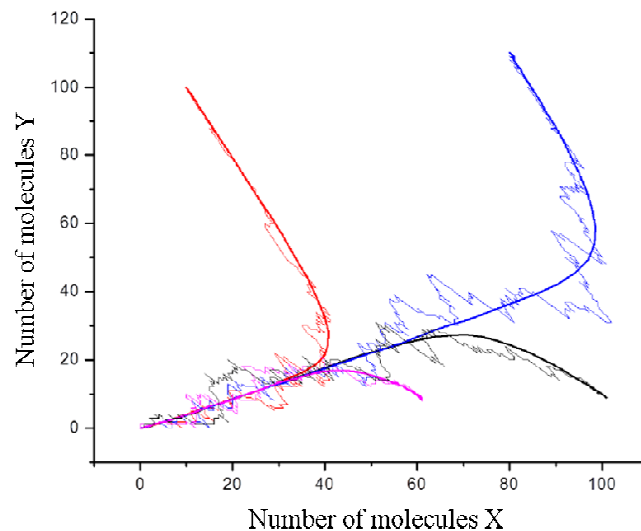
equilibrium takes place. The mutual correlation between species concentrations held on the SM allows one, in principle, to achieve the desired reduction of the system description. By means of simulations performed by us on simple kinetic schemes, it turned out that 1) an analogous of the SM indeed exists for the stochastic counterpart, and 2) a suitable state-dependent descriptor allows one to localize the SM in the space of the numbers of molecules. Simulations have been performed for several schemes by means of the basic Gillespie's stochastic algorithm [1-3] which allows the generation of an ensemble of trajectories $\mathbf{x}(t)$ as alternative to solve directly the CME. By plotting together several trajectories it is possible to note that, on average, they indeed tend to bundle on a common subspace.

Here we illustrate such behaviour for the following scheme:



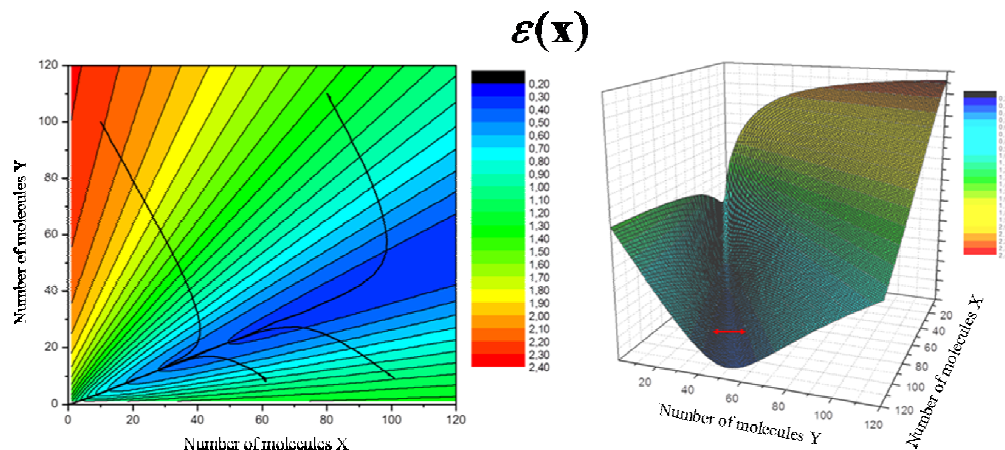
Model kinetic scheme with two reactants (X and Y) and a product (P) irreversibly formed. The coefficients which enter the expressions of the propensity functions according to notation of ref. [1] have been set to $c_1=2$, $c_2=1$, $c_3=20$, $c_4=3$, $c_5=10$ (they are meant to be expressed in units t_s^{-1} where t_s is a time unit). The arrows in the right panel show the variations of the reactants particle numbers when the possible reactions occur.

The figure below shows some stochastic trajectories. The underlying smoothed lines are average trajectories obtained from an ensemble of trajectories all departing from the same points. One may see that a SM-like phenomenology emerges when considering the average trajectories.



Examples of stochastic and average trajectories (beginning from the same starting points), projected on the reactants plane, for the kinetic scheme given above.

As a step beyond, we have considered a set of candidate descriptors to be employed to localize such a SM in the space of the numbers of molecules. Presently, the best descriptor, $\mathcal{E}(\mathbf{x})$ here below, turned out to be the simple Euclidean norm of the “weighted average move” that the system can take from the actual state (where the weights are provided by the normalized propensity functions). Namely, the figures below show that some features of the $\mathcal{E}(\mathbf{x})$ landscape (its high-curvature “groove”) may allow the delimitation of the perceived SM.



Contour plot (left) and landscape (right) of the dimensionless descriptor $\mathcal{E}(\mathbf{x})$ for the kinetic scheme given above. The immaterial product species is ignored in this representation.

These preliminary inspections, mainly of phenomenological kind and targeted to stimulate the scientific community active in this field of research, suggest that a proper formal definition and construction of Slow Manifolds in the context of stochastic chemical kinetics might be of use to achieve a simplification of the kinetics description itself.

References

- [1] D. T. Gillespie, A. Hellander, L. R. Petzold, *J. Chem. Phys.* **138**, 170901 (2013)
- [2] D. T. Gillespie, *Annu. Rev. Phys. Chem.* **58**, 35 (2007)
- [3] D. T. Gillespie, *J. Phys. Chem.* **81**, 2340 (1977)
- [4] P. Smadbeck, Y. N. Kaznessis, *Proc. Natl. Acad. Sci. USA* **110**, 14261 (2013)
- [5] R. T. Skodje, M. J. Davis, *J. Phys. Chem. A* **105**, 10356 (2001)

Acknowledgements: This work is funded by the University of Padova – Progetti di Ricerca di Ateneo 2013 (PRAT2013).

Mathematical description of the kinetics of photochemical reactions

Katalin Ósz, Virág Kiss, Éva Józsa

Department of Physical Chemistry, University of Debrecen,

Egyetem tér 1, H-4032 Debrecen, Hungary, e-mail: osz.katalin@science.unideb.hu

Photochemistry is interested in chemical reactions induced by light.¹ The kinetics of such processes differs very characteristically from the kinetics of thermally activated reactions because light intensity and light absorption play major parts in determining reaction rates. Classical kinetic studies in photochemistry are typically based on monitoring a short-lived excited state species after a substantial pulse of light. The role of this pulse light is only to generate an intermediate species in this approach, but the process itself can be fully described by conventional kinetics as the detection only begin after the light pulse is over and the sample is not illuminated in this period. Another common classical source of information is spectrofluorimetry, but this is typically carried out under steady state conditions where no substantial chemical change occurs in the solution. A third approach is based on sampling and offline chemical analysis of a reaction carried out in a photoreactor, which can rarely yield high-quality kinetic data for evaluation.

Recently, some efforts have been devoted to monitoring the major chemical changes during a photochemical reaction by online detection.²⁻⁵ The solid evaluation of such experiments requires the theoretical calculation of concentration changes occurring under illumination. Earlier studies in this field²⁻⁵ have attempted to develop a specialized solution to this problem, but more general sequences of thought are clearly needed.

This poster will present analytical and numerical methods to solve differential equations following from the kinetic description of photochemical processes. The general form of such ordinary differential equations is as follows:

$$\frac{d[A]}{dt} = -\int \frac{\Phi_{P,\lambda} \Phi_{\lambda}}{V} \left(1 - 10^{-\varepsilon_{A,\lambda} l [A] - \sum \varepsilon_{i,\lambda} l [B_i]} \right) \frac{\varepsilon_{A,\lambda} [A]}{\varepsilon_{A,\lambda} [A] + \sum \varepsilon_{i,\lambda} [B_i]} d\lambda$$

In this equation, A is the photoactive species, B_i are various non-photoactive species that absorb light, [A] signifies the concentration of the species A, $\Phi_{P,\lambda}$ is the spectral photon flux of the illumination, Φ_{λ} is the differential quantum yield, V is the volume of the reactor, l is the optical pathlength, whereas $\varepsilon_{A,\lambda}$ and $\varepsilon_{i,\lambda}$ are the molar decadic

absorption coefficients of the respective species. The terminology used here follows the current recommendations of IUPAC.⁶ The quantities shown with the subscript λ are dependent on the wavelength and the integration is done for the entire wavelength range of the illumination.

The ordinary differential equation shown above is further complicated by the fact that concentrations $[B_i]$ are also dependent on time and their change is governed by a separate but coupled ordinary differential equation. The only analytical solution available in the previous literature⁷ is for the very simple case when illumination is monochromatic (eliminating the need for integration) and all $\varepsilon_{i,\lambda}$ values are zero (none of the other components have absorption). This solution is of the following form:

$$[A] = \frac{\ln 10}{\varepsilon_{A,\lambda} l} \ln \left[1 + 10^{-\Phi_{P,\lambda} \Phi_{\lambda} / \nu t - \varepsilon_{A,\lambda} l t} \left(1 - 10^{-\varepsilon_{A,\lambda} l [A]_0} \right) \right]$$

The poster will present a number of further analytical solutions for other special cases and will also show how numerical solution methods can be used. In a few cases, actual experimental examples will also be used.

Acknowledgements:

The research was supported by the EU and co-financed by the European Social Fund under the project TÁMOP-4.2.2.B-15/KONV-2015-0001.

Hungarian Science Funding Agency OTKA is also acknowledged for support under contract no. NK105156.

The research performed by Virág Kiss was supported by NTP-TDK-14-0011.

The research work performed by Éva Józsa was supported by the European Union and the State of Hungary, co-financed by the European Social Fund in the framework of TÁMOP 4.2.4.A/2-11-1-2012-0001 'National Excellence Program'.

The authors wish to thank Gábor Lente for helpful discussions.

References:

1. N. J. Turro, V. Ramamurthy, J. C. Scaiano, *Principles of Molecular Photochemistry*; University Science Books, Sausalito, 2009.
2. G. Lente, J. H. Espenson, *J. Photochem. Photobiol. A: Chem.*, **2004**, *163*, 249-258.
3. I. Fábrián, G. Lente, *Pure Appl. Chem.*, **2010**, *82*, 1957-1973.
4. M. Gombár, É. Józsa, M. Braun, K. Ósz, *Photochem. Photobiol. Sci.*, **2012**, *11*, 1592-1595.
5. T. Lehoczki, É. Józsa, K. Ósz, *J. Photochem. Photobiol. A: Chem.*, **2013**, *251*, 63-68.
6. S. E. Braslavsky, *Pure Appl. Chem.*, **2007**, *79*, 293-465.
7. G. Lente, *Deterministic Kinetics in Chemistry and Systems Biology*; Springer: New York, Heidelberg, Dordrecht, London, 2015.

Exact analytical solution of a non-linear reaction-diffusion problem for full range of parameters values- multiplicity and dead zone coexistence.

Mirosław K. Szukiewicz

Rzeszów University of Technology, Department of Chemical and Process Engineering, al. Powstańców Warszawy 6, 35-959 Rzeszów, POLAND; ichms@prz.edu.pl

Theory

Diffusion and reaction problems are of great importance both in theory and practice. Nature abounds with distinct phenomena that can be modelled by closely analogous or even identical differential equations so the usefulness of many models usually go beyond only one branch. I show only three interesting and important cases for all technologies using porous structures in which reaction occurs: (i) heterogeneous catalysis, (ii) biochemical processes of different type e.g. for processes in which a biofilm is penetrated by oxygen; (iii) various technologies of the development of accumulators as the electrodes using porous materials, especially in the projects associated the alternative power engineering (hydrogen power engineering). The considered problem will be presented from a catalysis standpoint. A steady-state diffusion with an irreversible isothermal chemical reaction $A \rightarrow R$ with power law type kinetic equation is described equations presented in Table 1. External mass transfer resistances are not negligible. For simplicity, the model for which concentration in the pellet center is greater than zero “the regular model” will be called, while the model for which concentration inside the pellet reaches zero for $0 < x = x_{dz} < 1$ - “the dead zone model”.

Table 1. Mathematical foundations

	“regular model”	“the dead zone model”
mass balance	$\frac{d^2c}{dx^2} - \Phi^2 c^n = 0$	
BC 1	$\left. \frac{dc}{dx} \right _{x=1} = Bi_m(1 - c(1))$	
the boundary condition for	$\left. \frac{dc}{dx} \right _{x=0} = 0$	
the boundary condition, if concentration inside the pellet reaches zero for $x = x_{dz}$		$\left. \frac{dc}{dx} \right _{x=x_{dz}} = 0$
additional condition		$c(x_{dz}) = 0$

The regular model is most commonly used, and even from time to time it is overused by authors (namely it is used instead of the dead zone model; e.g. Scott Fogler in his commonly known textbook, example 5.9B in the second edition, made this mistake). It can produce even large errors because a mass flux at $x=0$ in steady state is not equal to zero. The problems result from a lack of the sufficient conditions for the applicability of the dead zone model (there are known only the necessary conditions of the dead zone formation for some types of kinetic equation). From practical standpoint this means that for the same kinetic equation can be used for both regular and dead zone model depending on Thiele modulus value.

Table 2. Table of solutions; the first equation in a cell gives concentration profile, from the second and the third ones c_0 and c_s should be calculated

n>1	$x = \frac{2}{\sqrt{\Phi^2(n+1)c_0^{n-1}}} \cdot \left(\frac{c}{c_0}\right)^{-n} \sqrt{\left(\frac{c}{c_0}\right)^{n+1} - 1} {}_2F_1\left(1, 1 - \frac{1}{n+1}; \frac{3}{2}; 1 - \left(\frac{c}{c_0}\right)^{-n-1}\right)$ $1 = \frac{2}{\sqrt{\Phi^2(n+1)c_0^{n-1}}} \cdot \left(\frac{c_s}{c_0}\right)^{-n} \sqrt{\left(\frac{c_s}{c_0}\right)^{n+1} - 1} {}_2F_1\left(1, 1 - \frac{1}{n+1}; \frac{3}{2}; 1 - \left(\frac{c_s}{c_0}\right)^{-n-1}\right); \sqrt{\frac{2\Phi^2}{n+1}} \sqrt{c_s^{n+1} - c_0^{n+1}} = Bi_m(1 - c_s)$	no solution with physical meaning
- 1<n <1	as above	$c = \left(\frac{1-n}{2} \sqrt{\frac{2\Phi^2}{n+1}}\right)^{\frac{2}{1-n}} (x - x_{dz})^{\frac{2}{1-n}}$ $1 - x_{dz} = \frac{2}{1-n} \sqrt{\frac{n+1}{2\Phi^2}} c_s^{\frac{1-n}{2}}; \sqrt{\frac{2\Phi^2}{n+1}} c_s^{\frac{n+1}{2}} = Bi_m(1 - c_s)$
n=1	$x = \frac{c_0}{\Phi} \sqrt{\frac{\pi}{2}} \operatorname{erfi}\left(\sqrt{\ln\left(\frac{c}{c_0}\right)}\right)$ $1 = \frac{c_0}{\Phi} \sqrt{\frac{\pi}{2}} \operatorname{erfi}\left(\sqrt{\ln\left(\frac{c_s}{c_0}\right)}\right); \sqrt{2\Phi^2 \ln\left(\frac{c_s}{c_0}\right)} = Bi_m(1 - c_s)$	c=0 (trivial solution) – reaction runs on the outer surface only
n<-1	$x = \frac{2}{\sqrt{-\Phi^2(n+1)c_0^{n-1}}} \cdot \frac{c}{c_0} \sqrt{1 - \left(\frac{c}{c_0}\right)^{n+1}} {}_2F_1\left(1, \frac{1}{2} + \frac{1}{n+1}; \frac{3}{2}; 1 - \left(\frac{c}{c_0}\right)^{n+1}\right)$ $1 = \frac{2}{\sqrt{-\Phi^2(n+1)c_0^{n-1}}} \cdot \frac{c_s}{c_0} \sqrt{1 - \left(\frac{c_s}{c_0}\right)^{n+1}} {}_2F_1\left(1, \frac{1}{2} + \frac{1}{n+1}; \frac{3}{2}; 1 - \left(\frac{c_s}{c_0}\right)^{n+1}\right); \sqrt{\frac{2\Phi^2}{-(n+1)}} \sqrt{c_0^{n+1} - c_s^{n+1}} = Bi_m(1 - c_s)$	c=0 (trivial solution) - reaction runs on the outer surface only
	$\eta = \sqrt{\frac{2}{\Phi^2(n+1)}} (c_s^{n+1} - c_0^{n+1})$	$\eta = \sqrt{\frac{2c_s^{n+1}}{\Phi^2(n+1)}}; \Phi_c = \frac{\sqrt{2(n+1)}}{1-n} \cdot c_s^{\frac{1-n}{2}}$

${}_2F_1$ - Gauss hypergeometric function; $c_0=c(0)$ is reagent concentration in the pellet center $c_s=c(1)$ is reagent concentration on the pellet surface

- NOTES:
- (i) some transformation of Gauss hypergeometric function were made to obtain convergence for all n-values
 - (ii) well-known solutions of the linear reaction-diffusion problems (n=1 or n=0) are omitted;
 - (iii) all expressions which include hypergeometric Gauss function and imaginary error function (erfi(x)) can be easily handled using mathematical programs as Maple, Mathematica, Matlab etc.

Theoretically, the validity of the model should be examined but in practice many author mishandled it.

Results and discussion

The solutions is based on proposed by Polyanin and Zaitsev (Handbook Of Exact Solutions For Odes, CRC Press, 1995) first integral of mass balance equation

$$\left(\frac{dc}{dx}\right)^2 - \frac{2\Phi^2}{n+1}c^{n+1} = C_1$$

The C_1 was determined using boundary condition. The resulting equation is separable ordinary differential equation. Integration of it gives results presented in Table 2 while in Fig.1 are presented effectiveness factor values for selected n values vs Thiele modulus.

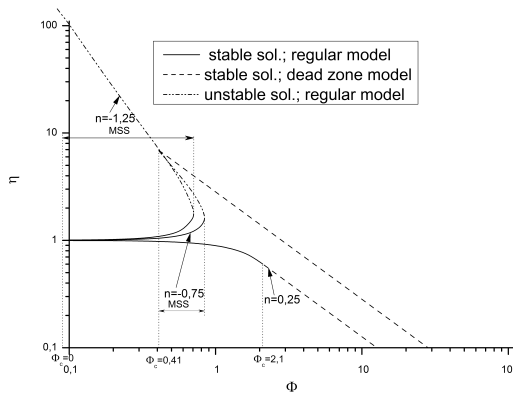


Fig. 1. Effectiveness factor vs. Thiele modulus for selected n values, $Bi_m \rightarrow \infty$; MSS – multiple steady states region

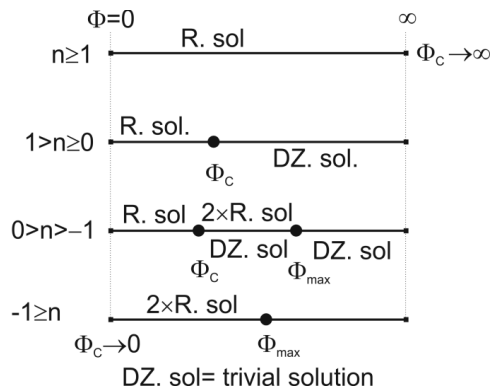


Fig. 2. Diagram existence of solutions; R. sol. = regular model solution, DZ. sol.=dead zone model solution, Φ_c – critical value of Thiele modulus, Φ_{max} - Thiele modulus value, for which lower and upper branch solutions of the regular model coincident.

The analysis of the results is as follows: (i) if $n \geq 1$ then the unique solution exists for any Thiele modulus value and c_0 is greater than 0 while $\Phi_c \rightarrow \infty$. The regular model should be used; (ii) if $0 \leq n < 1$ then the unique solution exists for any Thiele modulus value; for $\Phi < \Phi_c$ the regular model, while for $\Phi > \Phi_c$ the dead zone model should be used; (iii) if $-1 < n < 0$ then the unique solution exists for $0 < \Phi \leq \Phi_c$ (the regular model should be used) and for $\Phi > \Phi_{max}$ (the dead zone model should be used). For $\Phi_c < \Phi \leq \Phi_{max}$ the multiple solutions exist. In this region two solutions (stable and unstable) gives the regular model and one solution (stable) gives the dead zone model; (iv) if $n \leq -1$ then the multiple solutions exist and for $0 < \Phi \leq \Phi_{max}$ ($\Phi_c \rightarrow 0$). In this region two solutions (stable and unstable) gives the regular model. The dead zone extends over the entire space inside the catalyst, the reaction occurs on the pellet surface only. Scheme on existence of solutions is presented in Fig.2. If external resistances grows then Φ_c and Φ_{max} moves towards smaller values.

On basis of presented results the knowledge on regular and irregular phenomena was systematized and some misinterpretations will be corrected (presented in literature opinion that for $\Phi > \Phi_c$ the regular model is usefulness is not true for $n < 0$).

Modeling of gas flow – usefulness of the Laplace transform and CAS-type programs.

Miroslaw K. Szukiewicz*, Małgorzata Wójcik, Paweł Kowalik

Rzeszów University of Technology, Department of Chemical and Process Engineering, al. Powstańców Warszawy 6, 35-959 Rzeszów, POLAND
ichms@prz.edu.pl

* Institute of New Chemical Synthesis, Pulawy, Poland

Theory

The Laplace transform is an important integral transform with many applications in mathematics, physics, engineering etc. The Laplace transform is powerful tool of solving computational problems. It is not often met in chemical engineering because it is essentially limited to linear systems. However, in such cases, the advantages are evident analysis and solution of models are significantly simpler.

Here, application of Laplace transform technique for analysis of the process of two gases mixing on the basis of signal given by TCD-type detector is presented. The actual investigation have two main aims. The first one is determination of gas mixing in the continuous flow vessel. And the second one is checking out the hypothesis that the Laplace transform makes easier solution finding and the analysis of the answer of the analytic system.

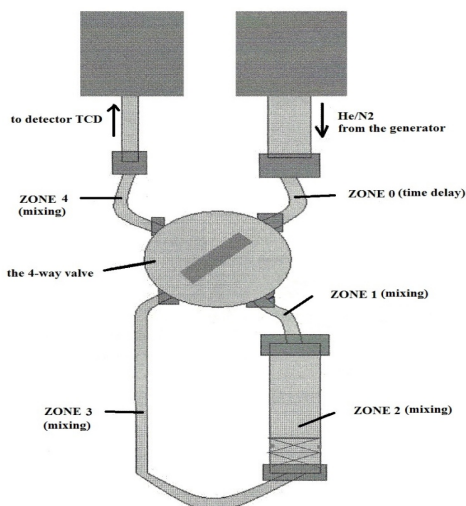


Fig. 1. The scheme of the measuring unit.

The unit consists of the following elements, the 4-way valve, u-shape vessel (empty in the actual investigations), thermal conductivity detector (TCD) and pipes connected the mentioned elements. The system was divided into five zones; they are distinguished on basis of geometry and/or its the function: <Zone 0>: the pipe connected inlet of gas and the 4-way valve; the length of the zone: 0.75dm, the diameter of the zone: 0.0125dm; <Zone 1>: the pipe connected the 4-way valve and a column inlet; the length of the zone: 1.8 dm, the diameter of the zone: 0.0125 dm; <Zone 2>: empty vessel; the length of the zone: 1.0 dm, the diameter of the zone: 0.056 dm; <Zone 3>: the pipe connected a column outlet and the 4-way valve; the length of the zone: 4.0 dm, the diameter of the zone: 0.0125dm; <Zone 4>: the pipe connected the 4-way valve and TCD detector; the length of the zone: 0.75dm, the diameter of the zone: 0.0125dm.

In order to identify the type of mixing, each zone were divided into n cells. Number of cells in each zone may be different. One cell in the zone corresponds to the ideal mixing in this zone. Infinite number of cells in the zone corresponds to the plug flow.

The study was conducted as follows. The system was flushed for 10 minutes with a constant flow of helium (flow rate of 0.04 dm³/min). Then the valve was closed the 4-way valve leading to shut off the flow of the gas through the vessel (Zone 1, 2, 3). For the next 15 minutes the system

(beside the vessel) was purged with a nitrogen (flow rate of 0.01dm³/min) until a stable base TCD signal was reached. After about seven minutes of stabilizing the system again turned over the 4-way valve to allow a constant flow of nitrogen with the volumetric flow rate of 0.01dm³/min or 0.04 dm³/min through the vessel. In result 'trapped' helium was removed and TCD signal was generated and recorded.

Model

Assumptions:

- The system is operated under isothermal conditions at constant pressure.
- Gases satisfy the equation of state of an ideal gas.

Mass balance of the nitrogen in the individual zones and for the number of cells of n leads to the following equations:

$$\text{Zone 1: } c_{1,k}(0) = c_T; k = 1..n1; \quad (1)$$

$$\text{Zone 2: } c_{2,1}(0) = c_T; k = 1..n2; \quad (2)$$

$$\text{Zone 3: } c_{3,1}(0) = c_T; k = 1..n3; \quad (3)$$

$$\text{Zone 4: } c_{4,1}(0) = 0; k = 1..n4 \quad (4)$$

Initial conditions:

$$\text{Zone 1: } c_{1,k}(0) = c_T; k = 1..n1; \quad (5)$$

$$\text{Zone 2: } c_{2,1}(0) = c_T; k = 1..n2; \quad (6)$$

$$\text{Zone 3: } c_{3,1}(0) = c_T; k = 1..n3; \quad (7)$$

$$\text{Zone 4: } c_{4,1}(0) = 0; k = 1..n4 \quad (8)$$

Inlet concentration is described by $c_{in} = \begin{cases} 0 & \text{for } t < 0 \\ c_T & \text{for } t \geq 0 \end{cases}$; time delay by $t_d = \frac{V_0}{q}$; and $c_T = \frac{P}{R_g \cdot T \cdot 10^3}$

Analysis of the model and its solution

Presented in previous section model is simple, but obtaining a solution can be a little difficult. The variable of interest is $c_{4,n4}$ as measurable concentration. For different values of n_1, n_2, n_3 and n_4 the model consist various number of equations. Moreover the values of $n_1..n_4$ have to be determined using trial and error method to obtain the best fit between model solution and experiments. For this reason it is necessary to solve the system repeatedly, the system can contain large number of equations, and finally the number of equations changes for each try. It is very inconvenient situation. One can try to eliminate variables out of interest from the system, but as a result high order differential equation will be obtained and the order of equation will changes for each try. Due to mentioned reasons we paid our attention on well-known tool of analysis and solution of non-stationary models namely Laplace transform. Model transformed into algebraic equations model one can easily solve with respect to variable $c_{4,n4}$.

$$c_{4,n4} = \frac{1}{s} \cdot \left[\left(\frac{q}{n_4 \cdot V_{c4} \cdot s + q} \right)^{n_4} \left(\frac{q}{n_3 \cdot V_{c3} \cdot s + q} \right)^{n_3} \left(\frac{q}{n_2 \cdot V_{c2} \cdot s + q} \right)^{n_2} \left(\frac{q}{n_1 \cdot V_{c1} \cdot s + q} \right)^{n_1} \cdot c_{in} + \left(\frac{q}{n_4 \cdot V_{c4} \cdot s + q} \right)^{n_4} \cdot c_{in} \right] \cdot e^{-t_d s} \quad (9)$$

It is noteworthy, that initial conditions and time delay are considered in the equation.

It is expected, that above equation for real conditions will be of high order. In that case a solution will contain many terms and its obtaining would arduous. But currently there exists computer

programs, usually called Computer Algebra Systems which can help to obtain model solution. We use one of this type program, namely Maple®. It operates Laplace transform. Trial and error method calculations were made fast and evaluation of $n_1..n_4$ coefficients and thereby evaluation of the mixing did not cause problems.

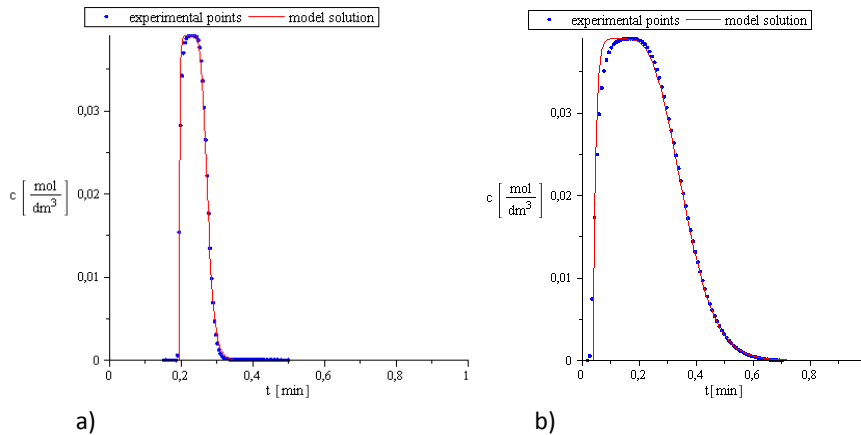


Fig. 2. Experimental and theoretical profiles gas concentrations for a) $q=0.04\text{dm}^3/\text{min}$ and $n_1=1, n_2=40, n_3=1, n_4=1$; b) $q=0.01\text{dm}^3/\text{min}$ and $n_1=1, n_2=12, n_3=1, n_4=1$.

The best fit the smaller gas flow is presented in Fig. 2a and for the larger gas flow in Fig. 2b. The best fit was determined on the basis of minimal value of sum of squares of differences between calculations and experiments. Differences results from the simplicity of the used model which do not consider all theoretically predicted phenomena (axial dispersion). As a result of dispersion a slope of a recorded curve is not as sharp as theoretical one. In our opinion precision of the presented model is satisfactory, especially for the higher gas flow. Consideration of dispersion phenomenon in model results in much complicated system of equations, more difficult for solution. Expected in this case improvement of fit is rather not large.

Following conclusion can be drawn on the basis presented investigations:

1. The theoretical model fits experimental results pretty well. It shows that the presented model of the process is correct. The fitting is better for larger gas velocity.
2. Gas in the pipes is perfectly mixed; in the column the flow approaches the plug, especially for larger gas velocity.
3. The main advancement of Laplace transform method application for solving such class of problems is its higher efficiency and convenience of calculations comparing to classical methods.
4. Using of CAS-type program (Maple®) significantly makes calculations simpler and faster.

This work was supported by The National Centre for Research and Development (Poland) under a grant PBS1/A1/6/2012.

Quadrature-Based Moment Methods in Chemical Engineering

Rodney O. Fox

Anson Marston Distinguished Professor in Engineering
Department of Chemical and Biological Engineering
Iowa State University, USA

Population balance models are a useful mathematical framework for developing models that account for complex physics. For many applications, direct solution of the population balance equation is intractable due to the high-dimensionality of the phase space. Thus a key challenge is to reduce the dimensionality of the problem without losing the underlying physics. At the same time, the reduced description must be numerically tractable and possess the favorable attributes of the original population balance equation. Starting from the seminal work of McGraw on the quadrature method of moments (QMOM), we have developed a general closure approximation referred to as *quadrature-based moment methods*. The basic idea behind these methods is to use the local (in space and time) values of the moments to reconstruct a well-defined local distribution function (i.e. non-negative, compact support, etc.). The reconstructed distribution function is then used to close the moment transport equations (e.g. spatial fluxes, nonlinear source terms, etc.). In this talk, I will review the underlying theoretical and numerical issues associated with quadrature-based reconstructions. The transport of moments in real space, and its numerical representation in terms of fluxes, plays a critical role in determining whether a moment set is *realizable*. Using selected examples from chemical engineering applications, I will describe our work on *realizable* high-order flux reconstructions developed specifically for finite-volume schemes.

Extended Abstract: Conference on Mathematics in (bio)Chemical Kinetics and Engineering, Ghent, Belgium, July 2-3, 2015

Coping with heterogeneity and stochasticity in microbial processes

D. Pischel ^{*1}, R. J. Flassig^{†2} and K. Sundmacher^{‡1,2}

¹Otto-von-Guericke University Magdeburg,
Universitätsplatz 2, 39106 Magdeburg, Germany

²Max Planck Institute for Dynamics of Complex Technical Systems,
Sandtorstr. 1, 39106 Magdeburg, Germany

April 22, 2015

The shift from fossil to renewable biomass feedstock is driving an emerging economy of microbial production based on rationally designed biochemical processes. The rational comes from recent acquired knowledge in the field of systems bio(techno)logy and advances in tools for engineering efficient and sustainable processes that transform biomass into chemicals, material and electricity. Although microorganisms hold a diverse spectrum of valuable products, they often come at very low yield. Further process stability and scale-up or -down can be hampered by unaccounted adaptation or interaction mechanisms: Especially the interplay between heterogeneity of a microbial cell population and stochasticity at the individual cell level can lead to unexpected behavior. Heterogeneity of a cell population refers to individual cell state differences determined by various inter- and extra-cellular factors (protein amounts, cell viability, cell cycle state, nutrients). The origin of heterogeneity is a complex interplay of external, extrinsic and intrinsic noise (5, 1). External noise refers to fluctuations of external environmental factors such as inlet flows or flow composition, but also local environmental fluctuations, e.g. nutrient supply or stress conditions as a consequence of mixing effects in the bioreactor. On the cell level, extrinsic noise is linked to fluctuations in the amount of proteins, which may also result from external noise. Finally, intrinsic noise results from stochasticity in gene expression (low copy number effects), which is propagated on several temporal and spatial scales. Importantly to note, external noise increases with system size, whereas extrinsic and intrinsic noise decrease and vice-versa. Besides system size, external factors leading

*pischel@mpi-magdeburg.mpg.de

†flassig@mpi-magdeburg.mpg.de, corresponding author

‡sundmacher@mpi-magdeburg.mpg.de

to extrinsic noise are important tuning targets for engineering a competitive microbial process, e.g. large product yields at high growth rates.

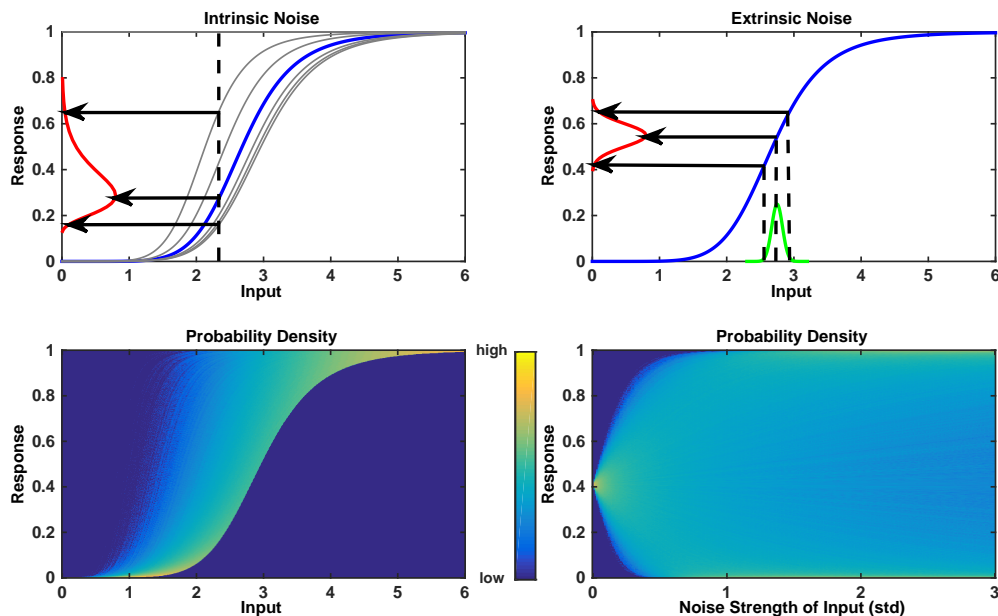


Figure 1: Effects of intrinsic (stochasticity) and extrinsic/external noise on sigmoidal-like system response (Hill kinetics). We see that stochasticity (left) alone can alter the distribution shape (left/right tailed) of a population response, e.g. size distribution, growth rate or yield. On the other hand, fluctuations in the input can result into a bimodal response (right, see contour plot for increasing noise strength=level of standard deviations of the input signal). Colour levels of the contour plots correspond to frequency of occurrence (=density) of a specific response.

However as by now, the complex interplay between external, extrinsic and intrinsic fluctuations and its consequences for microbial process design is poorly understood (2, 1). The potential for bioprocess design is therefore also hard to be exploited by engineers. This is due to the fact that experimental monitoring as well as numerical modeling of the temporal evolution of a heterogeneous cell population remains challenging (1). Therefore, in our contribution we present a hybrid approach for modeling distributed stochastic processes modeled by means of stochastic ordinary differential equations. Our approach is based on a combination of the sigma point method and Haseltine-Rawlings algorithm (4, 3). Whereas the former one allows to efficiently describe external and extrinsic fluctuations as stochastic inputs to the model equations, the latter provides an efficient approximation to the solution of the chemical master equation for describing stochasticity in the biochemical reactions. In this way, we have an effective simulation and analysis tool to rapidly study and exploit the interplay between external, extrinsic

and intrinsic fluctuations for microbial process design.

We apply our approach to several instructive examples including synthetic examples (see Fig. 1, where we give a flavor of effects one may observe for intrinsic and extrinsic/external noise for a simple sigmoidal response-curve), simple and complex biochemical reaction networks from the life- and bio-science. The results of this work pave the way to a bioprocess design and analysis tool that explicitly accounts for fluctuating factors in microbial processes.

References

- [1] F. Delvigne and P. Goffin. Microbial heterogeneity affects bioprocess robustness: Dynamic single-cell analysis contributes to understanding of microbial populations. *Biotechnology Journal*, 9(1):61–72, 2014.
- [2] R. L. Fernandes, M. Nierychlo, L. Lundin, A. E. Pedersen, P. P. Tellez, A. Dutta, M. Carlquist, A. Bolic, D. Schäpper, A. C. Brunetti, et al. Experimental methods and modeling techniques for description of cell population heterogeneity. *Biotechnology Advances*, 29(6):575–599, 2011.
- [3] E. L. Haseltine and J. B. Rawlings. Approximate simulation of coupled fast and slow reactions for stochastic chemical kinetics. *The Journal of Chemical Physics*, 117(15):6959–6969, 2002.
- [4] S. Julier, J. Uhlmann, and H. F. Durrant-Whyte. A new method for the nonlinear transformation of means and covariances in filters and estimators. *Automatic Control, IEEE Transactions on*, 45(3):477–482, 2000.
- [5] P. R. Patnaik. External, extrinsic and intrinsic noise in cellular systems: analogies and implications for protein synthesis. *Biotechnology and Molecular Biology Review*, 1:121–127, 2006.

**THE SWITCHING POINT BETWEEN KINETIC AND
THERMODYNAMIC CONTROL OF COMPETITIVE REACTIONS**

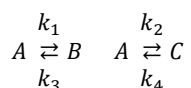
Branco P. Daniel (*), Constaes Denis

Numerical Analysis and Mathematical Modelling Research Group

Ghent University, Galglaan 2 S22 9000 Gent (www.cage.ugent.be/wa)

A new definition is proposed for the switching point t_s between the kinetic and thermodynamic control regimes of two competitive reactions: the time at which the rates of formation of the competing products are equal. According to this definition, the kinetic control regime is present from the beginning of the reaction, and is valid as long as the rate of formation of the kinetic product is larger than the rate of formation of the thermodynamic product. At the switching point t_s , both rates of formation are equal, so, from this switching point the thermodynamic product has a larger rate of formation, and the thermodynamic control is settled until the end of the reaction.

Given the following system of first order competitive reactions:



where A , B and C are chemical species, and k_i are kinetic constants, the solution consists of the functions that describe the temporal evolution of the concentrations of the chemical species involved. Assuming initial and equilibrium concentrations of A , B and C as A_o , B_o and C_o , and A_{eq} , B_{eq} and C_{eq} , respectively, it is possible to write the time dependent concentration of the chemical species accordingly; for example, for A :

$$A(t) = A_{eq} + (A_o - A_{eq} - A_x)e^{-\alpha_p t} + A_x e^{-\alpha_m t} \quad (1)$$

where α_p and α_m , $\alpha_p > \alpha_m$, are:

$$\alpha_p, \alpha_m = \frac{1}{2} \left(k_1 + k_2 + k_3 + k_4 \pm \sqrt{(k_1 + k_2 + k_3 + k_4)^2 - 4(k_1 k_4 + k_2 k_3 + k_3 k_4)} \right) \quad (2)$$

and a new term A_x appears:

$$A_x = \frac{\alpha_m \left(\frac{(\alpha_p - \alpha_m) + k_4}{A_o + B_o + C_o} B_{eq} + \frac{(\alpha_p - \alpha_m) + k_3}{A_o + B_o + C_o} C_{eq} - (k_1 + k_2) \right) A_o + 2B_o k_3 (\alpha_m - k_4) + 2C_o k_4 (\alpha_m - k_3)}{2\alpha_m (\alpha_p - \alpha_m)} \quad (3)$$

Similar expressions to Eq. (1) can also be written to describe the temporal evolution for the concentrations of the products B and C . The expressions B_x and C_x consist of a collection of terms comprising kinetic constants and both initial and equilibrium concentrations of all chemical species, similar to the expression for A_x given in Eq. (3). Opposed to the typical set up experiment devised to present the definition of the kinetic vs thermodynamic competition in the basic and organic chemistry textbooks, where $B_o = C_o = 0$, in our study the initial

(*). Corresponding author. Emails: Daniel.BrancoPinto@UGent.be (Branco D.) and Denis.Constaes@UGent.be (Constales D.)

concentrations of both competing products are valid parameters and are not restrained to these values.

The classical definition of the switching point corresponds to the value of time when the concentration profiles of both competing products intersect, i.e., $B(t) = C(t)$. This intersection point is impossible to express in an exact, closed form, but can only be calculated in a numerical, approximated form; numerical methods to calculate this switching point has been proposed elsewhere [see Caravaca M. *et. al.*, *Phys. Chem. Chem. Phys.*, 16 (2014) 25409]. We propose a new definition of the switching point: the time t_s when the rate of formation of both competing products is the same. So, the kinetic product is the one which is produced faster at the beginning of the reaction, and the kinetic control regime extends until the proposed switching point is reached. The rate of formation of the kinetic product is larger not only at $t = 0$, but as long as the kinetic control regime prevails. At the switching point t_s , no actual crossing occurs in both concentration profiles, but in both rate of formation – time curves, as seen in Fig. 1b. After this time, and until equilibrium is achieved, the rate of formation of the thermodynamic product is larger, so eventually his concentration will reach and surpass the concentration of the kinetic product. Then, the thermodynamic control regimes extends from the proposed switching point t_s until the end of the reaction.

We can obtain a closed form expression for the switching time t_s , equating the time derivatives of the corresponding concentration – time expressions for the competing products B and C , similar to Eq. (1), at $t = t_s$:

$$t_s = \frac{\log \left[\frac{\alpha_p - \Delta}{\alpha_m - \Delta} \right]}{\alpha_p - \alpha_m} \quad (4)$$

where:

$$\Delta = \alpha_p \alpha_m \left(\frac{(B_{eq} - B_o) - (C_{eq} - C_o)}{(A_o k_1 - B_o k_3) - (A_o k_2 - C_o k_4)} \right) \quad (5)$$

If the initial concentrations are $A_o \neq 0$, $B_o = C_o = 0$, Eq. (5) is reduced to:

$$\Delta = \frac{\alpha_p \alpha_m}{A_o} \left(\frac{B_{eq} - C_{eq}}{k_1 - k_2} \right) \quad (6)$$

It is interesting to study the fraction inside the parentheses in Eq. (6): the denominator corresponds to the difference between the initial rates of formation of the competing products, whereas the numerator corresponds to the difference between the equilibrium concentrations. In order to observe both control regimes, the product with the largest initial rate of formation should have the smallest equilibrium concentration (and viceversa; the given description corresponds to the kinetic product), so the value of the fraction inside the parentheses, and therefore the value of Δ , must be strictly negative. This conclusion can also be extended to the case where $B_o \neq C_o \neq 0$; this is, the value of the fraction enclosed in parenthesis in Eq. (5) is also negative. In this case, both equilibrium concentrations are referred to their corresponding initial concentrations, so, for example, the difference $B_{eq} - B_o$ accounts for the amount of B produced in the reaction. Therefore, if $B_o \neq C_o \neq 0$, not the

equilibrium concentration, but the amount produced of the thermodynamic product must be larger than the amount produced of the kinetic product.

In Fig. 2 is shown a plot of the value of the proposed switching time t_s , normalized to a constant corresponding to the time $t_{s(\Delta=0)} = \log(\alpha_p/\alpha_m)$ when $\Delta = 0$, as a function of the value of Δ . Given that Δ is restricted to negative values, the maximum value of t_s corresponds to that when $\Delta = 0$:

$$t_{s(\Delta=0)} = t_{s(\max)} = \frac{\log\left[\frac{\alpha_p}{\alpha_m}\right]}{\alpha_p - \alpha_m} \quad (7)$$

so the value of the switching time t_s is bounded between zero (when Δ tends to large negative values) and $t_{s(\max)}$.

Further studies were performed where the initial concentrations of one or both of the competing products are not zero. Restrictions for the maximum values of the initial concentrations were settled, in order to guarantee the presence of both competing control regimes and the existence of at least a crossing point between the concentration profiles of the competing products. For example, starting from the top value for the initial concentration of the thermodynamic product, the intersection of both concentration profiles is unique and will occur at a time equivalent to the switching time t_s . Besides, the inconvenience of the classical definition of the switching point, where the crossing points are also control regime switching points, is evident when the initial concentration of the thermodynamic product is non-zero; being this the case, two crossing points will occur between the concentration profiles, therefore we can identify three consecutive control regimes: thermodynamic, followed by kinetic, and then thermodynamic control until the end of the reaction. Finally, we extended the definition proposed of the switching time to a different initial set up: the decomposition of two competing reagents, for instance B and C , to give an unique product A ; we demonstrated that the expression given for the switching time t_s , Eq. (4), can be used as it is and without change.

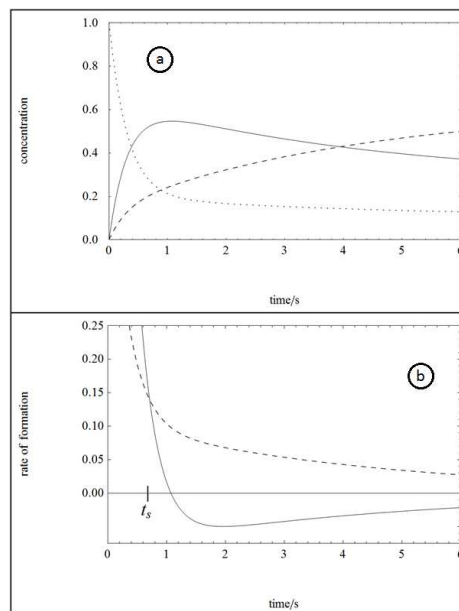


Fig 1. a) Concentration profiles for A (dotted line), B (solid line) and C (dashed line). b) Rates of formation as a function of time for the products B (solid line) and C (dashed line). $A_o = 1.0$; $B_o = C_o = 0$; $k_1 = 2.0$; $k_2 = 0.6$; $k_3 = 0.75$; $k_4 = 0.1$.

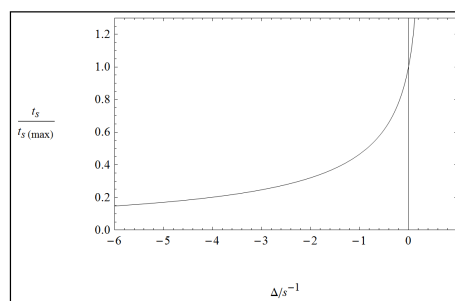


Fig 2. Value of the switching time $t_s / t_{s(max)}$, as a function of Δ . $A_o = 1.0$; $B_o = C_o = 0$; $k_1 = 2.0$; $k_2 = 0.6$; $k_3 = 0.75$; $k_4 = 0.1$.

Fischer-Tropsch Synthesis SSITKA simulation: balancing between model complexity, computational effort and relevance of the included features

Jonas Van Belleghem, Joris W. Thybaut* and Guy B. Marin
Ghent University, Laboratory for Chemical Technology, Technologiepark 914
Ghent B-9052 Belgium

*Corresponding author – e-mail: Joris.Thybaut@UGent.be

Introduction

A fundamental understanding of the intrinsic reaction kinetics of heterogeneously catalyzed reactions is of great importance for the chemical industry. Insight in the effect of reaction conditions on catalyst activity and selectivity is indispensable for the design and safe operation of chemical reactors and even entire processes. In the pursuit of novel catalyst design, an adequate understanding of promoter, support, metal particle size,... effects on the catalyst performance is essential. A technique providing such key insights is Steady State Isotopic Transient Kinetic Analysis (SSITKA).

While quite some relevant information can already be obtained from the experimental analysis itself, the modeling of SSITKA data will further increase the insights in the reaction pathway and how it is affected by the aforementioned phenomena. These additional insights can be used in a model guided design procedure. One must take care, however, not to drown in the acquired experimental information and to keep the computational effort, while modeling, within manageable limits.

The present work focuses on the modeling of SSITKA data acquired for complex reactions. Specific attention is devoted to the stable and fast integration of the reactor model equations as well as to the extent of the reaction network that is accounted for in molecular detail. Fischer-Tropsch Synthesis (FTS) has been selected as the model reaction.

Procedures

In a SSITKA experiment an isotopic label in the reactants and products is monitored as a function of time after an abrupt switch of a reactant by its isotopic counterpart.¹ For FTS, this is typically a switch between ^{12}CO and ^{13}CO . Apart from the isotopic labeling, the experiment is performed at steady state conditions. The preferred reactor configuration for SSITKA experimentation is a plug flow reactor. The resulting reactor model equations, hence, comprise partial differential equations, PDEs, for the species which take part in the isotopic exchange and ordinary differential equations, ODEs, and algebraic equations, AEs for the species that are not taking part in the isotope exchange reactions and for the various sums of isotopologues and isotopomers of a specific species.² The PDEs are purely convective in nature, necessitating the use of a non-linear discretization scheme to avoid spurious oscillations during the numerical integration.³ As non-linear discretization scheme, the Flux Limiter³ (FL) approach has been selected. Due to the vast number of FL functions proposed in the literature, a case study has been performed in which the 14 most relevant FL functions are compared to each other in terms of accuracy and computational time as function of the residence time in the reactor and abruptness of the isotopic switch. Two more ways to further reduce the computational time are considered, i.e., a semi-analytical calculation of the Jacobian matrix and selection of an appropriate stiff ODE solver.

The Single-Event microkinetic (SEMK) methodology⁴ is applied for the microkinetic modelling. The isotope effects merely impact on the symmetry number of the reaction rate coefficients in the SEMK methodology. An available automated reaction network generation algorithm⁵ has been

extended with the capability to account for isotopes. The size of the resulting reaction network, however, exhibits an exponential dependency on the carbon number of the longest hydrocarbon chain, see Figure 1. It not only leads to computationally too intensive calculations but goes beyond the detail which can reasonably be obtained with present-day analytical techniques. As a result, a reaction network size reduction technique has been devised. The hydrocarbons considered in the network are split up into two groups. A group with a maximum carbon number for which isotopologues and isotopomers are accounted for in full detail. In the second group of heavier hydrocarbons, sets of species are introduced which allow tracking the isotopic labeling at specific positions in the chain. This is illustrated in Figure 1 for metal propyl species in which the maximum carbon number for which isotopically labeled species are accounted for in detail is set at 2. The eight metal propyl species are distributed over six sets. Two of these sets follow the total amount of metal propyl species with a ^{12}C or ^{13}C atom bonded to the metal atom of the catalyst. The four other sets follow the total amount of metal propyl species with an isotopic labeling of the two terminal carbon atoms as indicated in Figure 1. For the heavier hydrocarbon, only the total fraction of ^{12}C or ^{13}C as a function of time can be simulated. Of course, the example presented for metal propyl species serves illustrative purposes only and the corresponding gain is practically none. The gain for heavier species, however, is much more significant as evident from Figure 1, left.

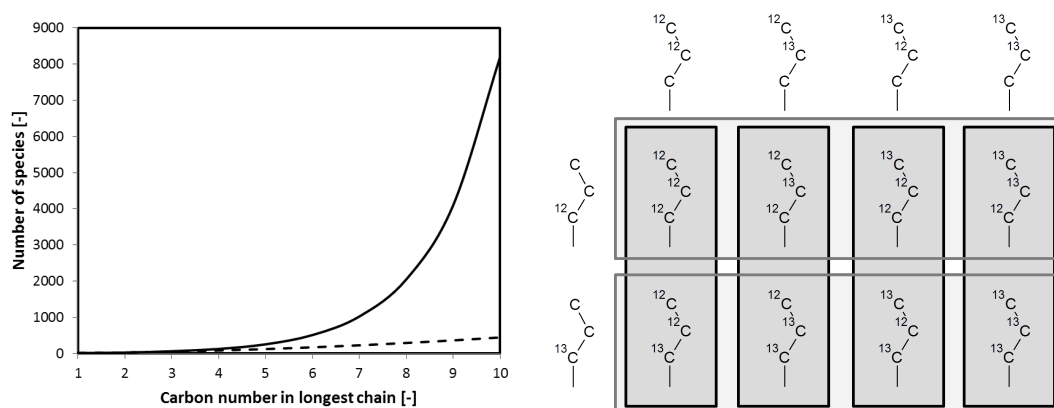


Figure 1: Left - The number of species in the reaction network as function of the carbon number in the longest hydrocarbon chain. The full black line represents the number of species in the reaction network generated with the reaction network generation code. The dashed line corresponds to the number of species when only the formation of C_2 species is described in detail. Right - Graphical representation of the sets introduced in the reduced kinetics scheme.

Results and discussion

Most of the FL functions show competitive convergence behavior with respect to the step size used in the discretization for the application considered in this work. Hence, the selection of a FL function for the simulation of SSITKA data was focused on the required computational time. The simulations clearly illustrate that a careful selection of a FL function for a specific application can considerably speed up the simulations, e.g., the difference in computational time between the SMART FL and the Van Leer FL amounts to several orders of magnitude, see Figure 2. Based on the results of the case study, continuous FL

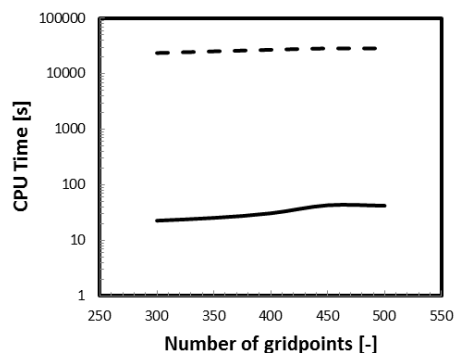


Figure 2: CPU time as function of the number of gridpoints. SMART FL (---) and Van Leer (—)

functions were selected as the best FL functions for the modeling of SSITKA data.

The semi-analytical calculation of the Jacobian matrix allows reducing the computational time with a factor 4 to 7. Of the four backward differentiation solvers, i.e. DASPK, LSODE, VODE and LSODA, the DASPK solver was found to outperform the others.

Table 1 shows the reduction in computational time between simulations performed with the kinetics scheme accounting for all the isotopologues and isotopomers of all the hydrocarbons, the so-called detailed network, and the simulations performed with the kinetics scheme accounting for a detailed labeling of only a subset of the hydrocarbons, the so-called reduced network. The carbon number of the longest hydrocarbon in the simulations is 5 and the carbon number of the longest hydrocarbon chain in the subset is 2. The simulations indicate that a reduction in computational time up to a factor 10 can be achieved.

Table 1: Computational time for the different kinetics schemes. The carbon number of the longest hydrocarbon in both schemes is 5. In the reduced kinetics scheme, the carbon number of the longest hydrocarbon chain which is described in full detail is 2.

τ [s]	H2/CO	CPU time detailed network	CPU time reduced network
	[-]	[s]	[s]
0.01	2	1779	175
	5	1764	173
0.1	2	2153	349
	5	2296	329
1.0	2	21052	3022
	5	19093	2734

Conclusions

A careful assessment of Flux Limiter (FL) functions is essential to select an appropriate FL function for a specific application. The case study presented in this work illustrates how for the modeling of Steady State Isotopic Transient Kinetic Analysis (SSITKA) data, continuous FL functions are the best choice. A semi-analytical calculation of the Jacobian matrix further reduces the computational time with a factor 4 to 7. The DASPK solver is selected as the best backward differentiation solver. A method to track the isotopic labeling in full detail has been devised together with a technique to reduce the reaction network size and fine-tune the information generated by the simulations to the level of detail accessible by current analysis methods. Simulations results show that a reduction in computational time of a factor 10 can be achieved.

Acknowledgements

This work was supported by a doctoral fellowship from the Fund for Scientific Research Flanders (FWO) and the 'Long Term Structural Methusalem Funding by the Flemish Government'. This work was carried out using the STEVIN Supercomputer Infrastructure at Ghent University, funded by Ghent University, the Flemish Supercomputer Center (VSC), the Hercules Foundation and the Flemish Government – department EWI.

References

1. Shannon, S.L. and J.G. Goodwin, Chem Rev, 1995. **95**(3): p. 677-695.
2. Berger, R.J., et al., Appl Catal, A, 2008. **342**(1-2): p. 3-28.
3. Waterson, N.P. and H. Deconinck, J Comput Phys, 2007. **224**(1): p. 182-207.
4. Lozano-Blanco, G., et al., Ind Eng Chem Res, 2008. **47**(16): p. 5879-5891.
5. Lozano-Blanco, G., et al., Oil Gas Sci Technol, 2006. **61**(4): p. 489-496.

Novel heuristics for mediating radical chain reactions: a stochastic simulation of the synthesis of copolymers with tailored monomer sequences

Paul H.M. Van Steenberge¹, Dagmar R. D'hooge^{1,2,*}, Marie-Françoise Reyniers¹ and
Guy B. Marin¹

¹Laboratory for Chemical Technology, Ghent University, Technologiepark 914 B-9052 Gent, Belgium

²Department of Textiles, Ghent University, Technologiepark 907, B-9052 Gent, Belgium

Introduction

A novel kinetic Monte Carlo modeling methodology is presented, allowing control over monomer sequences for each individual macromolecule in radical polymerization [1,2]. The methodology is applied for controlled radical polymerization (CRP), in which macroradicals R_i (i : chain length) can be temporarily deactivated into dormant species (R_iX ; X : end-group functionality) by a mediating agent (e.g. catalyst). Under well-chosen conditions termination reactions which lead to loss of X and formation of dead polymer P can be minimized.

In this contribution, focus is on Initiators for Continuous Activator Regeneration Atom Transfer Radical Polymerization (ICAR ATRP; Figure 1a) aiming at the controlled synthesis of linear gradient copolymers (Figure 1b) made of methyl methacrylate (red and n -butyl acrylate (green) monomer units. A temperature of 80°C is selected and $\text{CuBr}_2/\text{PMDETA}$ (N,N,N',N'',N'' -pentamethyldiethylenetriamine) is considered as catalyst with amounts as low as 50 ppm (molar with respect to monomer).

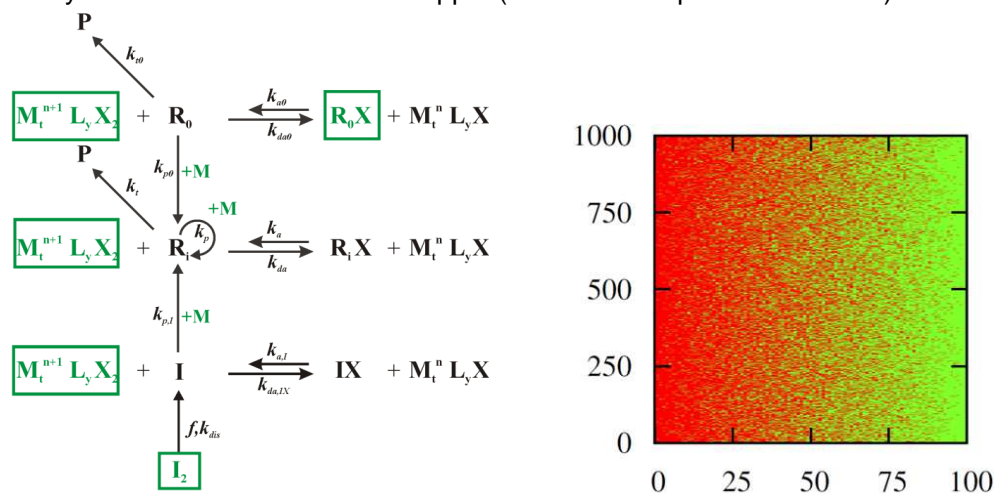


Figure 1: (a) ICAR ATRP, initial compounds boxed (R_0X : ATRP initiator; I_2 : conventional radical initiator; M : monomer; $M_1^{n+1}L_yX_2$: deactivator); X : functionality; $k_{a,da,dis,p,t}$: rate coefficient for activation, deactivation, dissociation, propagation (b) Targeted linear gradient copolymer (methyl methacrylate (red) and n -butyl acrylate (green) monomer units).

Methodology

Linear gradient quality ($\langle GD \rangle$) is calculated based on the comparison of kinetic Monte Carlo simulated monomer sequences of a representative number of chains with predefined ideal gradient monomer sequences [1]. Mayo-Lewis monomer

incorporation kinetics are exploited to determine the optimal multicomponent fed-batch policy that results in a fast ATRP initiation and a good control over monomer sequences [2]. The conventional radical initiator flow rate is determined based on the simulated termination rate profile, in order to mimic a steady radical concentration. The comonomer flow rates are adjusted to maintain starved feed operation (90% monomer conversion; low monomer concentrations) and the catalyst/deactivator flow rate is varied so that a constant ppm level is obtained with respect to the added amount of monomer. These heuristics follow from the design premise to incorporate a quasi-constant number of monomer units per activation-growth-deactivation cycle and, hence, to limit as much as possible the perturbation of the ATRP pseudo-equilibrium between R and RX species.

Results

Kinetic Monte Carlo simulations show that starved feed operation and fed-batch feeding of the catalyst ensure the incorporation of an approximately constant number of monomer units during each activation/growth/deactivation cycle, leading to higher uniformity in the monomer sequences. Combined with fine-tuning of the conventional radical initiator flow rate, *i.e.* maintaining a constant radical concentration, a relatively fast ICAR ATRP (Figure 2a), a linear number average chain length evolution (Figure 2b), a high end-group functionality (Figure 2c) and suppressed termination in the initiation phase (Figure 2d) can be obtained.

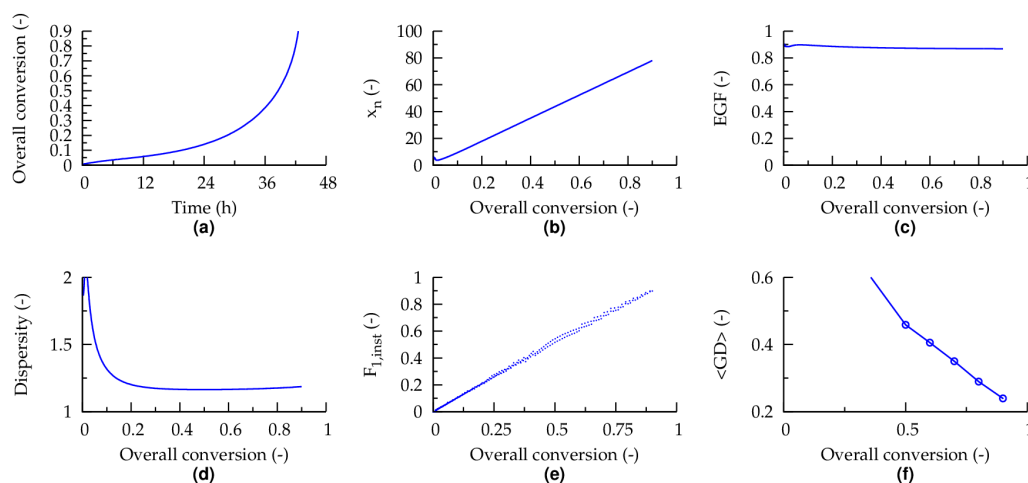


Figure 2: (a) Overall conversion (based on total monomer amount of corresponding batch case) as a function of polymerization time (b) Number average chain length x_n as a function of overall conversion (c) End-group functionality EGF as a function of overall conversion. (d) Dispersity as a function of overall conversion (e) Evolution of instantaneous copolymer composition $F_{1,inst}$ as a function of the overall conversion (MMA:1) (f) Gradient deviation $\langle GD \rangle$ as a function of conversion; initial conditions: $[M]_0; [R_0X]_0$ 100; fed-batch addition of dissolved I_2 : $27 \mu\text{mol L}^{-1}$ with flow rate of $0.001 \mu\text{L s}^{-1}$ per liter reaction mixture of the corresponding batch case; fed-batch addition of comonomer via Mayo-Lewis equation each time an in situ conversion of 0.9 is reached (with at the start 1% of the batch amount in pure MMA form); comonomer addition accompanied by addition of deactivator so that Cu level is always 50 ppm (with respect to the monomer and monomer units).

The fed-batch addition of comonomer yields a linear probability profile for incorporating the first monomer (Figure 1e), as desired for linear gradient polymers. The proposed heuristics yield at high conversion copolymers with $\langle GD \rangle$ values near zero (Figure 1f). Chain initiation and propagation are improved, while chain

termination remains uncharacteristically low for starved feed conditions (Figure 3 right).

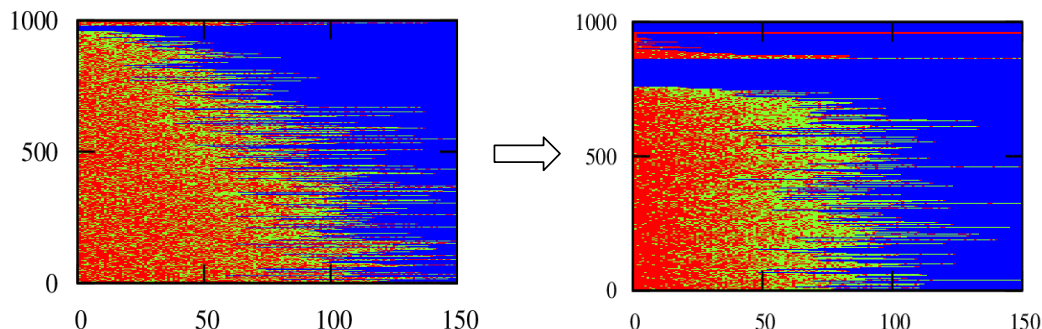


Figure 3: (left) sample of polymer molecules when adding all reagents at $t = 0$ (batch); (right) sample of polymer molecules when adding all reagents according to the heuristics (fed-batch)

Conclusions

Novel heuristics for controlled radical polymerization using isothermal ICAR ATRP of MMA and nBuA for the synthesis of tailored linear gradient copolymers are established and their feasibility is demonstrated. A continuous addition of dissolved conventional radical initiator suppresses initial termination and leads to higher time-averaged radical concentrations and, hence, an increase of the overall polymerization rate. To establish stable activation/growth/deactivation cycles, the monomer is added in a fed-batch manner so that the monomer concentration remains approximately constant. The relative comonomer flows are set in such way that a linear probability of finding MMA along the polymer backbone results, controlling the monomer sequences of individual copolymer chains. Per monomer addition, deactivator is added to compensate for the volume increase, again ensuring stable activation/growth/deactivation cycles. Hence, the highest polymer gradient quality results when a multi-component fed-batch procedure is selected.

Acknowledgements

The authors acknowledge financial support from the Long Term Structural Methusalem Funding by the Flemish Government, the Interuniversity Attraction Poles Program–Belgian State–Belgian Science Policy, and the Fund for Scientific Research Flanders (FWO; G.0065.13N). Dagmar R. D’hooge acknowledges the Fund for Scientific Research Flanders (FWO) for a postdoctoral fellowship.

- [1] P.H. M. Van Steenberge *et al.* *Macromolecules*, **2012**, 45, 8519.
- [2] D.R. D’hooge *et al.* *Polymers*, **2014**, 6, 1074.

Calibration And Analysis Of A Direct Contact Membrane Distillation Model Using Monte Carlo Filtering and good modelling practice

^{1,2}I. Hitsov, ^{2,3}L. Eykens, ²K. De Sitter, ²C. Dotremont, ⁴L. Pinoy, ³B. Van der Bruggen, ¹I. Nopens*

¹BIOMATH, Department of Mathematical Modelling, Statistics and Bioinformatics, Faculty of Bioscience Engineering, Ghent University, Coupure Links 653, 9000 Ghent, Belgium

²VITO - Flemish Institute for Technological Research, Boeretang 200, 2400 Mol, Belgium

³Department of Chemical Engineering, Process Engineering for Sustainable Systems Section, KU Leuven, W. de Croijlaan 46, 3001 Leuven, Belgium

⁴Department of Chemical Engineering, Cluster Sustainable Chemical Process Technology, KU Leuven, Gebroeders Desmetstraat 1, Ghent B-9000, Belgium

*Corresponding author – Ingmar Nopens, Ingmar.Nopens@ugent.be

Introduction

Membrane distillation is an emerging technology to separate non-volatile components from an aqueous feed stream. Mathematical models have proven useful to pursue breakthrough in the economics of the technology and for further improvement through membrane and module design as well as operational optimization.

Many models for direct contact membrane distillation (DCMD) are based on the Dusty Gas Model for the mass transfer inside the membrane, while the heat transfer inside the channels is typically modelled with Nusselt type equations. In most of the MD models the researchers use an "of-the-shelf" Nusselt equation. In our work, we show that the existing Nusselt equations cannot directly be applied to simulate the heat transfer in the spacer filled channels and instead the existing equations should be pre-calibrated using aluminium foil [1], operating the system as a heat exchanger.

In this contribution a Monte Carlo filtering method was applied to calibrate and study the structure of a typical DCMD model. This is not common practice and the calibration efforts in the literature are typically not treated correctly. Often too many parameters are being calibrated and issues related to identifiability usually are not discussed. The method showed that in order to properly calibrate the model for a single layer membrane, only 2 parameters are needed, that correct the heat and mass transfer inside the membrane. The study revealed that a three dimensional interaction between the porosity, tortuosity and pore size exists when the Dusty Gas Model is used, revealing that the tortuosity could be used successfully as a single calibration parameter for the membrane mass transfer. It should be stressed that a multitude of solutions exist to predict the same mass and heat transfer.

Finally, a simple, yet physical method for the simulation of supported membranes is developed that enables to model the system by reducing the heat transfer coefficient in the permeate channel, where the membrane support is physically located. The model structure did not need adaptation and addition of parameters.

Results and discussion

In order to choose which parameters should be used in the calibration of the model, the resistances in the DCMD system are split into different categories - Figure 1.

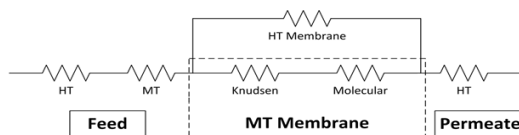


Figure 1 Heat (HT) and mass transfer (MT) resistances in DCMD system

The heat transfer inside the channels is modelled using the Nusselt equation (eq.1), similarly to heat exchanger models. Likewise, the mass transfer is modelled using the Sherwood equation (eq. 2).

$$Nu = aRe^bPr^c \tag{1}$$

$$Sh = aRe^bSc^c \tag{2}$$

The Nusselt equation is calibrated by replacing the membrane with an aluminium foil and performing heat transfer experiments in order to obtain the coefficients a, b and c in eq. 1. Since the Sherwood equation is the mass transfer equivalent of the Nusselt equation [2], the experimentally obtained coefficient a, b and c were also used in the Sherwood equation.

In order to study the model structure for the Knudsen and molecular resistances in the Dusty Gas model a Monte Carlo filtering method was applied – Figure 2.

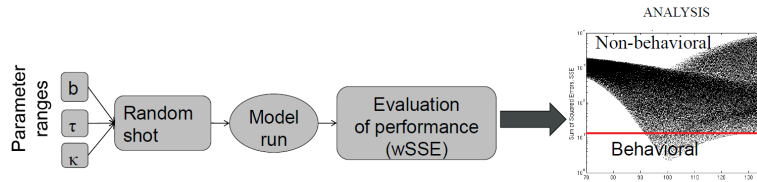


Figure 2 Flow diagram representation of the Monte Carlo Filtering method used in this work

A sampling range was chosen for the parameters studied in this work. Next, a random shot is taken for each of the parameters and the model is run using the given parameters set for all of the experiments of a given membrane. The prediction performance of the model is estimated using the weighted sum of squared errors (wSSE) using an objective function that includes model output variables, i.e. the flux and the energy efficiency. The weights were assigned based on the experimental errors, estimated by the difference of flux and energy efficiency between the feed and the permeate channels. In this way it is estimated how well a simulation based on a certain parameter set fits all of the available experimental data. It was found that the membrane mass transfer parameters interact in a three dimensional way (Figure 3) which would make it dangerous to estimate them simultaneously as this point towards a problem of structural identifiability. This simply means that, based on the available data, no “unique” set of parameter estimates can be found. Since the membrane tortuosity is the most uncertain parameter and cannot be measured it was decided to leave it as the only calibration parameter for the mass transfer. The only resistance left to be calibrated is the thermal conductivity of the membrane matrix. This parameter is very uncertain since it cannot be reliably measured and the models that predict the thermal conductivity of the membrane rely on a pre-defined structure of the air-polymer matrix that is different for every membrane type. Therefore, it was decided to include this parameter in the calibration – Figure 4. The initial value of the thermal conductivity had to be increased by about 50% in order to obtain a good fit for the particular membrane.

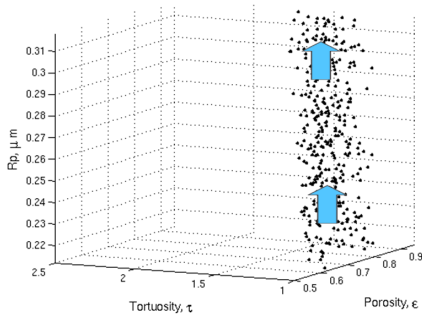


Figure 3 Three dimensional interactions

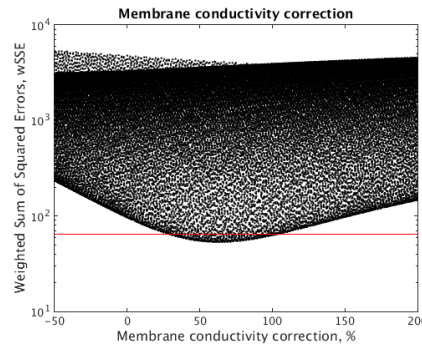


Figure 4 Weighted sum of squared errors as a

between the membrane parameters. Only the behavioural (good) solutions are plotted.

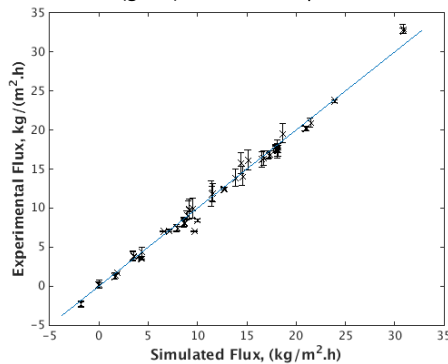


Figure 5 The simulated versus predicted flux for an **unsupported** membrane, eq. Experimental conditions: T_f 53- 61 °C, T_p 25-54 °C, salinity 0-327 g/l, channel velocity 2 to 28 cm/s

function of membrane thermal conductivity correction. Good solutions lie below the red line.

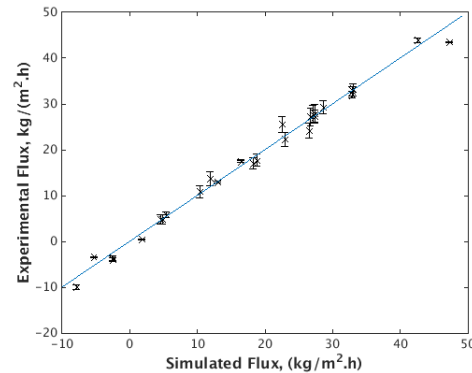


Figure 6 Simulated versus experimental flux for a **supported** membrane. Experimental conditions: T_f 54-59 °C, T_p 39-49 °C, salinity 0-347 g/l, channel velocity 4 to 28 cm/s

To improve the mechanical stability of the very thin membranes, non-woven support is often used. Traditionally, the support is modelled by assuming that the support is completely filled with water and the thermal conductivity of the support (water and polymer mixture) is calculated by another submodel. This approach is flawed, mainly because it neglects the convection in the support material and adds uncertainty of the model and additional parameters to the model. Moreover, the thermal conductivity of the polymers depend strongly on their orientation and degree of crystallinity. On the other hand, by recognizing that the support brings only an additional heat transfer resistance because it is located at the permeate side (Figure 1), we decided to model the support simply by reducing the Reynolds exponent b in the Nusselt equation (eq. 1) since this is the lumped parameter for these phenomena. The resulting fit for the newly proposed method can be seen in Figure 6. We will also show how this additional parameter impacts the identifiability of the parameters and how one needs to be careful when choosing degrees of freedom for optimisation problems.

Conclusions

By applying the Monte Carlo filtering technique to this model we were able to study the model structure and to derive a new method for simulation of supported membranes. Moreover, the proper parameters for system optimization could be chosen in order to avoid identifiability issues. This is important, because if one parameter is used to compensate for another, the predictive power of the model will be impacted.

Bibliography

- [1] Phattaranawik et al. (2003). Heat transport and membrane distillation coefficients in direct contact membrane distillation. *J. Membrane Sci.* 212, 177-193.
- [2] L. Martínez-Díez et al. (1999), Temperature and concentration polarization in membrane distillation of aqueous salt solutions, *J. Membrane Sci.* 156, 265–273

Optimal design of chemical processes with joint chance constraints

M. Ostrovsky¹, N. N. Ziyatdinov², T. V. Lapteva², I.V. Zaitsev¹Karpov G.Institute of Physical Chemistry, Vorontsovo Pole, 10, Moscow, 103064, Russia²Kazan State Technological University, Karl Marx str., 65, Kazan, 420111, Russia

1. Introduction

We consider a problem of a chemical process (CP) design in the case of the presence of uncertainty in the process models. One of two following formulations of a problem of the optimal design of chemical processes (CP) under uncertainty is usually used: a) the formulation of *the two-stage optimization problem* (TSOP) takes into account the possibility of the change of control variables at the operation stage b) the formulation of *the one-stage optimization problem* (OSOP) implies that the control variables are constant at the operation stage.

Methods of solving the TSOP with hard constraints (TSOPHC) and the OSOP with chance constraints (OSOPCC) have been developed extensively. Significantly less attention was given to formulation and solving of the TSOP with soft constraints. One of the main issues in solving the TSOPCC is a calculation of multiple integrals to determine the expected value of the objective function and the probability of constraints satisfaction. This operation is very intensive computationally. The use of the standard Gaussian quadrature for the calculation of the multiple integrals is very intensive computationally even for small dimensionality of vector θ of the uncertain parameters. We consider a method of solving TSOPCC based on the reduction of chance constraints to deterministic ones.

The two-stage optimization problem with chance constraints (TSOPCC) has the following form

$$f_1 = \min_{d, z(\theta)} \int_T f(d, z(\theta), \theta) \rho(\theta) d\theta \quad (1)$$

$$\Pr\{g_j(d, z(\theta), \theta) \leq 0, j = 1, \dots, m\} \geq \alpha \quad (2)$$

We showed that constraint (2) can be substituted with the following $m+1$ constraints

$$\Pr\{\theta \in T_\alpha\} \geq \alpha \quad (4)$$

$$\max_{\theta \in T_\alpha} g_j(d, z(\theta), \theta) \leq 0, \quad (5)$$

Hence, problem (1) can be rewritten in the following form

$$f^* = \min_{d, z(\theta), T_\alpha} E[f(d, z(\theta), \theta)] \quad (6)$$

$$\max_{\theta \in T_\alpha} g_j(d, z(\theta), \theta) \leq 0, j = 1, \dots, m \quad (6)$$

$$\Pr\{\theta \in T_\alpha\} \geq \alpha, \quad (7)$$

The peculiarity of problem (6) is that

- we should look for optimal forms and positions of the regions T_{α_j} and
- the search variables $z(\theta)$ are multivariate functions

We will develop an iteration method of solving problem (6) which will be based on a partition of the uncertainty region T into subregions (multidimensional rectangles $R_i^{(k)}$). Let at the k -th

iteration the region T be partitioned on a set $R^{(k)}$ of the subregions $R_i^{(k)}$

$$R_r^{(k)} = \{\theta_i : \theta_i^{(k),L,r} \leq \theta_i \leq \theta_i^{(k),U,r}, r = 1, \dots, N_k\}, \quad (8)$$

$$R_1^{(k)} \cup \dots \cup R_{N_k}^{(k)} = T \quad (9)$$

$$(R_l^{(k)}) \cap (R_q^{(k)}) = \emptyset, \quad \forall l, q \quad 1 \leq q \leq N_k, \quad 1 \leq l \leq N_k \quad (10)$$

where $(R_l^{(k)})$ is a set of interior points of the region $R_l^{(k)}$, N_k is a number of regions $R_l^{(k)}$ at the k -th iteration and l is a number of a subregion in the set $R^{(k)}$. Unfortunately it is very difficult to look for the optimal form and location of the region T_α . Therefore, we will restrict a class of possible region T_α and look for some approximation $\tilde{T}_\alpha^{(k)}$ of the region T_α . At the k -th iteration of this procedure we will solve the following problem

$$\min_{d, \tilde{z}^{(k)}(\theta), \tilde{T}_\alpha^{(k)}} E_{ap}^{(k)} [f(d, \tilde{z}^{(k)}(\theta), \theta)] \quad (11)$$

$$\max_{\theta \in \tilde{T}_\alpha^{(k)}} g_j(d, \tilde{z}^{(k)}(\theta), \theta) \leq 0 \quad j = 1, \dots, m \quad (12)$$

$$\Pr\{\theta \in \tilde{T}_\alpha^{(k)}\} \geq \alpha \quad (13)$$

where $\tilde{z}^{(k)}$ is an approximation of multivariate function $z(\theta)$, $E_{ap}^{(k)} [f(d, \tilde{z}^{(k)}(\theta), \theta)]$ is an approximation of $E[f(d, z(\theta), \theta)]$.

Approximation of the region T_α . We will look for the approximation $\tilde{T}_{\alpha_j}^{(k)}$ in the form of some union of multidimensional rectangles $T_\alpha^{l,(k)} = \{\theta_i : \theta_i^{L,J,(k)} \leq \theta_i \leq \theta_i^{U,J,(k)}, i = 1, \dots, p\}$

$$\tilde{T}_\alpha^{(k)} = T_\alpha^{1,(k)} \cup T_\alpha^{2,(k)} \cup \dots \cup T_\alpha^{N_k,(k)} \quad (14)$$

where $T_\alpha^{l,(k)}$ is the l -th subregion in the set $\tilde{T}_\alpha^{(k)}$ and N_k is the number of subregions $T_\alpha^{jJ,(k)}$ at the k -th iteration and

$$(T_\alpha^{s,(k)}) \cap (T_\alpha^{t,(k)}) = \emptyset, \quad \forall s, t = 1, \dots, N_k \quad (15)$$

Note that the number of regions $T_\alpha^{l,(k)}$ is equal to the number of the regions $R_l^{(k)}$. We will require satisfaction of the following conditions

$$T_\alpha^{l,(k)} \in R_l^{(k)}, \quad l = 1, \dots, N_k \quad j = 1, \dots, m \quad (16)$$

Since conditions (10) are met then it follows from (16) that conditions (15) are met. Taking into account (14), (15) we obtain

$$\Pr\{\tilde{T}_\alpha^{(k)}\} = \Pr\{T_\alpha^{1,(k)}\} + \Pr\{T_\alpha^{2,(k)}\} + \dots + \Pr\{T_\alpha^{N_k,(k)}\} \quad (17)$$

In this case the search of the optimal forms and locations of the regions T_{α_j} is reduced to the search of the optimal upper and lower bounds $\theta_i^{L,J,(k)}$, $\theta_i^{U,J,(k)}$ of the sides of the multidimensional rectangles $T_\alpha^{l,(k)}$. Since all the parameters θ_i are independent and have the normal distribution then the probability measure of the multidimensional rectangle $T_\alpha^{l,(k)}$ is equal to multiplication of the probability measures of the intervals $I_i^{l,(k)} = [\theta_i^{L,J,(k)} \leq \theta_i \leq \theta_i^{U,J,(k)}]$. Thus, we have

$$\Pr\{\theta \in T_\alpha^{l,(k)}\} = \prod_{i=1}^p [\Phi((\theta_i^{U,J,(k)} - E[\theta_i])\sigma_i^{-1}) - \Phi((\theta_i^{L,J,(k)} - E[\theta_i])\sigma_i^{-1})], \quad (18)$$

where $\Phi(\eta)$ is the standard normal distribution function

Substituting the expressions for $\Pr\{T_\alpha^{l,(k)}\}$ from (18) in (17) we obtain

$$\Pr\{\tilde{T}_\alpha^{(k)}\} = \sum_{l=1}^{N_k} \prod_{j=1}^p [\Phi(\hat{\theta}_i^{U,J,(k)}) - \Phi(\hat{\theta}_i^{L,J,(k)})] \quad (19)$$

Approximation of multivariate functions. We will look for an approximate solution of problem (11) in the supposition that the control variables $z(\theta)$ will be piece-wise constant functions $\tilde{z}^{(k)}(\theta)$ of the following form

$$\tilde{z}^{(k)}(\theta) = z^{l,(k)} \text{ if } \theta \in R_l^{(k)}, \quad l = 1, \dots, N_k \quad (20)$$

It is easy seen that if at each iteration $N_k = 1$ then TSOPCC is transformed into OSOPCC. For the approximate calculation of the expected value of the function $f(d, \tilde{z}^{(k)}, \theta)$ we will use the piecewise linear approximation $\tilde{f}(d, \tilde{z}^{(k)}, \theta)$ of the function $f(d, \tilde{z}^{(k)}, \theta)$ of the following form

$$\begin{aligned} \tilde{f}(d, \tilde{z}^{(k)}, \theta) &= \tilde{f}(d, \tilde{z}^{l,(k)}, \theta, \theta_l^{(k)}) \text{ if } \theta \in R_l^{(k)} \quad l = 1, \dots, N_k \\ \tilde{f}(d, \tilde{z}^{r,(k)}, \theta, \theta_r^{(k)}) &= f(d, \tilde{z}^{r,(k)}, \theta_r^{(k)}) + \sum_{i=1}^{N_k} \frac{\partial f(d, \tilde{z}^{r,(k)}, \theta_r^{(k)})}{\partial \theta_i} (\theta_i - \theta_{ri}^q) \end{aligned} \quad (21)$$

and $\theta_{ri}^{(k)}$ is the i -th component of the vector $\theta_r^{(k)}$. For the expected value approximation we use the same partition of the uncertainty region as for approximation of the regions T_{α_j} and multivariable functions. The right-hand side of formula (21) is the linear part of the Taylor's expansion of the function $f(d, \tilde{z}^{r,(k)}, \theta)$ at the point $\theta_r^{(k)}$. The points $\theta_r^{(k)}$, $r = 1, \dots, N_k$ are the *linearization points*. They will coincide with the middle points of the subregions $T_r^{(k)}$. It is easy to obtain the following expression

$$\int_{T_r^{(k)}} \tilde{f}(d, \tilde{z}^{r,(k)}, \theta, \theta_r^{(k)}) \rho(\theta) d\theta = a_r f(d, \tilde{z}^{r,(k)}, \theta_r^{(k)}) + \sum_{i=1}^p \frac{\partial f(d, \tilde{z}^{r,(k)}, \theta_r^{(k)})}{\partial \theta_i} (E[\theta_i; T_r^{(k)}] - a_r \theta_{ri}^{(k)}) \quad (22)$$

where $a_r = \int_{T_r^{(k)}} \rho(\theta) d\theta$, $E[\theta_i; T_r^{(k)}] = \int_{T_r^{(k)}} \theta_i \rho(\theta) d\theta$. One can show that calculation of the values a_r and $E[\theta_i; T_r^{(k)}]$ is reduced to calculation of some one-dimensional integrals.

As an approximation of the expected value $E[f(d, \tilde{z}^{(k)}(\theta), \theta); T]$ we will use the following expression

$$E_{ap}^{(k)} [f(d, \tilde{z}^{(k)}(\theta), \theta)] = \sum_{r=1}^{N_k} \int_{T_r^{(k)}} \tilde{f}(d, \tilde{z}^{r,(k)}, \theta, \theta_r^{(k)}) \rho(\theta) d\theta \quad (23)$$

Using (23), (19), (22) it is easy to transform problem (11) into the following optimization problem which will be solved at k -th iteration

$$\begin{aligned} f^{(k)} &= \min_{d, \tilde{z}^{l,(k)}, \theta_r^{l,(k)}, \theta_r^{j,(k)}} E_{ap}^{(k)} [f(d, \tilde{z}^{(k)}(\theta), \theta); T] \\ &\max_{\theta \in \alpha^{l,(k)}} g_j(d, \tilde{z}^{l,(k)}, \theta) \leq 0, \quad j = 1, \dots, m, \quad l = 1, \dots, N_k \\ &\sum_{l=1}^{N_k} \prod_{r=1}^p [\Phi(\hat{\theta}_i^{U,j,l,(k)}) - \Phi(\hat{\theta}_i^{L,j,l,(k)})] \geq \alpha_j, \quad j = 1, \dots, m \\ &T_{\alpha}^{l,(k)} \in R_l^{(k)}, \quad l = 1, \dots, N_k \end{aligned} \quad (24)$$

Problem (24) is a semi-infinite programming problem. For solving problem (24) one can use the outer approximations method (Hettich, Kortanek, 1993). We will partition one or several subregions $R_l^{(k)}$ at each iteration for improvement of the approximations of the regions T_{α_j} , the piece-wise constant approximation of multivariate functions $z(\theta)$ functions and the approximation of the expected value of the goal function. Thus, the solution of problem (24) does not require the numerical calculation of multiple integrals.

Conclusion

References

Hettich R. and Kortanek K.O., 1993, Semi-infinite programming: Theory, methods and applications, SIAM Review, 35, 380-429.

Simulations of instationary operated heterogeneous catalytic reactions

F.J. Keil, A. Garayhi
Hamburg University of Technology, Hamburg, Germany

In general, in a temporal analysis of products (TAP) reactor a pulse-response experiment is executed by a small and narrow pulse of a gas mixture which is sent into an evacuated packed microreactor. The injected molecules of gas travel through the microreactor via Knudsen diffusion and eventually escape into an adjacent vacuum chamber containing a QMS detector. A rectangular pulse input corresponds to an infinite Fourier series of trigonometric functions. That means very many frequencies are simultaneously stimulated. Instead, we propose a sinusoidal input of the reactant gas mixture employing various frequencies and amplitudes. In doing so, one can find out many details about adsorption/desorption and reactions inside the pellets. For this purpose the catalyst pellets were modeled as heterogeneous supports. The gas phase and solid phase being spatially inhomogeneous, that means the catalyst distribution can be arbitrary, are taken into account. The diffusion is calculated by the dusty-gas model. Adsorption/desorption processes are considered as chemical reactions, i.e. gaseous and adsorbed species are modeled as different species. The elementary steps of reactions can be presented, and the reactors are simulated as networks of continuous stirred tanks which show the same residence time distribution as the real reactor. As an example one then obtains the following reduced system of equations for the isothermal case, whereby for each cell one has to solve the pellet equations:

$$\frac{\partial(\psi \mathbf{x})}{\partial \theta} = \frac{\partial}{\partial z} \left[\left(\beta^0 \frac{1}{\tau} (\psi \mathbf{x}) e^T + \delta \frac{1}{\tau} \right) \frac{\partial(\psi \mathbf{x})}{\partial z} \right] + \frac{1}{\varepsilon} \sum_{j=1}^{n_R} \mathbf{v}_j w_j \quad (\text{gas})$$

$$\frac{\partial(\psi \mathbf{x})}{\partial \theta} = \frac{\partial}{\partial z} \left(\delta^S \frac{1}{\tau} \right) \frac{\partial(\psi \mathbf{x})}{\partial z} + \frac{1}{1-\varepsilon} \sum_{j=1}^{n_R} \mathbf{v}_j w_j \quad (\text{adsorbed phase})$$

Reactor equation

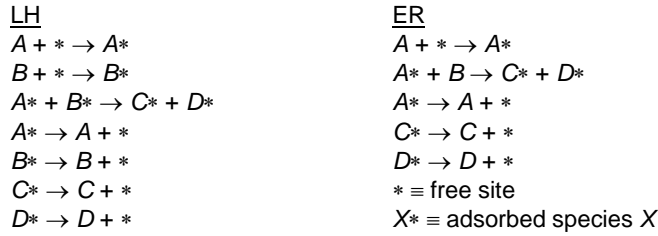
$$\frac{d\mathbf{x}_R}{d\theta} = \frac{1}{\theta_R} (\mathbf{x}_{in} - \mathbf{x}) - \kappa \cdot \varepsilon \cdot (1 - \mathbf{x}_R e^T) \left(\frac{1}{\tau} \mathbf{x} \Big|_{z=0.5} e^T + \delta \right) \frac{\partial \mathbf{x}}{\partial z} \Big|_{z=0.5}$$

Boundary conditions

$$\frac{\partial(\psi \mathbf{x})}{\partial z} = 0 \quad \text{and} \quad Bi \cdot (\mathbf{x}_R - \mathbf{x}) = \frac{1}{\tau} (\mathbf{x} e^T + \delta) \frac{\partial \mathbf{x}}{\partial z} \quad (\text{symmetry}) \quad \text{or} \quad x(z=0.5) = x_R$$

Bi \equiv Biot number, ψ \equiv pressure ratio ($p/p_{z=0.5}$) \mathbf{x} \equiv molar fraction, β^0 \equiv convective factor ($r_p^2 \cdot p|_{z=0.5} / (8\eta\Delta)$), δ \equiv dimensionless diffusion matrix, z \equiv pellet coordinate, τ \equiv residence time, \mathbf{v}_j \equiv stoichiometric coefficients, w \equiv dimensionless reaction rate, \mathbf{e} \equiv vector with all elements equal to one

By using the a. m. model, the instationary behavior of the reaction $A + B \rightarrow C + D$ has been investigated. The following Langmuir-Hinshelwood and Eley-Rideal schemes have been employed:



The inflow of component B is maintained constant whilst component A is supplied sinusoidal. An inert component is also fed into the reactor to keep the residence time constant.

A very important result is that component B oscillates also inside the reactor although its feed is constant. The oscillations are induced by various mechanisms. The first mechanism is a depletion of component A in the gas phase owing to penetration of the pores and adsorption. This results in a high concentration of B in one period when the concentration of A is also high. That means both components oscillate in phase. This phenomenon is more pronounced in the ER mechanism compared to the LH mechanism. Coadsorption may also induce oscillations if the sorption processes and equilibration are running very fast, but the surface reaction is so slow that a large part of the reactants desorbs before reacting. Fast chemical reactions also lead to oscillations of B which is depleted in case the concentration of A is high. In case of an ER mechanism the concentrations of A and B oscillate by a half period phase shift. If the surface reaction is rate determining, this phenomenon occurs also for the LH mechanism. Fig. 1 shows an example of the oscillations of B for a LH mechanism and various adsorption constants.

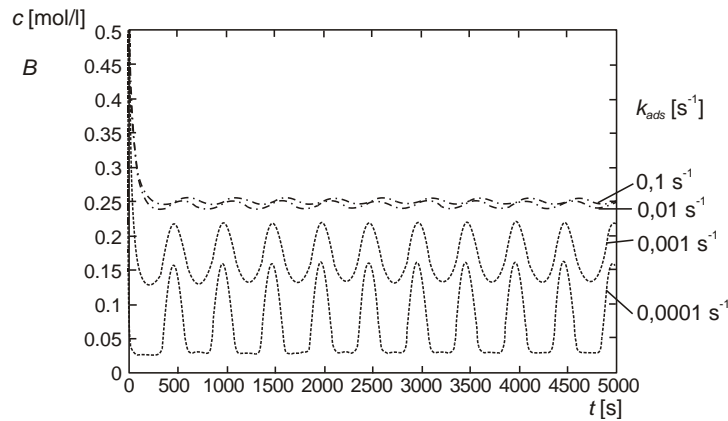


Fig. 1

As the three induction mechanisms lead to different phase shifts, the phase shifts give an indication of the rate determining step. A diffusion resistance has primarily effect on the phase shift. Additionally, nonlinear distortions of the response curves may be observed. This means that the fundamental frequency stimulates higher frequencies.

The influence of various parameters on the response will be demonstrated.

Integration of DFT calculations into microkinetic analysis: Application to carbon dioxide hydrogenation on ceria

Zhuo Cheng and Cynthia S. Lo
Department of Energy, Environmental and Chemical Engineering
Washington University in St. Louis

April 1, 2015

1 Introduction

Heterogeneous catalysis involves the complex interplay of structure, properties, and activity across length and time scales. Thus, multiscale modeling can be an effective method to predict catalyst behavior and guide experimental studies. In particular, density functional theory (DFT) calculations, coupled with microkinetic modeling, can give insight into how the electronic structure of the catalyst dictates activity and selectivity. Macroscopic reaction observables can thus be obtained, with quantitative accuracy, from first principles, given the atomistic structure of the reacting system. Transition state theory is employed with a modified Brønsted-Evans-Polanyi relation to obtain the input parameters to the reactor design equations, which, in turn, are solved to obtain the reaction rate coefficients, turnover frequencies, and surface coverages.

This method [1] is applied to model the hydrogenation of carbon dioxide to methanol (Figure 1) and methane on a reduced ceria catalyst. Carbon dioxide utilization is receiving increased attention due to both the industrial importance of fuel production and the environmental significance of greenhouse gas utilization [2, 3]. Methanol, as a liquid fuel, can be effectively used as a source of energy and thus close the carbon cycle. Alternatively, methanol can be used as the raw material for other synthetic hydrocarbons by the MTO (methanol to olefins) process. The hope is that the carbon dioxide generated from fossil fuel combustion can then be activated [4] and chemically recycled by converting it back to methanol via hydrogenation.

2 Results

Two reaction channels to methanol are identified: 1. COOH pathway via a carboxyl intermediate and 2. HCOO pathway via a formate intermediate. While formaldehyde (H_2CO) appears to be the key intermediate for methanol synthesis, other intermediates, including carbene diol, formic acid and methynol, are not feasible due to their high formation energies. Furthermore, direct formyl hydrogenation to formaldehyde is not feasible due to its high activation barrier (Figure 2).

Instead, we find that conversion of H-formalin (H_2COOH^*) to formaldehyde is kinetically more favorable. The formaldehyde is then converted to methoxy (H_3CO^*), and finally hydrogenated to form methanol. Our calculated results for vibrational entropy, heat capacity, and reaction enthalpy are in good agreement with corresponding values in the published literature, which validates our choice of methodology. Microkinetic analyses reveal the rate-limiting steps in the reaction network and establish that the HCOO route is the dominant pathway for methanol formation on this catalyst (Figure 3).

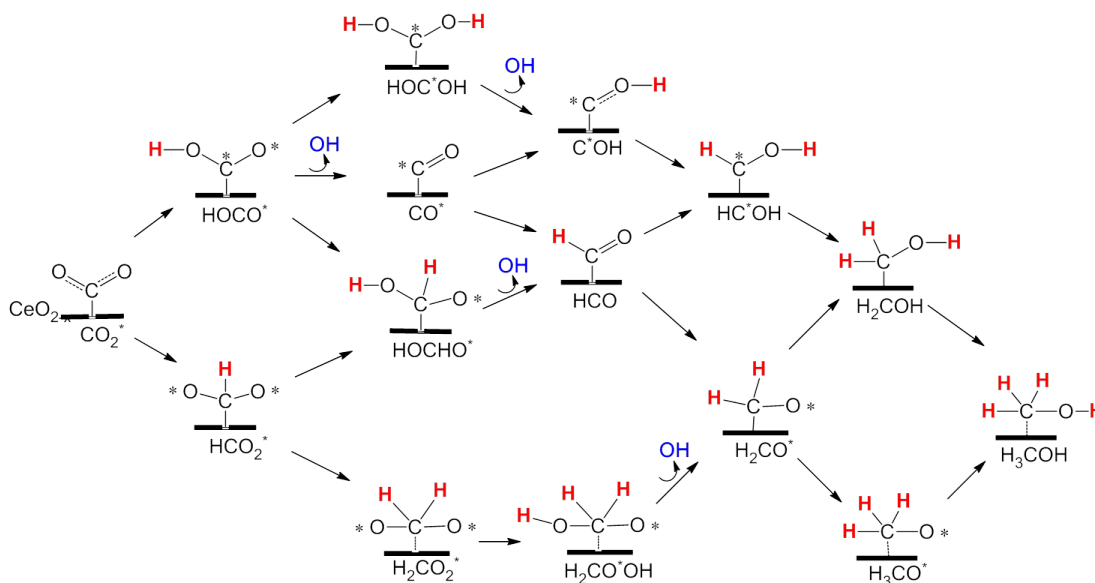


Figure 1: Schematic of hydrogenation network for upgrading CO₂.

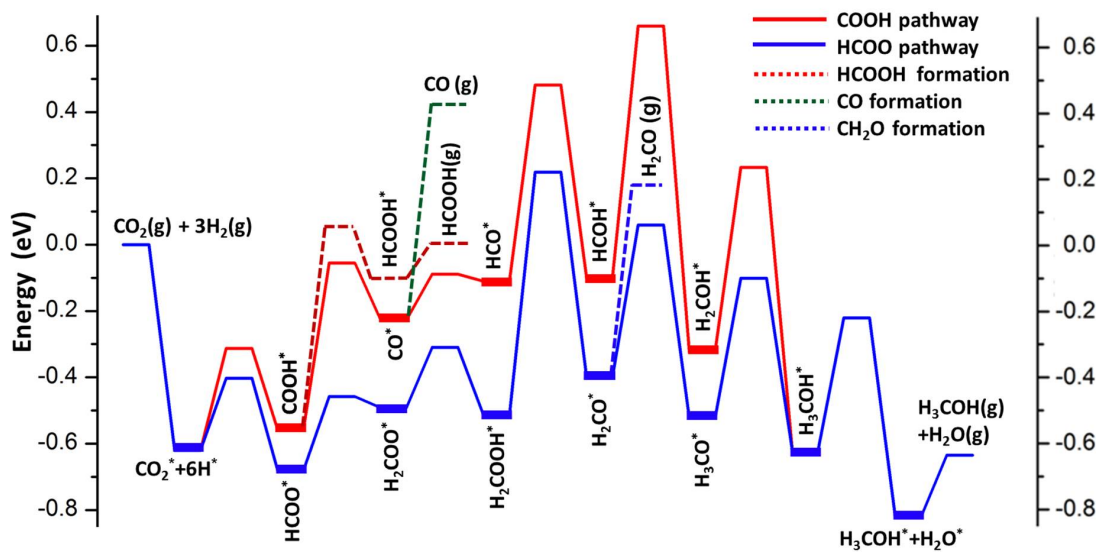


Figure 2: Hydrogenation Energy Profile

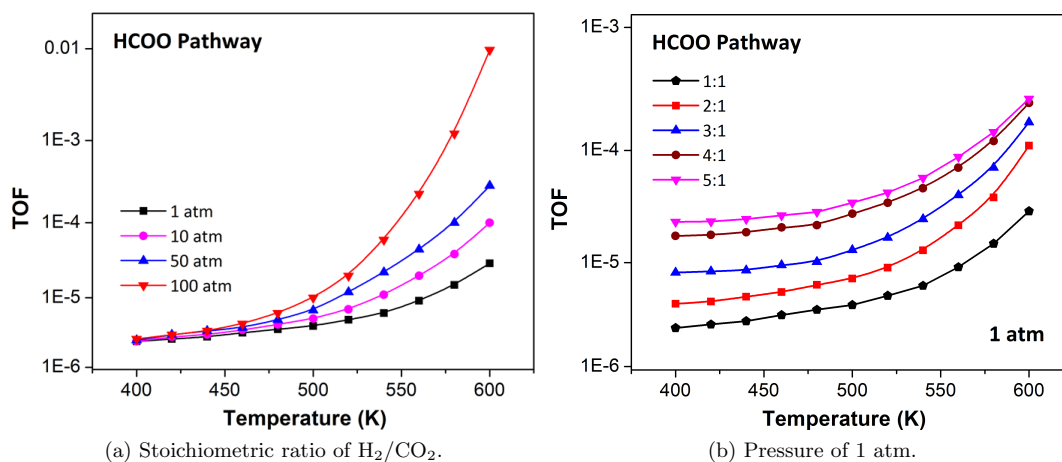


Figure 3: Temperature and (a) pressure and (b) H_2/CO_2 ratio dependence on TOF for HCOO pathway.

3 Conclusions

Carbon dioxide hydrogenation to methanol on a reduced ceria catalyst should predominantly follow the formate pathway. In this pathway, H-formalin is converted to formaldehyde in the rate-limiting step, followed by further hydrogenation to form a surface-bound methoxy group and finally, methanol. Furthermore, our analysis of the turnover frequency suggests that a moderately high H_2/CO_2 feed ratio can facilitate carbon dioxide hydrogenation to methanol. The methodology proposed here is also broadly applicable to the analysis of chemical reaction networks.

References

- [1] Zhuo Cheng and Cynthia S. Lo. Propagation of olefin metathesis to propene on WO_3 catalysts: A mechanistic and kinetic study. *ACS Catal.*, 5:59–72, 2015.
- [2] Vesna Havran, Milorad P. Duduković, and Cynthia S. Lo. Conversion of methane and carbon dioxide to higher value products. *Ind. Eng. Chem. Res.*, 50(12):7089–7100, 2011.
- [3] Eunmin Lee, Zhuo Cheng, and Cynthia S. Lo. Present and future prospects in heterogeneous catalysts for C1 chemistry. In James Spivey, editor, *Catalysis*, volume 27, pages 187–208. The Royal Society of Chemistry, Cambridge, 2015.
- [4] Zhuo Cheng, Brent J. Sherman, and Cynthia S. Lo. Carbon dioxide activation and dissociation on ceria (110): A density functional theory study. *J. Chem. Phys.*, 138(1):014702, 2013.

Explicit formulas for reaction probability in reaction-diffusion experiments

M. Wallace^{*1}, R. Feres^{†1}, G. Yablonsky^{‡2} and A. Stern^{§1}

¹Department of Mathematics, Washington University

²Department of Chemistry, Saint Louis University

1 INTRODUCTION

We consider reaction-diffusion systems of the following kind: Pulses of a reactant gas are injected into a chemical reactor whose interior has been filled with a chemically inert, permeable to gas diffusion, solid medium containing a number of small metal catalyst particles. Reaction at the catalytic sites is assumed to be of first order and gas transport is by Knudsen diffusion. The outflow of gas from the reactor is then measured for the fraction of reaction product in a mixture containing the product and unreacted gas. Our goal is to find formulas that express this value as a function of the chemical reaction constant and the reactor geometric configuration (position and number of catalyst particles, shape of reactor and of the catalyst particles, place of gas injection, etc.) Our main results are as follows. We first show that reaction probability can be effectively computed by a time-independent boundary value problem for Laplace's equation. This boundary value problem often admits relatively simple one-dimensional network models on so-called metric graphs. The usefulness of these network models, which we refer to as *generalized thin zone* systems, lies in that it provides explicit formulas for reaction probability that can be used as reference, or approximation, for the more realistic three-dimensional reactors. We also undertake a systematic study of Temporal Analysis of Products (TAP)-like configurations for one or more catalyst particles in which we solve the three-dimensional boundary value problem numerically and compare the results with explicit formulas obtained for the generalized thin-zone systems. The problem of determining optimal particle configuration that maximizes reaction probability is investigated in a few simple cases.

*One Brookings Dr., St. Louis, MO, 63130; matt@math.wustl.edu

†One Brookings Dr., St. Louis, MO, 63130; feres@math.wustl.edu; — Corresponding author

‡3450 Lindell Blvd, St. Louis, MO, 63103; gyablons@slu.edu

§One Brookings Dr., St. Louis, MO, 63130; astern@math.wustl.edu

2 MAIN RESULTS

- It is shown by stochastic analysis that the problem of conversion in general reactor configurations in dimensions 2 or 3 is solved by a time-independent boundary value problem for Laplace's equation (or, more generally, a Feynman-Kac equation) with mixed (Dirichlet, Neumann, Robin) boundary conditions. This provides an effective computational tool.

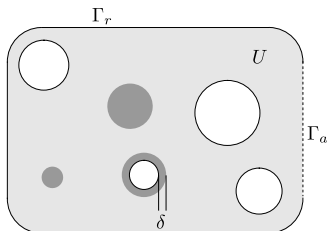


Figure 1: The reaction probability is the solution of a time independent boundary value problem for the Feynman-Kac operator on the domain U with Neumann boundary condition on the *reflecting boundary* Γ_r and boundary value 0 on the *absorbing boundary* Γ_a . The reaction rate term $kq(\mathbf{x})$ is assumed to be supported on a relatively small region of U , indicated by the darker grey sets, called *active sites*.

Here are some details. It is convenient to formulate the problem for the *survival function* $\psi(\mathbf{x})$, representing the probability that a single gas molecule of type A , injected into U at the initial position \mathbf{x} , will eventually leave U through Γ_a without having converted into B . The complementary probability of conversion to B will be denoted $\alpha(\mathbf{x}) = 1 - \psi(\mathbf{x})$. If the overall reaction constant is k and the diffusion constant is \mathcal{D} (assuming uniform Fickian diffusivity) then $\psi(\mathbf{x})$ satisfies

$$\mathcal{D}\Delta\psi - kq(\mathbf{x})\psi = 0 \text{ on } U$$

with boundary conditions

$$\begin{aligned} \mathbf{n} \cdot \nabla\psi &= 0 \text{ on } \Gamma_r \\ \psi &= 1 \text{ on } \Gamma_a. \end{aligned}$$

If the active sites are all collar regions of thickness δ as in Figure 1, the problem of finding the survival function can be restated in terms of Laplace's equation $\Delta\psi = 0$ in U with mixed Dirichlet-Neumann-Robin conditions on the boundary. Specifically, with Γ_c denoting the boundary of the region occupied by catalyst particles, and Γ_r now denoting the complement of Γ_c in the reflecting boundary, we have:

$$\begin{aligned} \mathbf{n} \cdot \nabla\psi &= 0 \text{ on } \Gamma_r \\ \mathbf{n} \cdot \nabla\psi &= \kappa\psi \text{ on } \Gamma_c \\ \psi &= 1 \text{ on } \Gamma_a \end{aligned}$$

Here $\kappa := \frac{\delta k}{\mathcal{D}}$ can be regarded as an *effective* reaction constant.

- We obtain general approximate solutions based on exact solutions for network models mentioned below. The following is shown to hold very well when the catalyst is a single particle of a relatively small size:

$$(2.1) \quad \alpha(\mathbf{x}) = P(\mathbf{x}) \frac{\lambda \kappa}{1 + \lambda \kappa}$$

Here, $P(\mathbf{x})$ is the probability that a molecule of A injected at \mathbf{x} will hit the catalyst particle. Under the assumption of Fickian diffusion $P(\mathbf{x})$ solves Laplace's equation $\Delta P(\mathbf{x}) = 0$ in U , together with the boundary conditions:

$$\begin{aligned} \mathbf{n} \cdot \nabla P &= 0 \text{ on } \Gamma_r \\ P &= 1 \text{ on } \Gamma_c \\ P &= 0 \text{ on } \Gamma_a \end{aligned}$$

- The above conversion formula is greatly generalized in a network approximation, where we suppose the catalyst to consist of a finite number of points. Then

$$\alpha(\mathbf{x}) = P_0(\mathbf{x}) - \sum_{v \in \mathcal{C}} P_v(\mathbf{x}) \frac{\lambda_v(\kappa)}{\lambda(\kappa)}$$

where $P_0(\mathbf{x})$ is the probability of hitting a catalyst at all and $P_v(\mathbf{x})$ is the probability of hitting at vertex v ; λ and λ_v are polynomial functions whose coefficients contain geometric information.

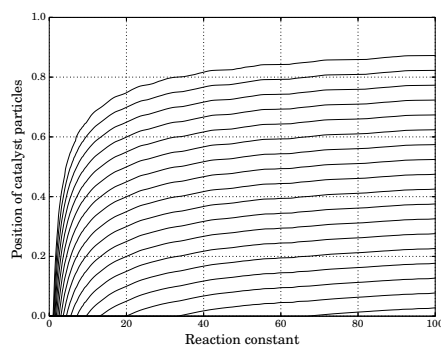


Figure 2: Optimal configuration of a multi-particle thin zone system.

- We undertake a detailed analysis of various configurations of a Temporal Analysis of Products (TAP)-reactor, including one catalyst particle, two particles, approximations of thin zone systems, among others. We obtain detailed dependence of conversion on particle shape and position parameters. We also study optimal configurations that maximize conversion in multiparticle systems.

Stochastic effects in autocatalysis

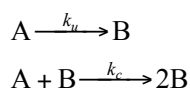
Gábor Lente

Department of Inorganic and Analytical Chemistry, University of Debrecen,
Egyetem tér 1, H-4032 Debrecen, Hungary, e-mail: lenteg@science.unideb.hu

The most widely used mathematical approach to chemical kinetics relies on concentrations, which are assumed to be continuous functions of time. However, it is now well understood that when very small amounts of substance are involved, the particulate nature of matter makes this approach untenable and the computationally often more demanding stochastic kinetics must be used as an alternative.¹

This contribution will show that the use of stochastic kinetics may be inevitable in interpreting experimentally observed results in autocatalytic systems even if the amounts of substance involved are quite macroscopic. Chemical examples of this phenomenon include seemingly random distributions of enantiomers in the Soai reaction,^{2,3} and large fluctuations in the clock time of certain Landolt-type reactions.^{4,5} Strong autocatalysis was confirmed in all of these systems²⁻⁵ and the stochastic approach was successfully used to interpret the enantiomeric excess and Landolt time distributions.⁶⁻⁸

Autocatalysis is a kinetic phenomenon that involves positive feedback. When the feedback is very strong compared to other processes, the kinetic role of just a handful of product molecules may be significant enough to influence the overall reaction, which provides exactly the conditions where the use of stochastic kinetics is inevitable. The following simple autocatalytic scheme will be of particular interest:



The deterministic rate equation describing the change of concentration of reactant A is as follows:

$$\frac{d[A]}{dt} = -k_u[A] - k_c[A][B] = -k_u[A] - k_c[A]([A]_0 + [B]_0 - [A])$$

In this rate equation, $[A]_0$ and $[B]_0$ represent the initial concentrations of these two species. This rate equation can be solved analytically.⁹

$$[A] = \frac{(k_u + k_c[A]_0 + k_c[B]_0)[A]_0 e^{-(k_u + k_c[A]_0 + k_c[B]_0)t}}{(k_u + k_c[A]_0 + k_c[B]_0) - k_c[A]_0 (1 - e^{-(k_u + k_c[A]_0 + k_c[B]_0)t})}$$

In the corresponding stochastic kinetic description, molecule numbers (a for A and $b = a_0 + b_0 - a$ for B) are used instead of concentrations. The direct equivalent of the rate equation is the stochastic master equation, which describes the time-dependent probability, denoted $P_a(t)$, that the systems contains exactly a molecules of species A at time instant t :

$$\frac{dP_a}{dt} = [\kappa_u(a+1) + \kappa_c(a+1)(a_0 + b_0 - a - 1)]P_{a+1} - [\kappa_u a + \kappa_c a(a_0 + b_0 - a)]P_a$$

As all master equations in stochastic kinetics, this a system of linear differential equations, whose solution can be given symbolically in the following form:

$$P_a = \sum_{i=0}^{a_0-a} X_{a,i} e^{-[\kappa_u(a_0-i) + \kappa_c(a_0-i)(b_0+i)]}$$

In this formula, $X_{a,i}$ represent multiplication factors that can be calculated in a recursive manner for $a = a_0, a_0 - 1, a_0 - 2, a_0 - 3$, etc.

The contribution will compare the two different approaches and identify the conditions under which the deterministic rate equation cannot be used. These results will be visualized by using stochastic maps, which were recently introduced in the case of first order reaction networks.¹⁰ Preliminary results will also be presented on how the dependence of the observations on stirring rate, a paramount feature in experimental systems,^{4,5} can be modelled using the stochastic approach.

References:

1. P. Érdi, G. Lente, *Stochastic Chemical Kinetics - Theory and (Mostly) Systems Biological Applications*; Springer: New York, Heidelberg, Dordrecht, London, 2014.
2. K. Soai, I. Sato, T. Shibata, S. Komiya, M. Hayashi, Y. Matsueda, H. Imamura, T. Hayase, H. Morioka, H. Tabira, J. Yamamoto, Y. Kowata, *Tetrahedron: Asymm.* **2003**, *14*, 185-188.
3. T. Kawasaki, K. Suzuki, M. Shimizu, K. Ishikawa, K. Soai, *Chirality* **2006**, *18*, 479-482.
4. I. Nagypál, I. R. Epstein, *J. Phys. Chem.* **1986**, *90*, 6285-6292.
5. I. Nagypál, I. R. Epstein, *J. Chem. Phys.* **1988**, *89*, 6925-6928.
6. G. Lente, *J. Phys. Chem. A* **2005**, *109*, 11058-11063.
7. G. Lente, *Symmetry* **2010**, *2*, 767-798.
8. É. Dóka, G. Lente, *J. Am. Chem. Soc.* **2011**, *133*, 17878-17881.
9. G. Lente, *Deterministic Kinetics in Chemistry and Systems Biology*; Springer: New York, Heidelberg, Dordrecht, London, 2015.
10. G. Lente, *J. Chem. Phys.* **2012**, *137*, 164101.

OSCILLATING REGIMES OF FIRST ORDER PHASE TRANSITION

Bykov V.I., Emanuel Institute of Biochemical Physics, Russian Academy of Sciences,

Russia, Moscow, Kosygin St., 4, vibykov@mail.ru

Tsybenova S.B., Emanuel Institute of Biochemical Physics, Russian Academy of Sciences,

Russia, Moscow, Kosygin St., 4, s.tsybenova@gmail.com

In this work we propose the simplest dynamic model of a first order phase transition [1] and perform its parametric analysis. Conditions have been recognized for the existence of three and five steady states; the ranges of the parameters where autooscillations exist in a dynamic system have been found; and parametric and phase portraits of the mathematical model have been built. The process dynamics in the vicinity of a phase transition point has been shown to can be rather complex. For phase transitions of the type

$$F_1 \leftrightarrow F_2 \quad (1)$$

in a system where there is heat exchange with the environment, a dimensionless spatially homogeneous model can be represented as

$$\frac{dx}{dt} = -f_1(y)x + f_2(y)(1-x), \quad (2)$$

$$\frac{dy}{dt} = \beta_1 f_1(y)x + \beta_2 f_2(y)(1-x) + s(1-y), \quad (3)$$

where

$$f_i(y) = Da_i \exp(\gamma_i(1-1/y)), \quad i = 1, 2, \quad (4)$$

x and y are dimensionless concentration and temperature, respectively; dimensionless parameters Da_i , s , γ_i , and β_i .

Parametric dependences are easily derived in an explicit form from the stationary equation, for example,

$$s(y) = \frac{(\beta_1 + \beta_2)f_1(y)f_2(y)}{(y-1)(f_1(y) + f_2(y))}, \quad (5)$$

$$(\beta_1 + \beta_2)(y) = \frac{s(y-1)(f_1(y) + f_2(y))}{f_1(y)f_2(y)}, \quad (6)$$

$$Da_1(y) = \frac{s(y-1)f_2(y) \exp(\gamma_1(1-1/y))}{(\beta_1 + \beta_2)f_2(y) - s(y-1)}, \quad (7)$$

$$\gamma_1(y) = \frac{y}{y-1} \ln \frac{s(y-1)f_2(y)}{Da_1(\beta_1 + \beta_2)f_2(y) - s(y-1)}, \quad (8)$$

The examples of parameter curves based on (5)–(8) are shown in Figs. 1 and 2, where we can see regions with one, three and five steady states. The multiplicity of steady states gives rise to a hysteresis on the temperature curves.

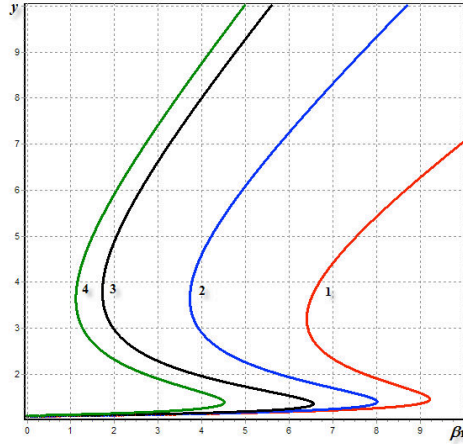


Fig. 1. Dimensionless steady state temperature vs. parameter β_1 for $s = 13$, $\gamma_1 = 5$, $\beta_2 = 8$, $Da_1 = 0.1$ and $Da_2 = 0.35$. Parameter γ_2 varies as follows: (1) 4, (2) 5, (3) 7, and (4) 20.

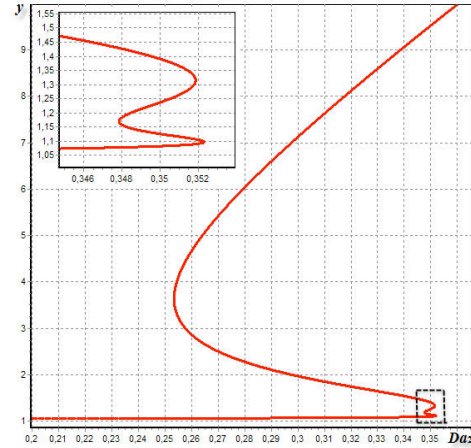


Fig. 2. Parametric dependence $y(Da_2)$ for $Da_1 = 0.1$, $\beta_1 = -4.4$, $\beta_2 = 8$, $\gamma_1 = 25.7$, $\gamma_2 = 5$, $s = 13$.

For example, bifurcation curve of multiplicity (L_Δ) is given by the condition

$$\frac{(\beta_1 + \beta_2)f_1^2(y)f_2^2(y)}{y^2(f_1(y) + f_2(y))^2} \left(\frac{\gamma_1}{f_1(y)} + \frac{\gamma_2}{f_2(y)} \right) = s. \quad (9)$$

and curve of neutrality (L_σ) by

$$\left(\beta_1 \frac{\gamma_1}{y^2} x - 1 \right) f_1(y) + \left(\beta_2 \frac{\gamma_2}{y^2} (1-x) - 1 \right) f_2(y) = s. \quad (10)$$

Together with (5)–(8) equalities (9) and (10) allow to write equations for curves L_Δ and L_σ in an explicit form on the plane of the two parameters.

Fig. 3 shows one of the possible parametric portraits of the nonlinear dynamic model (2) and (3). The curves of multiplicity L_Δ and neutrality L_σ define the range of parameters that differ in the number and stability of steady states. In the case of the one unstable steady state there are autooscillations for model (2), (3) (Fig. 4). From any initial data, the system goes to the autooscillation mode. The range of parameters for which there are oscillations is quite narrow. Therefore, for detection of autooscillation it requires a consistent parametric analysis of an investigated mathematical model.

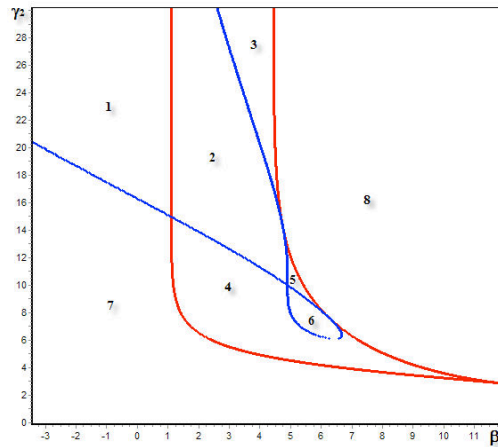


Fig. 3. Parametric portrait on the plane (β_1, γ_2) for $Da_1 = 0.1$, $Da_2 = 0.35$, $\beta_2 = 8$, $\gamma_1 = 5$, $s = 13$.

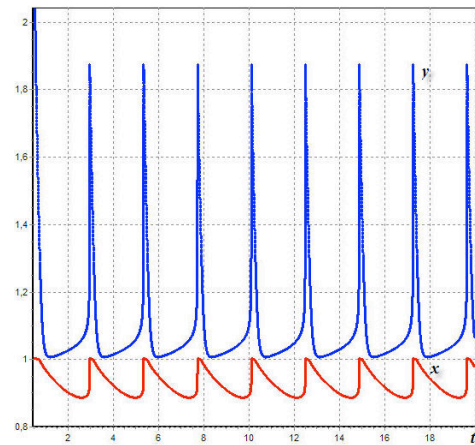


Fig. 4. Time dependences of the model (2), (3) $x(t)$, $y(t)$ for autooscillation mode $Da_1 = 0.1$, $Da_2 = 0.35$, $\beta_1 = -1$, $\beta_2 = 8$, $\gamma_1 = 5$, $\gamma_2 = 20$, $s = 13$.

To summarize, dynamic model (2), (3) can be regarded as the simplest basic model of a first order phase transition. The parametric analysis of this model shows that it can have one, three, or five steady states. The parameter regions have been found where autooscillations exist in a dynamic system; characteristic parameter and phase portraits have been built for the mathematical model [2–6]. The process dynamics in the vicinity of a phase transition point can be rather complex. Its characteristic features can be hysteresis of temperature dependences, undamped temperature and concentration oscillations, and considerable dynamic bursts as the system tends to acquire a steady state.

REFERENCES

1. Prigogine, I.R. and Kondepudi, D. *Modern Thermodynamics: From Heat Engines to Dissipative Structures*, Chichester: Wiley, 1998.
2. Bykov, V.I. and Tsybenova, S.B., *Teor. Osn. Khim. Technol.*, 2003, vol. 37, no. 1, pp. 64–75.
3. Bykov, V.I., Tsybenova, S.B., and Slin'ko, M.G., *Dokl. Phys. Chem.*, 2001, vol. 378, nos. 1–3, pp. 134–137 [*Dokl. Akad. Nauk*, 2001, vol. 378, no. 2, pp. 214–217].
4. Bykov, V.I., Tsybenova, S.B., and Slin'ko, M.G., *Dokl. Phys. Chem.*, 2001, vol. 378, nos. 1–3, pp. 138–141 [*Dokl. Akad. Nauk*, 2001, vol. 378, no. 3, pp. 355–358].
5. Bykov, V.I., *Modelirovanie kriticheskikh yavlenii v khimicheskoi kinetike (Modeling of Critical Phenomena in Chemical Kinetics)*, Moscow: Editorial URSS, 2006.
6. Bykov, V.I., Tsybenova, S.B. *Nelinejnye modeli himicheskoi kinetiki (Nonlinear models of chemical kinetisc)*, Moscow: Editorial KRASAND, 2011.

Low-dimensional Modeling of Reactions and Transport in Stratified Microflows

Jason R. Picardo^{*1} and S. Pushpavanam²

Department of Chemical Engineering, Indian Institute of Technology Madras,
Chennai, 600036, India

corresponding author*

^{*1}picardo21@gmail.com , ²spush@iitm.ac.in

1 Introduction

In recent years many mass transfer operations and two-phase reactions have been carried out in microchannels, with the aim of improving process efficiency. Microchannels offer advantages such as high surface to volume ratio, low inventories and well defined laminar flow fields. Applications of *stratified* microflows include liquid-liquid extraction [1], phase transfer catalysis [2, 3] and membraneless microfluidic fuel cells [4].

Mathematical models of these systems consist of partial differential equations (PDEs) for each phase, which describe transverse diffusion, axial convection and reactions. These models must generally be solved numerically. They contain a large number of parameters, all of which can affect the system performance. Thus analysis of the system, across parameter space, and optimization using these PDE models becomes quite tedious.

In this work, we derive reduced order models or averaged models of the system, which retain all the physical parameters. These models describe the evolution of the transversely averaged concentration along the length of the channel. They reduce computation time and aid in analysis, design and optimization. Such models can also be used to gain insight into the physics of the process.

To average the equations, we use the Lyapunov-Schmidt (LS) reduction technique. This technique has been effectively applied by Balakotaiah and coworkers to average partial differential equations of the convection-diffusion-reaction type [5, 6, 7]. Two different reduced order models are obtained: the One Equation Averaged (OEA) model and the Two Equation Averaged model (TEA).

2 Averaged Models for Reactive Extraction

In this section, we discuss averaged models developed for reactive extraction in stratified flow. The process consists of two fluids flowing alongside each other with a flat inter-fluid interface, in a microchannel. This flow is modeled as flow between two parallel flat plates. The carrier fluid enters with solute, while the solvent fluid enters without any solute. As the fluids flow along the channel, the solute diffuses from the carrier phase into the solvent phase, where it undergoes a reaction of the type $A \rightarrow \text{products}$.

Two reduced order models are obtained for this system. The One Equation Averaged model (OEA) and the Two Equation Averaged model (TEA).

In case of the OEA model, the LS reduction is applied to both fluids simultaneously. Mathematically the PDEs are formulated as a single operator equation in a direct sum space and then reduced. This approach was used by Ratnakar et al. [8] to develop an averaged model for a monolith catalytic reactor that consists of a core fluid phase and an annular solid catalyst. The final OEA model is given below:

$$h \frac{d\hat{c}_1}{dx} + \frac{(1-h)}{\omega} \frac{d\hat{c}_2}{dx} = Dar(\bar{c}_2)(1-h) \tag{1a}$$

$$\hat{c}_1 - \bar{c}_1 = pDa r(\bar{c}_2)(\beta_1) \tag{1b}$$

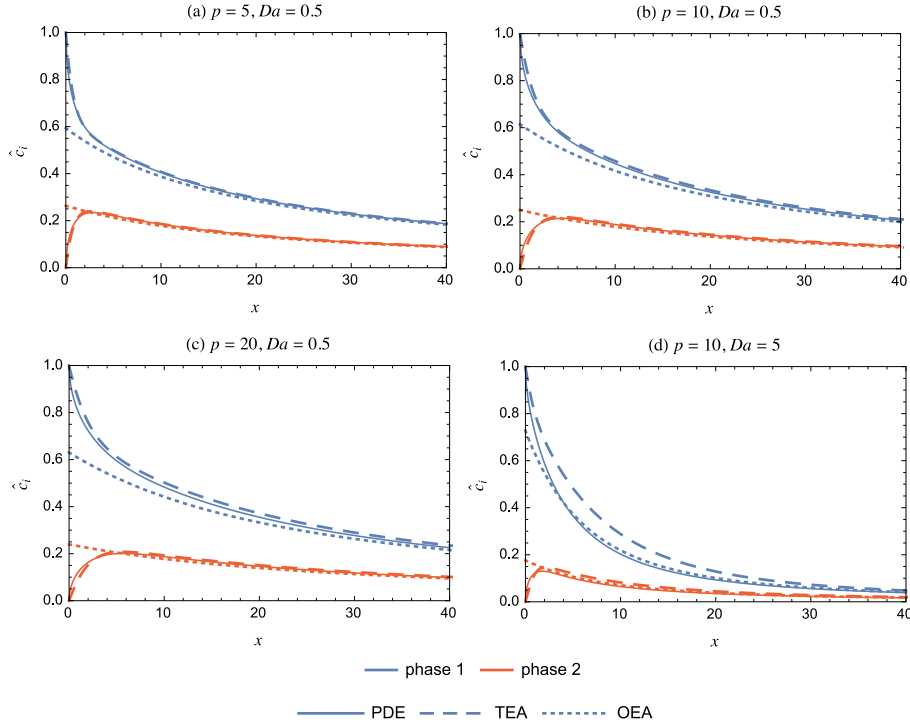


Figure 1: Comparison of the two equation averaged (TEA) model with the full PDE model and the one equation averaged (OEA) model for the case of second order reaction in phase 2. The variation of the cup-mixing average concentration along the length of the channel is plotted. Different values of p and Da are considered. At the inlet ($x = 0$), $\hat{c}_1 = 1$ and $\hat{c}_2 = 0$. Parameter values: $\mu_{12} = 1/2$, $D_{12} = 3$, $K = 2$, $h = 0.4$

$$\hat{c}_2 - \bar{c}_2 = pDaD_{12}r(\bar{c}_2)(\beta_2) \quad (1c)$$

$$\bar{c}_1 - K\bar{c}_2 = pDar(\bar{c}_2)(\beta_3) \quad (1d)$$

$$h\hat{c}_1 + \frac{(1-h)}{\omega}\hat{c}_2 = h + \frac{(1-h)}{\omega}\frac{\hat{c}_{2,in}}{\hat{c}_{1,in}} \quad \text{at } x = 0 \quad (1e)$$

Here \hat{c}_i and \bar{c}_i are cup-mixing and cross-section average concentrations of the carrier ($i = 1$) and solvent ($i = 2$). p is the transverse peclt number, which is small when transverse diffusion is much faster than axial convection. Da is the Damkohler number corresponding to the reaction in the solvent phase. β_i are constants that depend on the velocity profile, the ratio of solute diffusivities (D_{12}), the viscosity ratio (μ_{12}) and the distribution coefficient ($K = c_1^{eq}/c_2^{eq}$). h is the volume fraction of the carrier phase (fluid 1) and ω is ratio of the average velocity of the carrier fluid to the solvent.

This reduced model consists of **one** averaged mass balance equation ((1a)) which describes the evolution of the cup mixing averaged concentrations along the channel length. Eqs. (1b) and (1c) account for the difference between the cup-mixing and cross-section average concentrations in each phase (due to a finite time for transverse diffusion). Eq. (1d) accounts for the departure from equilibrium maintained between the two phases due to the reaction in phase 2.

Figure 1 presents a comparison of the predictions of the TEA and OEA reduced models with that of the PDE model. Different values of p and Da are considered, for the case of $\mu_{12} = 1/2$, $D_{12} = 3$, $K = 2$, $h = 0.4$. The reaction is assume to be second order: $r(\bar{c}_2) = -\bar{c}_2^2$. At the inlet, phase 2 (solvent) is taken to be pure ($\hat{c}_{2,in} = 0$).

This figure shows that the OEA model is able to predict the systems behavior well, except in the region close to the inlet. The OEA model cannot predict the initial mass transfer between the phases when they first come in contact. It can only capture the variations in concentration that occur after this inlet region, due to the chemical reaction in the solvent phase. This drawback is a result of averaging across both

phases simultaneously. As p increases, the diffusion time scale increases relative to convection, and the length of the inlet region over which the initial mass transfer occurs increases. Therefore, the predictions of the full PDE model matches the OEA after a greater channel length when p is larger.

To overcome this drawback of the OEA model, we develop the TEA model by applying the LS procedure to each phase separately. This requires identifying the flux between the phases explicitly ($J(x)$) and writing the equations in the form of two separate operator equations. The final result is given below:

$$p \frac{d\hat{c}_1}{dx} = \frac{-J(x)}{h} \quad (2a)$$

$$\hat{c}_1 - \bar{c}_1 = \gamma_1 J(x) \quad (2b)$$

$$\frac{p}{\omega} \frac{d\hat{c}_2}{dx} = \frac{J(x)}{(1-h)} + pDa r(\bar{c}_2) \quad (2c)$$

$$\hat{c}_2 - \bar{c}_2 = \gamma_2 J(x) + pDa \gamma_3 r(\bar{c}_2) \quad (2d)$$

$$J(x) = \frac{(\bar{c}_1 - K\bar{c}_2)}{\gamma_4} - pDa r(\bar{c}_2) \frac{\gamma_5}{\gamma_4} \quad (2e)$$

$$\hat{c}_1 = 1 \quad \text{and} \quad \hat{c}_2 = \frac{\hat{c}_{2,in}}{\hat{c}_{1,in}} \quad \text{at} \quad x = 0 \quad (2f)$$

Here γ_i are constants that depend on fluid properties.

This model consists of **two** differential equations for the evolution of the cup-mixing average concentrations along the channel. Two more equations account for the difference between the cup-mixing and the cross-section averages. The last equation gives an expression for the flux between the fluids.

The flux $J(x)$ is composed of two terms. The first is due to the departure of the average concentrations in the two fluids from equilibrium. The second term is a correction to the flux due to a chemical reaction.

Figure 1 shows that the TEA model predicts the average concentrations much better than the OEA model, when Da is small (Figs. 1(a)-1(c)). This improvement is pronounced near the inlet; the TEA model captures the variation of the average concentrations right from the entrance of the channel. The TEA model deteriorates, however, as Da is increased beyond unity. In this case the OEA model performs much better, as seen in Fig. 1(d). This was found to be the case in other comparisons as well, which were carried out for a range of parameter values. Thus, when modeling reactive extraction, the TEA model should be used if Da is small ($Da < 1$) while the OEA model should be used for relatively high Da ($Da > 1$).

3 Conclusions

Reduced order models have been derived that describe mass transfer and reactions in stratified micro flows accurately. While the averaged models have been developed for a relatively simple reactive-extraction process, they can be easily extended to processes involving multiple species and multiple reactions, occurring within the fluids or on the surface of the walls. These models will be useful for design, analysis, optimization and model predictive control.

We have shown how the LS technique can be applied to each phase separately, to derive an averaged model that predicts inter-fluid mass transfer more accurately. This procedure can be applied to average models for a wide range of systems involving stratified flows that sustain transport and reactions.

References

- [1] N. Assmann, A. Ladosz, and P. Rudolf von Rohr, "Continuous Micro Liquid-Liquid Extraction," *Chemical Engineering & Technology*, vol. 36, pp. 921–936, June 2013.
- [2] S. Aljbour, H. Yamada, and T. Tagawa, "Sequential reaction-separation in a microchannel reactor for liquidliquid phase transfer catalysis," *Top. Catal.*, vol. 53, pp. 694–699, Apr. 2010.
- [3] E. Šinkovec, A. Pohar, and M. Krajnc, "Phase transfer catalyzed esterification: modeling and experimental studies in a microreactor under parallel flow conditions," *Microfluid. Nanofluid.*, vol. 14, pp. 489–498, Oct. 2013.
- [4] S. Ali, M. Shaegh, N.-t. Nguyen, and S. H. Chan, "A review on membraneless laminar flow-based fuel cells," *Int. J. Hydrogen Energy*, 2011.

- [5] S. Chakraborty and V. Balakotaiah, “Low-dimensional models for describing mixing effects in laminar flow tubular reactors,” *Chem. Eng. Sci.*, vol. 57, pp. 2545–2564, 2002.
- [6] S. Chakraborty and V. Balakotaiah, “Spatially averaged multi-scale models for chemical reactors,” in *Advances in Chemical Engineering Multiscale Analysis* (G. B. Marin, ed.), vol. 30 of *Advances in Chemical Engineering*, pp. 205 – 297, Academic Press, 2005.
- [7] V. Balakotaiah and R. R. Ratnakar, “On the use of transfer and dispersion coefficient concepts in low-dimensional diffusion convection-reaction models,” *Chem. Eng. Res. Des.*, vol. 88, no. 3, pp. 342–361, 2010.
- [8] R. R. Ratnakar, M. Bhattacharya, and V. Balakotaiah, “Reduced order models for describing dispersion and reaction in monoliths,” *Chem. Eng. Sci.*, vol. 83, pp. 77–92, 2012.

Modeling the chaotic dynamics of heterogeneous catalytic reactions with fast, intermediate, and slow variables

G. A. Chumakov^{a,d}, L. G. Chumakova^b, N. A. Chumakova^{c,d,*}

^a*Sobolev Institute of Mathematics, Novosibirsk 630090, Russia*

^b*School of Mathematics, The University of Edinburgh,
Edinburgh, EH9 3FD, Scotland, UK*

^c*Borshakov Institute of Catalysis, Novosibirsk 630090, Russia*

^d*Novosibirsk State University, Novosibirsk 630090, Russia*

Abstract

Examples of the most amazing phenomena in catalysis are self-oscillations and chaotic behavior of the reaction rate accompanied by spatial and temporal self-organization in the adsorbed layer on the catalyst surface. One of the first heterogeneous catalytic systems in which the rate self-oscillations were found was hydrogen oxidation on a nickel catalyst. In spite of a wide variety of different heterogeneous catalytic systems that demonstrate the critical phenomena of this kind, up to now there is no common theoretical explanation of such a complex dynamics.

One of the approaches to theoretical studying the complex dynamics in heterogeneous catalysis consists in development of a mathematical model as a system of nonlinear ordinary differential equations that describes the temporal changes of the concentrations of the individual intermediates on the catalyst surface.

Our paper presents some results of studying chaotic behavior in the low-dimensional dynamical systems with a hierarchy of characteristic times. Under study is a kinetic model of three nonlinear ordinary differential equations

*Corresponding author at: Borshakov Institute of Catalysis, Pr. Akad. Lavrent'eva 5, Novosibirsk 630090, Russia. Tel.: +7 383 326 6426; fax: +7 383 330 6878

Email addresses: chumakov@math.nsc.ru (G. A. Chumakov),
Lyuba.Chumakova@ed.ac.uk (L. G. Chumakova), chum@catalysis.ru
(N. A. Chumakova)

with fast, intermediate, and slow variables to illustrate that the influence of adsorbed species on the rate of a catalytic reaction may lead to sustained oscillations and chaos under isothermal conditions. Such a situation may occur, for example, when the heterogeneity of the catalytic active surface sites causes the activation energy of some rate constants to change with surface coverage by one of the intermediate substances.

In our recent paper [1] we studied a scheme that allowed us to generate the multi-peak oscillations in the three-dimensional kinetic system with fast, intermediate, and slow variables. Our approach was based upon the examination of global dynamics of the one-parameter family of the two-variable subsystems with intermediate and fast variables. A distinctive feature of the study in [1] was the scenario of transition from periodic behavior corresponding to a stable cycle on the strongly deformed torus to the chaotic multi-peak oscillations by the bifurcation of the invariant torus. It was of great interest to clarify how the torus should lose its smoothness with respect to the control parameter.

In this paper, we study a scheme that allows us to generate homoclinic chaos in the three-dimensional system with fast, intermediate, and slow variables. In this case, for generation of the chaotic dynamics we find the parameters of the model under which the system exhibits a Feigenbaum cascade of period-doubling bifurcations. Numerical simulations are used to demonstrate the different types of periodic and chaotic behavior predicted by the model. In particular, as some parameter is varied, the subharmonic period-doubling cascade leads to generation of a global attractor in the system.

Unstable manifolds of the periodic orbits in the cascade are topologically equivalent to Möbius bands, so we call such orbits *Möbius orbits*. Using the one-dimensional approximations of the Poincaré map and its second iteration, we find a transversal homoclinic orbit to the Möbius orbit which appears as a result of the first bifurcation in the period-doubling cascade.

It is important to note that the saddle Möbius orbits from the track of the direct period-doubling cascade and the standard Kaplan-Yorke formula can give a lower bound for the Lyapunov dimension of the global attractor.

References

- [1] G. A. Chumakov, N. A. Chumakova, E. A. Lashina. “Modeling the complex dynamics of heterogeneous catalytic reactions with fast, intermediate, and slow variables,” Chem. Eng. J. (2014, in press).

Modelling of Influence of Oxygen Bulk Diffusion in Nickel on Oscillatory Kinetics of Catalytic Oxidation of Methane

V. Ustugov^{1,*}, E. Finkelstein², E. Lashina¹, N. Chumakova¹, A. Gornov²,

V. Kaichev¹, V. Bukhtiyarov¹

¹ Borekov Institute of Catalysis, Lavrentieva Ave. 5, Novosibirsk 630090, Russia

² Institute for System Dynamics and Control Theory, Lermontov str. 134, Irkutsk 664033, Russia

(*) corresponding author: ustugov@catalysis.ru

evgeniya.finkelstein@gmail.com, lashina@catalysis.ru, chum@catalysis.ru, gornov.a.yu@gmail.com

Keywords: kinetic oscillations, methane oxidation, oxygen bulk diffusion

Introduction

Oscillatory reaction kinetics is unusual and, nevertheless, well-known phenomenon in heterogeneous catalysis. Sinusoidal or relaxation-type oscillations, and chaotic behavior have been observed in approximately 70 catalytic reactions in a wide pressure range, from ultrahigh vacuum up to atmospheric pressure, over all types of catalysts, including single-crystals, polycrystalline foils, wires, and supported catalysts. Several mechanisms describing the rate oscillations for different reactions were proposed. However, the most of them is based on the Langmuir-Hinshelwood mechanism and do not take into account the diffusion in subsurface layers of catalysts. This study is devoted to theoretical analysis of the influence of the diffusion of oxygen atoms into nickel on the self-sustained rate oscillations in the catalytic oxidation of methane.

Methodology

The microkinetic scheme for the oxidation of methane over nickel was published elsewhere [1]. Parameters of elementary reactions, such as enthalpies and activation energies, were determined using a phenomenological approach suggested by E. Shustorovich [2]. Pre-exponential factors of elementary steps were evaluated in the framework of the transition state theory [3]. The diffusion coefficients of oxygen atoms in nickel were determined on the basis of experimental data. The mathematical model of the reaction consists of a system of ordinary differential equations and takes into account concentrations of surface intermediates, an oxygen concentration in subsurface layers, and the heat balance.

Results and discussion

The set of elementary reactions included in the model of the catalytic oxidation of methane over nickel is shown Table 1, where [*] denotes to free vacancies on the nickel metal surface; [Ox] is nickel oxide; [CH₄*], [CH₃*], [CH₂*], [CH*], [H*], [O*], [CO*], [OH*] are adsorbed intermediates on the catalyst surface; CH₄(g), O₂(g), CO(g), CO₂(g), H₂(g), H₂O(g) are gas phase concentrations. The model was amended with a step of the diffusion of oxygen atoms from the nickel surface into subsurface layers. It allows us to study the influence of this step on the characteristics of the oscillatory behavior (fig. 1). In full agreement with previous study [1] the model without the oxygen diffusion under certain parameters has oscillatory solution (fig. 2). In this case the oscillations starts without any delay. In contrast in the model with the oxygen diffusion we found a long induction period before arising the self-sustained oscillations. Similar effect was observed experimentally. Also we found that the concentration of oxygen in the subsurface layers of nickel oscillates synchronously with the concentrations of reaction products in the gas phase.

In both cases we found the partial pressure oscillations of products and reactants as well as the concentration oscillations of main intermediates on the catalyst surface. Simultaneously the catalyst temperature oscillated with the amplitude of several Celsius degrees. Typical oscillations are presented in fig. 1.

Table 1. The mechanism of catalytic oxidation of methane over nickel.

No	Reaction
1	CH ₄ (g) + [*] → [CH ₄ *]
2	[CH ₄ *] → CH ₄ (g) + [*]
3	[CH ₄ *] + [*] → [CH ₃ *] + [H*]
4	[CH ₃ *] + [*] → [CH ₂ *] + [H*]
5	[CH ₂ *] + [*] → [CH*] + [H*]
6	[CH*] + [*] → [C*] + [H*]
7	O ₂ (g) + 2[*] → 2[O*]

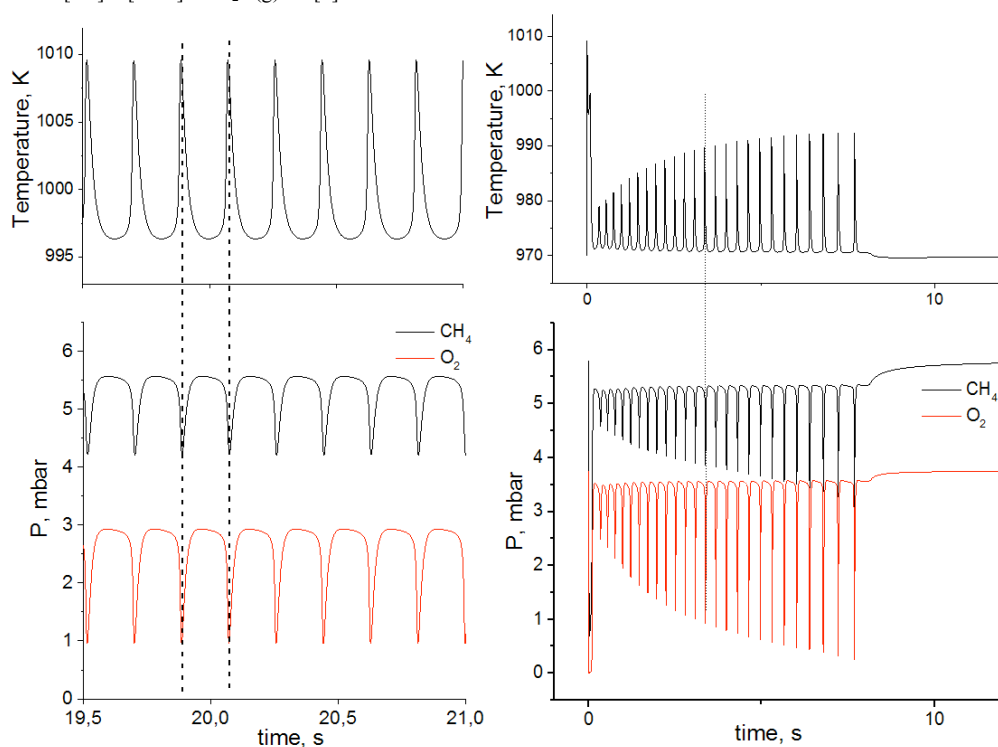
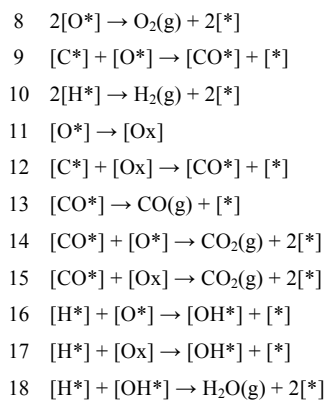


Fig. 1. Synchronous stable oscillations of temperature and gas phase concentrations (left). Unstable oscillations on the border of oscillatory region (right).

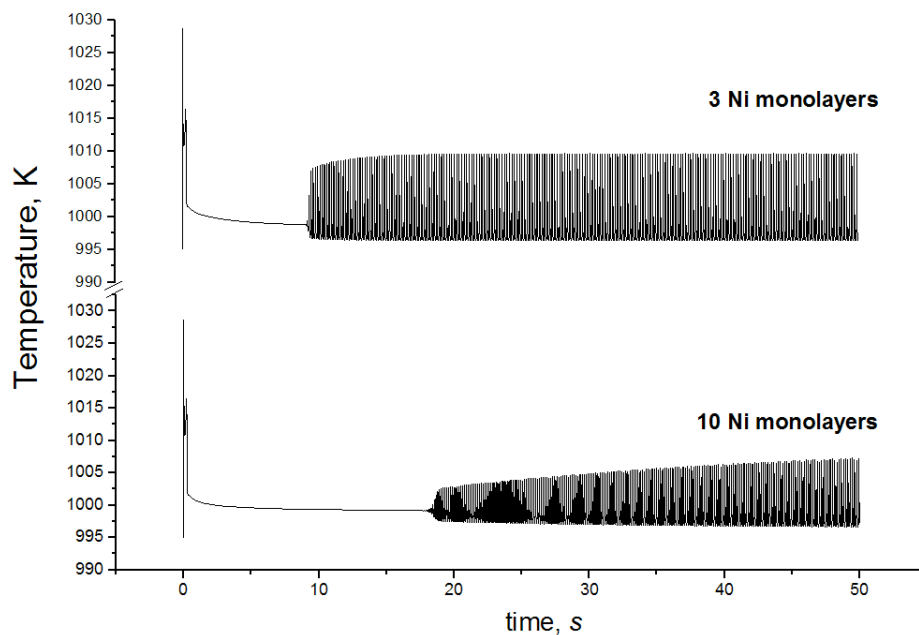


Fig. 2. Oscillations of catalyst temperature in the models of methane oxidation with 3 and 10 nickel monolayers.

Conclusions

The addition of the oxygen diffusion into the model leads to the appearance of an induction period before the self-sustained rate oscillations. The concentration of oxygen in the subsurface layers of nickel oscillates synchronously with the concentrations of reaction products in the gas phase.

Acknowledgements

The work was partially supported by the Grant of President of Russian Federation for government support of Leading Scientific Schools (SS-5340.2014.3).

References

- [1] E.A. Lashina, V.V. Kaichev, N.A. Chumakova, V.V. Ustyugov, G.A. Chumakov, V.I. Bukhtiyarov, *Kinet. Catal.* 53 (2012) 374.
- [2] E. Shustorovich, in: D.D. Eley, H. Pines, P.B. Weisz (Eds.), *Adv. in Catal.* 37 (1990) 101.
- [3] J.A. Dumesic, D.F. Rudd, L.M. Aparicio, J.E. Rekoske, A.A. Trevino, *The Microkinetics of Heterogeneous Catalysis*. American Chemical Society, Washington, 1993.

Application of population balance concept in modeling of FCC riser reactions

Dariusz S. Orlicki¹ and Uriel Navarro

Dariusz.Orlicki@Grace.com

Uriel.Navarro@Grace.com

Grace Davison Refining Technologies
7500 Grace Drive
Columbia, MD 21044
USA

Fluid Catalytic Cracking is an important unit operation in most of the petroleum refinery operations for the conversion of crude oil into useful products. The FCC process plays a major role in the conversion of high molecular weight hydrocarbons, which comprise FCC feedstock, into lower molecular weight and lower boiling range but higher market value hydrocarbons. The chemical composition of the feedstocks affects the slate and quality of major FCC products thus influencing the whole refinery economics. The FCC catalyst enables this economic value of raw materials to be harnessed under the unit operating conditions constraints. While the quality of FCC catalyst is important to unlock the feedstock potential and to produce the valuable products, the maximum value depends on the initial feedstock composition. Understanding complex catalyst-feedstock interactions is the key to proper catalyst selection and optimum unit operation. The industry standard is to evaluate catalyst-feed interactions in the Advanced Catalyst Evaluation (ACE) apparatus. This is a high throughput bench top system with a fluidized bed reactor to simulate commercial riser operations. While the interpretation of the experimental data within the envelope of testing equipment operating conditions is mathematically trivial, scaling-up the results onto different operation conditions, especially commercial operations, or understanding the effect of feedstock or catalyst change on unit performance requires a thorough understanding of the combined reactor hydrodynamics, unit heat balance, and kinetics of complex chemical reactions involved in the cracking process.

Over the years, methods have been developed, mostly in the form of heuristic correlations, to predict cracking products yield and quality based on the properties of the catalyst and feed. Correlations are however limited in applications to the domain of the experimental data set used for their derivations. Models allow to expand these heuristic observations onto new systems and to provide a detailed understanding of complex phenomena that are difficult to experiment with. Modeling of FCC processes is not trivial because of the enormous number of chemical compounds involved, the type of chemical families those compounds belong to (paraffins, isoparaffins, olefins, aromatic, naphthenic, saturates, resins, asphaltenes, etc.) that would affect reaction mechanism and pathways, and the type of cracking process pathways that can be either thermal or catalytic with Bronsted acid sites promoting protolytic cracking and Lewis acid sites associated with a β -scission mechanism. Literature provides numerous examples of kinetic schemes to deal with those complexities.

¹ Author of correspondence

This paper describes the evolution of the six-lump model that we successfully employed for the interpretation of experimental data. While such a lumping scheme is adequate to describe selectivity of major products, the reaction rate constant did not correlate well with initial composition of the feedstock. A collection of over two hundred feeds originated from different geographical locations was thoroughly characterized. All those feeds were tested in the ACE apparatus against three families of commercial FCC catalysts using a range of severities (cat-to-oil ratio from 0 to 100, and reactor temperatures from 778 to 817 K). Cracking products were identified and thoroughly characterized. Distribution models for the feedstock initial properties and cracking product attributes were formulated based on the discretized form of the gamma distribution function. The cracking process is described in terms of the discrete population balance assuming deterministic reaction pathways. While a good agreement was achieved between model predictions and the yield of major products using a univariate distribution, a bivariate approach might be needed for other properties such as Gasoline RON and MON.

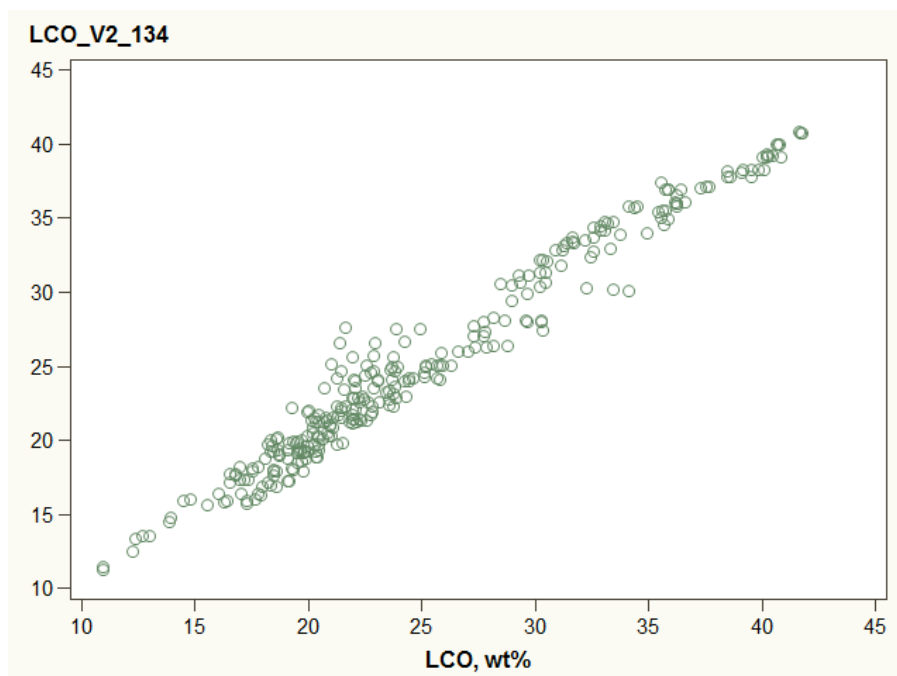


Figure 1. Comparison of model predictions with LCO yield data from ACE experiments – 289 data points.

Use of Hybrid Monte-Carlo Models in Online Control of Product Quality in Emulsion Copolymerization

Alexandr Zubov, Tomáš Chaloupka, Juraj Kosek*

*Department of Chemical Engineering, University of Chemistry and Technology Prague
Technická 5, 166 28 Praha 6, Czech Republic, *corresponding author, E-mail: juraj.kosek@vscht.cz*

1 Introduction

Although emulsion (co)polymerization is an industrially important process used in the production of adhesives, coatings and paintings, its mathematical modeling is challenging due to: (i) complex mass transfer and partitioning of monomer(s) among three phases, (ii) complicated kinetic schemes involving chain-branching and cross-linking, (iii) practical problems associated with latex production, e.g., coagulation of polymer particles and fouling on equipment surfaces.

This contribution deals with the work carried out in two EU collaborative projects. First of them, named “COOPOL” (No. 280827) was focused on the development of system for model-based predictive control (MPC) of semi-batch emulsion copolymerization of four monomers (two water soluble + two hydrophobic). The project ended in February 2015 and the functionality of the MPC system was successfully demonstrated at BASF pilot plant reactor. Probably the most important outcome of this project was the reduction of batch duration by up to 10% while maintaining the product quality characterized by solid content in latex and number-average molecular weight of the produced copolymer.

The aim of the ongoing project “RECOBA” (No. 636820) is shifted more towards the detailed molecular architecture of the formed copolymer, i.e., it is necessary to predict on-line full structure of branched and cross-linked polymer network, which cannot be done by the method of polymer moments used in the macroscopic model developed in the COOPOL project. For this purpose, we use Monte Carlo (MC) simulation which utilizes some of the state variables pre-calculated by the macroscopic model. Therefore we call our approach “hybrid”. Since we do not have a complete experimental characterization of the product molecular architecture (full molecular weight distribution, branching density etc.) up to now, in this abstract we demonstrate the feasibility of the hybrid MC approach on a simple case of emulsion copolymerization of two hydrophobic monomers without long chain-branching (LCB) and cross-linking. Hybrid MC predictions including branching / cross-linking are already available, but they are not validated yet.

2 Macroscopic Process Model of Semi-Batch Emulsion Copolymerization Reactor

The process model of semi-batch emulsion copolymerization of 4 monomers (2 water soluble + 2 water insoluble) developed within the COOPOL project is based on several simplifying assumptions, of which the most important are:

- Nucleation of polymer particles is neglected, because the polymer seed is used. The process is thus assumed to proceed in Stage II and III of emulsion polymerization.
- It was found that for typical process conditions, the solubility of hydrophobic comonomers in aqueous phase is low (< 5%) and also the solubility of hydrophilic comonomers in polymer particles is low. Therefore we neglect the presence of comonomers that are not compatible with a given phase and the reaction medium is finally divided into two simultaneously running 2-monomer copolymerizations with different kinetics: (i) emulsion copolymerization in latex particles, and (ii) solution polymerization in aqueous phase.
- Dynamic evolution of average number of radicals per polymer particle \bar{n} is predicted using approach of Li & Brooks^[1].
- Besides traditional steps as initiation, propagation and termination, the copolymerization kinetic scheme contains also chain transfer to monomer (and to chain-transfer agent) and intramolecular chain transfer (backbiting) leading to the formation of short-chain branches.

The model is formulated as a system of ODEs represented by:

- Material balances of non-polymeric species in all phases.
- Material balance of radicals in polymer and aqueous phase.
- Population balance of polymer moments (summed over polymer and aqueous phase).
- Heat balance of reaction mixture and reactor cooling jacket.

The method of polymer moments was used in this model because the main characteristic of product quality was number-average molecular weight of copolymer M_n and the long-chain branching and cross-linking was not considered in the model. However, in the presence of excessive branching and cross-linking, the use of polymer moments becomes unsuitable, because near the gel point the moments of higher order increase dramatically (approaching infinity at gel point), making integration of model equations stiff or impossible. Moreover, method of moments can provide only information about average molecular weights of polymer, while prediction of the detailed molecular architecture (cf. Section 3) provides valuable information, which can be used for instance for the estimation of polymer viscosity or film-forming properties.

In MPC system, the developed model is implemented as a C++ code and the simulation of several hours of semi-batch reaction is carried out in approx. 1.5 s. The model of semi-batch reactor was validated by 15 laboratory experiments with varying conditions for: (i) conversion of individual monomers, (ii) solid content in latex, and (iii) average molecular weights of the produced copolymer.

Moreover, the model became a central part of the MPC system implemented in the pilot plant reactor of our industrial partner and its functionality was successfully tested by three scenarios of increasing complexity:

1. On-line control of reaction mixture temperature.
2. Minimization of batch time while keeping the standard product quality (characterized by average molecular weight).
3. Minimization of batch time and change in product quality (increase/decrease in average polymer molecular weight).

Regarding the average molecular weights, we mean the experimentally (by SEC/GPC) determined value of the final product, which was not available on-line during the batch, but rather measured afterwards and compared with model predictions. Not only that this work represents the first successful case of on-line control of polymer quality implemented at larger than laboratory scale, it also allowed for the reduction in reaction time by approx. 10%. Results generated at the pilot plant are, however, confidential and can be presented only with scaling in arbitrary units.

3 Hybrid Monte Carlo Simulation of Polymer Chains Architecture Evolution

With respect to the evolution of copolymer molecular architecture, the classical approach represented by simulation of the growth of individual chains would be extremely time-consuming for the on-line control. Therefore we follow the so-called “competition technique” developed by Prof. Hidetaka Tobita in 1990s^[2], significantly reducing the simulation time.

In the competition technique, each event leading to the termination of the active chain growth (e.g., exit to the aqueous phase, termination, transfer to monomer or to other polymer chain) is given its probability distribution with respect to the given chain length. For each of these events and each radical (active/growing chain) in polymer particle, the imaginary time of the radical growth (until it is ceased by the event) is calculated based on the probability distribution and random numbers. The event with shortest time is then selected as the “real”, i.e., as the one that actually happened. In one step of MC algorithm, we thus propagate all active chains in the particle by much higher number of monomeric units than in the conventional MC simulations, which leads to enormous reduction of computational time. Information about the structure of macromolecules (formed over several hours of real time) can be obtained in approx. 10 seconds in MATLAB on a standard desktop PC.

In order to estimate the probabilities of individual events, Monte Carlo simulation utilizes physical-chemical parameters of the modeled system as well as evolution of several state variables previously evaluated by macroscopic process model, namely:

- reaction mixture temperature,
- concentration of radicals in the aqueous phase,
- concentration of monomers sorbed in polymer particles.

The predicted information about the evolution of polymer network topology can be easily translated into full molecular weight distribution (MWD), branching/cross-linking density, polymer particle size distribution (PSD), conversion at gel point and other desired product/process characteristics.

Up to now we are awaiting the detailed experimental information about the architecture of copolymer formed during the simulated reaction, therefore we can present at least the comparison of average product characteristics calculated by the MC simulation and macroscopic process model for a simplified system with long-chain branching and cross-linking neglected, i.e., semi-batch emulsion copolymerization of two water-insoluble monomers. However, the evolution of polymer network due to long-chain branching and cross-linking is already implemented and will be validated as soon as the experimental data are available.

It is evident that the agreement between Monte Carlo and process model is very good for average particle diameter (Fig. 1a) and average molecular weights of the produced copolymer (Fig. 1b), especially with respect to the final (product) values. The differences between the models are probably caused by the different approach to modeling of radicals distribution in polymer particles. While the process models uses purely statistical approach^[1], MC approach simulates each event (radical absorption into particle, exit from the particle or termination) separately.

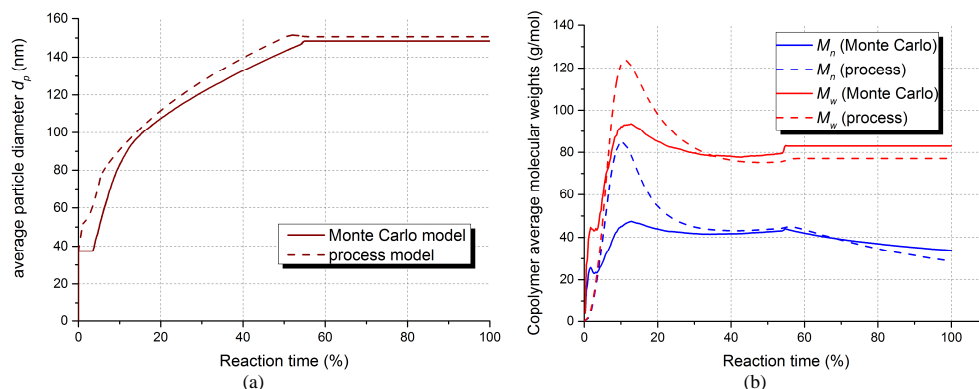


Figure 1. Comparison of the dynamic evolution of the product characteristics predicted by Monte Carlo and macroscopic process model of emulsion copolymerization of two hydrophobic comonomers. (a) Average diameter of polymer particle, (b) number and weight-average molecular weight of copolymer.

4 Conclusions and Future Work

The MPC system for on-line control and optimization of 4-monomer semi-batch emulsion copolymerization was developed and successfully demonstrated in industrial pilot-scale reactor, thus representing state-of-the-art in the control of emulsion polymerization processes. The developed control model can be extended with the hybrid Monte Carlo approach, resulting in the prediction of the detailed molecular architecture of the produced copolymer with sufficient speed for the use in on-line control system.

With respect to polymer quality, only data on average molecular weights of copolymer were available up to now for the validation of models. Therefore, the experimental validation of hybrid MC model will be performed as soon as the experimental data on more detailed molecular architecture (e.g., full MWD, branching density) are available. Polymer network architecture predicted by MC simulation is further used for the prediction of polymer melt viscosity using the extended tube theory^{[3],[4]}.

5 References

- [1] B.-G. Li, B.W. Brooks: Prediction of the Average Number of Radicals per Particle for Emulsion Polymerization. *Journal of Polymer Science: Part A: Polymer Chemistry*, **31**, 2397-2402 (1993)
- [2] H. Tobita, Y. Takada, M. Nomura: Molecular Weight Distribution in Emulsion Polymerisation. *Macromolecules*, **27**, 3804-3811 (1994)
- [3] R. G. Larson: Combinatorial Rheology of Branched Polymer Melts. *Macromolecules*, **34**, 4556-4571 (2001)
- [4] C. Das, N. Inkson, D.J. Read, M.A. Kelmanson, T.C.B. McLeish: Computational linear rheology of general branch-on-branch polymers. *Journal of Rheology*, **50**, 207-235 (2006)
- [5] A. Zubov, J. Pokorny, J. Kosek: Styrene-butadiene rubber (SBR) production by emulsion polymerization: Dynamic modeling and intensification of the process. *Chemical Engineering Journal*, **207**, 414-420 (2012)
- [6] R. Pokorny, A. Zubov, P. Matuska, F. Lueth, W. Pauer, H.-U. Moritz, J. Kosek: Robust process model for styrene and n-butyl acrylate emulsion copolymerization in smart-scale tubular reactor (submitted 2015).
- [7] M. Kroupa, M. Vonka, J. Kosek: Modeling the Mechanism of Coagulum Formation in Dispersions. *Langmuir*, **30**, 2693-2702 (2014)

Slow Manifolds identification for dimensionality reduction of chemical kinetics

Paolo Nicolini **, Alessandro Ceccato *, Diego Frezzato *

* *Department of Chemical Sciences, University of Padova,
Via Marzolo 1, I-35131, Padova, Italy. E-mail: diego.frezzato@unipd.it*

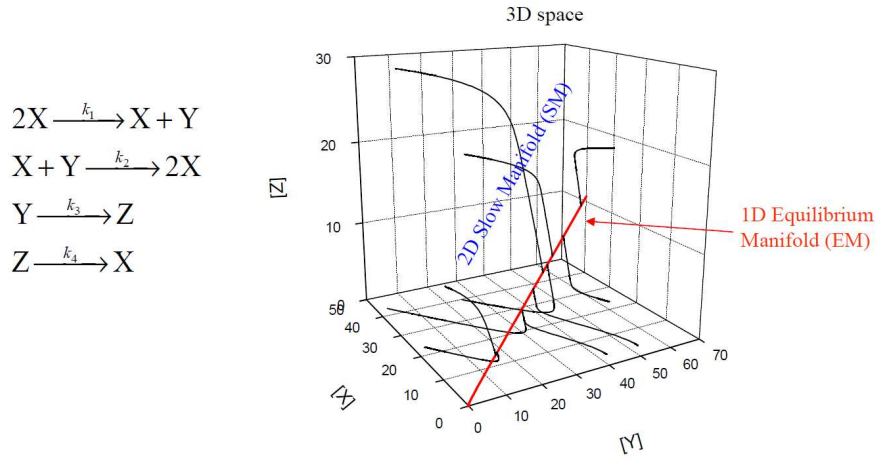
** *Department of Control Engineering – K335, Faculty of Electrical Engineering, Czech Technical
University in Prague, Karlovo náměstí 13, 121 35, Prague 2, Czech Republic. E-mail:
nicolpao@fel.cvut.cz*

Chemical reactions, in laboratory/industrial practice and in natural contexts, often occur via a complex mechanism involving many species and many elementary steps (or “parallel reactions”). Even in the ideal situation of perfectly stirred medium and isothermal conditions, for which the system of Ordinary Differential Equations (ODEs) yielding the trajectory in the concentrations space are of simple polynomial type, one may encounter severe problems on computational and/or interpretative grounds. For example, the large spread of kinetic constants may originate a “stiffness” which imposes the use of extremely short propagation time-steps for integrating the equations. Thus one aims to achieve a “reduced” but accurate enough description of the kinetics such that only the relevant features are kept, the dimension of the algebraic problem is lowered, and the stiffness is removed. This goal is termed “dimensional reduction” of kinetics description.

Here we exploit an almost ubiquitous trait which is “observed” in the concentrations space when several trajectories, originating from different initial points, are plotted together. After a fast transient, the trajectories seem to “converge” to a hypersurface, named Slow Manifold (SM), of lower dimension than that of the whole space; the trajectories then remain close to the SM up to equilibrium and the slow tail of evolution takes place in its neighbourhood. An illustration of a 2-dimensional SM, embedded in a 3-dimensional space, is given in the figure below for a simple kinetic scheme.

The existence of a region in which trajectories converge, implies the appearance of mutual correlation between the species concentrations, suggesting that some degrees of freedom can be removed from the description of the system. The strategy is particularly efficient considering that SMs of very low dimension can be featured in reacting systems involving very many species. For example, a 1-dimensional SM is found in a 9-species model scheme for hydrogen combustion [1].

From the mid of 1980s, several theoretical-computational approaches have been proposed to define and detect SMs in chemical kinetics. Amongst them we mention strategies which exploit the idea of the existence of a timescale separation between fast and slow processes. In such a category we find the Computational Singular Perturbation method [2] and the construction of Intrinsic- [1] and Attracting [3] Low-Dimensional Manifolds. Other methods are inspired by thermodynamic-like criteria [4].



Example of 2-dimensional Slow Manifold in the 3-dimensional concentrations space. Solid lines are trajectories starting from initial points generated at random. The red line is the 1-dimensional manifold of stationary points. The SM can be figured out as the surface which is approached by trajectories in going towards the stationary points. Values of the kinetic constants here used are $k_1 = 2 c_s^{-1} t_s^{-1}$, $k_2 = 1 c_s^{-1} t_s^{-1}$, $k_3 = 0.6 t_s^{-1}$, $k_4 = 3 t_s^{-1}$ where c_s and t_s are arbitrary units for volumetric concentrations and time.

In such a scenario, a formal/operative definition of SM has been recently presented by us [5, 6]. Our guess is that the SM, being a common trait, should emerge from a “universal format” of the evolution law of the reacting system. In this communication we outline the theoretical approach and present some issues concerning low-computational-cost algorithmic implementations. Hereafter only the main features are outlined.

The starting point in ref. [5] was to derive an extended system of ODEs from the original one having the following mass-action-based form

$$\dot{x}_j = \sum_{m=1}^M (v_{P_j}^{(m)} - v_{R_j}^{(m)}) r_m(\mathbf{x}) \quad , \quad r_m(\mathbf{x}) = k_m \prod_{i=1}^N x_i^{v_{R_i}^{(m)}} \quad , \quad j = 1, \dots, N \quad , \quad m = 1, \dots, M \quad (1)$$

where x_j is the volumetric concentration of the species j , $v_{R_j}^{(m)}$ and $v_{P_j}^{(m)}$ are its stoichiometric coefficients as reactant and product, respectively, in the m -th elementary step/reaction, and k_m is the kinetic constant. Our transformation, as a whole, consists in turning from the N variables x_j to the following $N \times M$ variables $V_{jm, j'm'}(\mathbf{x})$ having physical dimension of rates:

$$V_{jm, j'm'}(\mathbf{x}) = \left[v_{P_{j'}}^{(m)} - v_{R_{j'}}^{(m)} \right] \left[\delta_{j, j'} - v_{R_{j'}}^{(m)} \right] k_m \prod_i x_i^{v_{R_i}^{(m)} - \delta_{i, j'}} \quad (2)$$

By introducing the cumulative index $Q = (j, m)$ which labels the pair species-step, the new variables are collected in the square matrix \mathbf{V} of dimension $Q_s \times Q_s$ with $Q_s = N \times M$, whose time evolution results to be governed by

$$\dot{V}_{QQ'} = -V_{QQ'} \sum_{Q''} V_{Q''Q'} \quad (3)$$

A backward transformation $\mathbf{V}(\mathbf{x}) \rightarrow \mathbf{x}$ then allows one to retrieve the actual state of the system in the concentrations space [5]. Eq. (3) is an extended system of ODEs (for the Q_s^2 variables mutually related by non-linear constraints such that the actual number of independent quantities remains N) whose quadratic format is the same regardless of the features of the specific kinetic scheme.

We stress that the change from Eq. (1) to Eq. (3) fits into the class of transformations named “quadratization” or “embedding into Lotka-Volterra format” [7]. By considering that general ODEs systems can be firstly put into a polynomial format [8] and then “quadratized”, the present study may be of interest in different fields even outside the chemical kinetics context.

In ref. [5] we have shown that the rates

$$z_Q(\mathbf{x}) := \sum_{Q'} V_{QQ'}(\mathbf{x}) \quad (4)$$

have peculiar properties. First, they fix the timescale of evolution of the matrix \mathbf{V} (as it appears from Eq. (3)), and hence of the reacting system. Moreover, we have recently established that the inverse of the Euclidean norm of the array \mathbf{z} is directly proportional to the time-step to be employed in a forward propagation scheme, hence such a norm quantifies the local “slowness” of the evolution. Second, by means of phenomenological inspections, in ref. [5] we formulated the conjecture that a “typical” trajectory for a “typical” kinetic scheme enters a region of the concentrations space, termed by us as the “Attractiveness Region” (AR), within which the high-order time-derivatives $z_Q^{(n)}(\mathbf{x}(t)) = d^n z_Q(\mathbf{x}(t)) / dt^n$ tend to become multiple one of the others and monotonically decay to zero. The SM was defined as the hypersurface within AR where $z_Q^{(n)}(\mathbf{x}) = 0$, for all Q , as $n \rightarrow \infty$ (on the equilibrium manifold, the stronger and exact condition $z_Q^{(n \geq 1)}(\mathbf{x}) = 0$ holds). This provides a geometric *definition* of SM as a global object in the concentrations space [6]. Remarkably, such a definition emerged (and indeed it was detected *via* a phenomenological inspection) by the structure of the evolution law in Eq. (3), without the need of subjective choices or assumptions.

In ref. [6] we have proved such a conjecture on simple model kinetic schemes, showing that the SM can be detected once an algorithmic implementation of its definition is adopted. On the other hand, we have also pointed out that facing high-dimensional cases is a hard task. The major problem is to devise an efficient way to approach the neighborhood of the SM, *before* starting the check of conditions on the high-order derivatives. Indeed, although the AR is specified in mathematical terms [5], there are still no ways to state, *via* a low-computational-cost route, if a point in the concentrations space belongs to it or not. Without such a guide, the search for the SM would be like “to find a needle in a (multi-dimensional) haystack”. However, we have recently recognized that approximations of the SM can be obtained by using only the low-order derivatives $z_Q^{(n)}(\mathbf{x})$. Some recent outcomes along this way will be presented here, while for technicalities we refer to our companion communication *Slow Manifolds identification for dimensionality reduction of chemical kinetics: a computational route*.

References

- [1] R. T. Skodje, M. J. Davis, *J. Phys. Chem. A* **105**, 10356 (2001)
- [2] S. H. Lam, D. A. Goussis, *Int J. Chem. Kinet.* **26**, 461 (1994)
- [3] U. Maas, S. B. Pope, *Combust. Flame* **88**, 238 (1992)
- [4] D. Lebiecz, *Entropy* **12**, 706 (2010)
- [5] P. Nicolini and D. Frezzato *J. Chem. Phys.* **138**, 204101 (2013)
- [6] P. Nicolini and D. Frezzato *J. Chem. Phys.* **138**, 204102 (2013)
- [7] B. Hernández-Bermejo, V. Fairén, *Phys. Lett. A* **206**, 31 (1995)
- [8] E. H. Kerner, *J. Math. Phys.* **22**, 1366 (1981)

Acknowledgements: This work is funded by the University of Padova – Progetti di Ricerca di Ateneo 2013 (PRAT2013).

Lyapunov functions and stability of kinetics: from Boltzmann to present days

*A.N. Gorban*²

The talk gives a review of Lyapunov functions and stability analysis of kinetic systems from Boltzmann's $f \log f$ to the present. New families of universal Lyapunov functions for nonlinear kinetics are introduced. Differential inclusions produced by kinetics with partially known reaction rate constants are studied. For them, the forward-invariant peeling procedure is constructed. This procedure produces a forward-invariant subset of the concentration space from an initially given domain. The general constructions are illustrated by simple examples from chemical kinetics.

²University of Leicester, U.K.

Methods and tools for kinetic model identification

Rafiqul Gani

Department of Chemical & Biochemical Engineering
Technical University of Denmark
DK-2800 Lyngby, Denmark

Abstract

Process systems engineering (PSE) has been traditionally concerned with the understanding and development of systematic procedures for the design, control, and operation of chemical process systems. Systematic computer aided methods and tools have been successfully used in the solution and analysis of problems related to process-product engineering, covering a wide range of topics and disciplines. This presentation will discuss the role and importance of modelling with special emphasis on kinetic model identification. Although, models are an integral part of all computer aided methods/tools, the development of mathematical models for representation of the domain chemical process/product knowledge is still principally a manual task. A significant reduction in time and resources spent on problem solving in general and modelling in particular, can be made through the development and use of a computer aided modelling framework that can aid in the systematic generation/creation of the needed models, which is usually the first-step of any model-based approach. A versatile and flexible modelling framework with features such as model reuse, model decomposition and aggregation, model identification coupled with a library of predictive constitutive models and numerical solvers will have the capability to generate process-product models for a wide range of problems at a fraction of the time and resources spent currently. The presentation will highlight the use of a systematic model based approach coupled with a computer aided modelling framework in solving interesting problems in model development, model analysis, model validation and model application of models. Issues such as model applicability, data consistency, model discrimination and numerical solution strategies will also be discussed.

Lack of fit and degrees of freedom in kinetic modelling

Jonas Jansson and Bengt Andersson*

Department of Chemistry and Chemical Engineering

Chalmers University, Sweden

There are many sources of errors both in experiments and the kinetic model that affect the quality of a kinetic model. It is not always possible to model all change in the catalyst during a large series of experiments. Average deactivation or the effect of regeneration may be included but small changes due the complete history of the catalyst is more difficult to identify and model. This may be observed as a difference between two identical experiments as seen in Figure 1.

Identical repeated experiments may show systematic errors i.e. 'lack of fit'. Now it can be argued if this 'lack of fit' is random or due to a poor model that cannot model the change in catalyst due to the history of the catalyst.

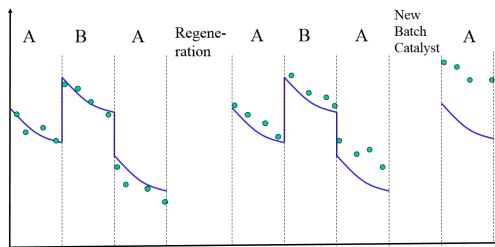


Figure 1 Observed and simulated reaction rates with different experiments and catalyst treatments.

In kinetic modeling we fit the model by minimizing the residual between model and experiment

$$e_u = Y_u - f(C_u, T_u, p)$$

This residual may have different sources

$$E(e_u) = \psi_k + \sigma_l + \tau_m + \epsilon_u$$

ψ = error from catalyst batch

σ = errors from different test series

τ = errors from different experiments

ϵ = errors from different observations

With a correct model we expect that the same parameters are valid for all data points and the residual will be randomly distributed. A prediction using these parameters should have a correct expected value and the problem arises in calculating the confidence interval. The degrees of freedom is the number of observations of the error and we need to find the largest sources of error. If the residual from repeated experiments is larger than the residual from repeated observations it is not sufficient to increase the number of observations to improve predictability, we need more experiments and the degrees of freedom is estimated from the number of experiments minus the number of parameters.

A poor model with lack of fit will not describe all data equally well and the resulting parameters will depend on what experiments that are performed. The predictions from such a model will have even larger confidence intervals depending on the expected variations of the parameters in addition to the random effects.

One way to analyze such data is bootstrapping (random sampling with replacement). There are different ways of performing the data selection but one common method is to randomly remove a fraction of the data e.g. 1/10 of the data and make a least squares minimization to obtain new parameters. You repeat this until all data has been used and an estimation of the confidence interval is obtained from the variation in parameters between the different data sets.

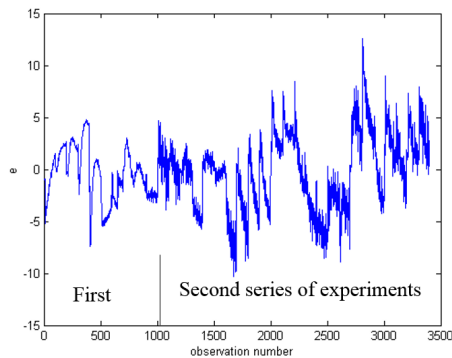


Figure 2 Residual of 24 experiments in two series with in total 3400 observations.

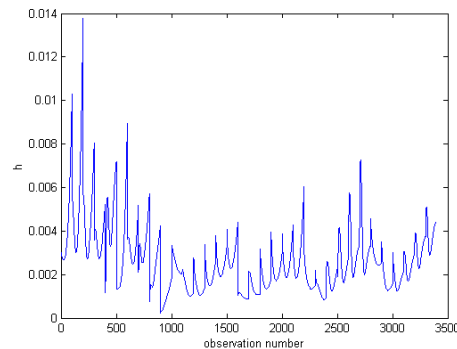


Figure 3 Influence of the observations on the parameters estimated from the H-matrix

Figure 2 shows typical residuals from kinetic modelling of transient experiments. The graph shows 10 experiment from a first series of experiments and then additional 24 experiments. From least squares minimization we obtain that the sum of errors are zero and the sum of squares has a minimum. However it does not guarantee that the main errors are due to errors in the individual observations. On the contrary we observe a large residual in the transient transition from one experimental condition to another and that the residual for the experiments are much larger than the residual for repeated observations.

The degrees of freedom is the number of observations of the main error i.e. $34-p$ in this case and in this case 20 parameters, the degrees of freedom is 14 and not 3380.

The rate of accumulation and desorption can only be observed during transients and only the equilibrium constant can be determined from steady state experiments. Figure 3 shows the influence of the different experimental points on the parameters estimated from the H-matrix. We can clearly see that some observations have minor influence on the parameters and in reality we could estimate the parameters from 1/5 of all the experiments. In text book parameter estimation with one type of errors the extra experiments contributes to a more accurate estimation of the error as seen in the increased degrees of freedom. However, when the main error arises from the experiments and not to the individual observations these extra experiments do not contribute at all.

The residual during transients are much larger than the average residual and it turns out that some parameters are determined from a few observations with large errors while other parameters are determined more accurately from more data points with less errors.

Figure 4 shows a normal probability plot of the average residual for each experiment. They fit very nice into a straight line but it is not possible to conclude that these errors are random since with sufficient number of observations the distribution tend according to the central limit theorem to be normal distribution. We need a more thorough analysis to identify if the model can be improved e.g. plot the residuals vs the temperature in the previous experiments.

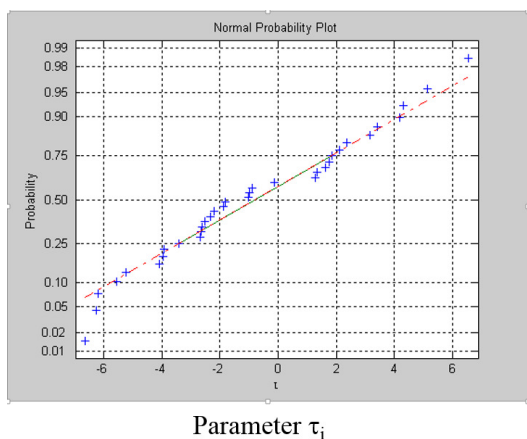


Figure 4 Normal probability plot of the residual τ

Conclusion

A proper parameter fitting require an analysis of the residual as well. Identification of what experiments that contribute to the parameter estimation and the errors in these experiments are required for a proper regression analysis. Adding more observations may not always improve the quality of the model.

Traditional lack of fit analysis based on comparison between repeated identical experiments and the total sum of squares must be performed with different sources of errors.

Future work

Analysis of the quality of predictions from models with lack of fit.

THE NATURE OF VORTEX BREAKDOWN

Vladimir N. Shtern¹ and Guy B. Marin²

¹Shtern Research and Consulting, Houston, TX 77096, USA, vshtern40@gmail.com

²Ghent University, LCT, Technologiepark 914, B-9052, Gent, Belgium, Guy.Marin@ugent.be

Introduction Swirling counterflows play an important role in the environment (tornadoes) and technology: chemical¹⁻³, bio and nuclear reactors; delta-wing aircraft; vortex combustors⁴. Their nature has been discussed more than a half-century, but no consensus has been achieved. We argue that swirl decay and acceleration cause the flow reversals. These mechanisms clearly show why counterflows develop along and normal to the axis of rotation, how counterflows emerge, expand, becomes double and multiple. This understanding can potentially help design conventional and novel vortex devices. It also indicates possible means of the counterflow control.

The development of a local circulation region in a swirling flow, often referred to as vortex breakdown (VB) bubble, was first observed on a delta wing. The vortex arises where the wing and fuselage meet. The swirl and longitudinal velocities increase downstream, reach their peaks near the wing middle, then decay, and vanish far away. VB occurs near the location of maximal swirl velocity and reduces the lift force. As the angle of attack varies, the lift and drag forces have jumps. These sudden changes can cause the loss of flight control.

Being problematic for aircraft, VB is beneficial for combustion. A flame front propagates via diffusion with a speed around 1 m/s. For applications in turbines, the front must be stationary. Therefore, a flow is required which moves slowly against the flame propagation. A circulatory motion, induced by VB, has such necessary feature. The reversed flow transports the combustion heat back to a fuel source and warms up a fuel and an oxidizer that makes combustion stable and clean. Due to these and other applications, the VB problem attracted the attention of many researches.

Different conjectures⁴ were proposed to explain VB: (a) inertial wave roll-up (more than 500 citations!), (b) collapse of the near-axis boundary layer, (c) flow separation, (d) fold catastrophe, and (e) transition from convective to absolute instability. We argue below that VB develops via the swirl-decay mechanism (SDM) which explains VB features.

Swirl decay mechanism In a few words, SDM is the following. In a rapidly rotating flow, the centrifugal force induces the radial gradient of pressure p , according to the cyclostrophic balance, $\partial p / \partial r = \rho v^2 / r$, where ρ is the fluid density, v is the swirl velocity, and r is the distance from the rotation axis. Therefore, p increases with r . The reduction of pressure near the axis, compared with its peripheral value, is larger (smaller) in the vicinity (downstream) of a swirl source because the swirl decays, e.g., due to friction at a wall. Therefore, the near-axis pressure is smaller (larger) in the vicinity of (away from) the swirl source. This pressure difference drives the backflow near the axis. If a swirling flow converges to the axis, the near-axis pressure reduces, decelerating and reversing the downstream flow, i.e., a VB bubble develops as Figure 1 illustrates.

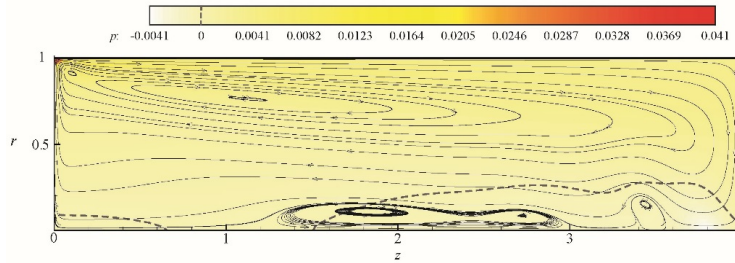


Figure 1: VB bubbles of the cylindrical container flow driven by the rotating left disk.

Swirl acceleration mechanism In a few words, this mechanism (SAM) is the following. The cyclostrophic balance, $\partial p/\partial r = \rho v^2/r$, can occur only away from a wall. The no-slip condition renders that $v = 0$ at a wall, i.e., the centrifugal force drops to the second-order zero. It drops in a thin near-wall boundary layer of a high-speed flow. In contrast, pressure remains nearly invariant across the boundary layer. If a wall is tangential to the r -direction, then $\partial p/\partial r$ is also nearly invariant across the boundary layer and being not balanced by the centrifugal force there, generates a strong near-wall jet propagating in the direction of decreasing r .

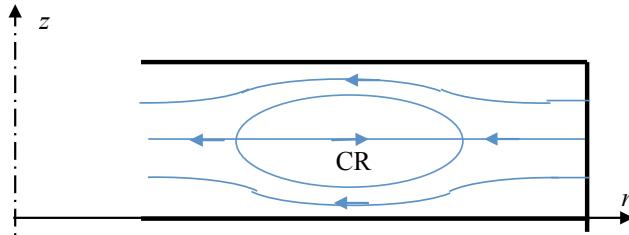


Figure 2. Schematics of circulation region CR in a disk-like vortex chamber.

The jet can be very strong if the bulk flow accelerates in the same direction. Such jets measured⁵ and numerically simulated⁶ in disk-like vortex chambers, DVC, developed for nuclear reactors, but their mechanism has not been adequately explained. Our explanation is that the jet entrains an ambient fluid that can cause a local reversal of the radial velocity. Figure 2 is a schematic of the meridional motion in the disk part of a DVC. A fluid nearly tangentially enters the DVC through its sidewall and develops a vortex-sink motion. The flow accelerates while moving inward the disk. In an accelerating flow, the velocity distribution becomes nearly uniform in the normal-to-end-wall directions. With no swirl, the radial velocity also would be uniform, but the presence of swirl radically changes this by the development of near-wall jets. If the swirl-to-radial entrance velocity ratio is sufficiently large, then the jet entrains not only upstream fluid but downstream fluid as well causing the radial velocity reversal and the formation of circulation region CR schematically shown in Fig. 2. Thus SAM explains the counterflow normal to the rotation axis observed in disk-like vortex chambers. For more details see papers⁵⁻⁸.

Conclusion Based on the above discussion, we can conclude that SDM and SAM resolve two vortex-dynamic enigmas each having a more than half-century history.

1. Marin, G. B. & Yablonsky, G. S. Kinetics of Chemical Reactors, Wiley-VCH, (2011).
2. Kovacevic, J. Z., Pantzali, M. N., Heynderickx, G. J. & Marin, G. B. Bed stability and maximum solids capacity in a Gas–Solid Vortex Reactor: Experimental study. *Chem.Eng.Sci.* **106**, 293-303 (2014).
3. Kovacevic, J. Z., Pantzali M. N., Niyogi, K., Deen, N. G., Heynderickx, G. J. & Marin, G. B. Solids velocity fields in a cold-flow Gas–Solid Vortex Reactor. *Chem.Eng.Sci.* **123**, 220-230 (2015).
4. Shtern, V. *Counterflows*. Cambridge University Press (2012).
5. Savino, J. M. & Keshock, E. G. Experimental profiles of velocity components and
6. Vatistas, G. H., Fayed, M. & Soroardy, J. U. Strongly swirling turbulent sink flow between two stationary disk, *Journal of Propulsion and Power*, **24**, 296-301 (2008).
7. Shtern, V. & Borissov, A. Counter-flow driven by swirl decay. *Phys. Fluids* **22**, 063601 (2010).
8. Shtern, V.N., Torregrosa, M.M., & Herrada, M.A. Effect of swirl decay on vortex breakdown in a confined steady axisymmetric flow. *Phys. Fluids* **24**, 043601 (2012).

Contents

M. Kraft: <i>On the detailed modelling of high temperature nanoparticles synthesis</i>	1
R. Bürger: <i>On reactive settling of activated sludge</i>	2
B. Celse: <i>Parameter fitting: which algorithm to choose?</i>	5
Guanghua Ye: <i>Probing pore blocking effects on multiphase reactions at the particle level using a discrete model</i>	8
S. Kar: <i>A comparative study of optimization algorithms for a cellular automata model</i>	11
S. Alzyod: <i>The Sectional Quadrature Method of Moments (SQMOM): An Application to Liquid-liquid Extraction Columns</i>	13
A. Ceccato: <i>Slow Manifolds identification for dimensionality reduction of chemical kinetics: a computational route</i>	15
P. Nicolini: <i>Traits of regularity in stochastic chemical kinetics: analogy with the Slow Manifolds feature in deterministic kinetics</i>	19
K. Osz: <i>Mathematical description of the kinetics of photochemical reactions</i>	22
M. Szukiewicz: <i>Exact analytical solution of a non-linear reaction-diffusion problem for full range of parameters values: multiplicity and dead zone coexistence.</i>	24
M. Szukiewicz: <i>Modeling of gas flow: usefulness of the Laplace transform and CAS-type programs</i>	27
R.O. Fox: <i>Quadrature-Based Moment Methods in Chemical Engineering</i>	30
D. Pischel: <i>Coping with heterogeneity and stochasticity in microbial processes</i>	31
D. Branco Pinto: <i>The switching point between kinetic and thermodynamic control of competitive reactions</i>	34

J. Van Belleghem: <i>Fischer-Tropsch Synthesis SSITKA simulation: balancing between model complexity, computational effort and relevance of the included features</i>	38
P.H. Van Steenberge: <i>Novel heuristics for mediating radical chain reactions: a stochastic simulation of the synthesis of copolymers with tailored monomer sequences</i>	41
I. Hitsov: <i>Calibration And Analysis Of A Direct Contact Membrane Distillation Model Using Monte Carlo Filtering and good modelling practice</i>	44
M. Ostrovsky: <i>Optimal design of chemical processes with joint chance constraints</i>	47
F.J. Keil: <i>Simulations of instationary operated heterogeneous catalytic reactions</i>	50
C. Lo: <i>Integration of DFT calculations into microkinetic analysis: Application to carbon dioxide hydrogenation on ceria</i>	52
R. Feres: <i>Explicit formulas for reaction probability in reaction-diffusion experiments</i>	55
G. Lente: <i>Stochastic effects in autocatalysis</i>	58
V.I. Bykov: <i>Oscillating regimes of first order phase transition</i>	60
J. Picardo: <i>Low-dimensional Modeling of Reactions and Transport in Stratified Microflows</i>	63
N.A. Chumakova: <i>Modeling the chaotic dynamics of heterogeneous catalytic reactions with fast, intermediate, and slow variables</i>	67
V. Ustyugov: <i>Modelling of Influence of Oxygen Bulk Diffusion in Nickel on Oscillatory Kinetics of Catalytic Oxidation of Methane</i>	69
D.S. Orlicki: <i>Application of population balance concept in modeling of FCC riser reactions</i>	72
A. Zubov: <i>Use of Hybrid Monte-Carlo Models in Online Control of Product Quality in Emulsion Copolymerization</i>	74
D. Frezzato: <i>Slow Manifolds identification for dimensionality reduction of chemical kinetics</i>	77
A.N. Gorban: <i>Lyapunov functions and stability of kinetics: from Boltzmann to present days</i>	81
R. Gani: <i>Methods and tools for kinetic model identification</i>	82
B. Andersson: <i>Lack of fit and degrees of freedom in kinetic modelling</i>	83
V.N. Shtern: <i>The nature of vortex breakdown</i>	86

ISBN 9789082401004
EAN: 9789082401004

An issue of the journal *Computers & Chemical Engineering* will publish the full papers corresponding to some of these abstracts.